UC San Diego

UC San Diego Electronic Theses and Dissertations

Title

Informative Touch for Intelligent Soft Robots

Permalink

https://escholarship.org/uc/item/1f4889nq

Author

Shih, Benjamin

Publication Date

2020

Peer reviewed|Thesis/dissertation

eScholarship.org Powered by the California Digital Library
University of California

UNIVERSITY OF CALIFORNIA SAN DIEGO

Informative Touch for Intelligent Soft Robots

A dissertation submitted in partial satisfaction of the
requirements for the degree
Doctor of Philosophy

in

Engineering Sciences (Mechanical Engineering)

by

Benjamin Shih

Committee in charge:

Professor Michael T. Tolley, Chair
Professor Shengqiang Cai
Professor Andrea Chiba
Professor Henrik I. Christensen
Professor Tania Morimoto
Professor Michael Yip

2020

Copyright
Benjamin Shih, 2020
All rights reserved.

The dissertation of Benjamin Shih is approved, and it is acceptable in quality and form for publication on microfilm and electronically:

_____

_____

_____

_____

Chair

University of California San Diego

2020

EPIGRAPH

Any sufficiently advanced technology is indistinguishable from magic.

—Arthur C. Clarke

TABLE OF CONTENTS

Signature Page . . . iii

Epigraph . . . iv

Table of Contents . . . v

Acknowledgements . . . ix

List of Figures . . . xii

List of Tables . . . xxi

Vita . . . xxii

Abstract of the Dissertation . . . xxiv

Chapter 1 Introduction . . . 1
1.0.1 Soft robotics . . . 1
1.0.2 Design and fabrication of integrated e-skins . . . 4
1.0.3 Skin-based sensing for soft robots . . . 7
1.0.4 Machine learning for soft e-skins . . . 9

Chapter 2 Custom soft robotic gripper sensor skins for haptic object visualization . . . 12
2.1 Design . . . 16
2.1.1 Actuator module design . . . 16
2.1.2 Sensor design . . . 18
2.1.3 Gripper design . . . 18
2.2 Analytical model . . . 19
2.2.1 2D actuator model . . . 19
2.2.2 Sensor model . . . 21
2.3 Fabrication . . . 22
2.3.1 Fabrication of actuator module . . . 22
2.3.2 Fabrication of sensor skin . . . 22
2.3.3 Assembly of finger module . . . 24
2.4 Results . . . 25
2.4.1 Experimental validation . . . 25
2.4.2 2D tactile object modeling . . . 27
2.4.3 3D tactile object modeling . . . 29
2.5 Conclusion and future work . . . 30

Chapter 3 Design considerations for 3D printed, soft, multimaterial resistive sensors for soft robotics . . . 33
3.1 Materials and methods . . . 38
3.1.1 Design and fabrication of the resistive sensors . . . 38
3.1.2 Removal of support material . . . 39
3.1.3 Mechanical strain relief . . . 40
3.1.4 Experimental setup for measurement and characterization . 41
3.1.5 Removal of water content by desiccation . . . 42
3.1.6 Preferential strain response of the multi-dimensional sensor 42
3.1.7 Model of strain response . . . 43
3.1.8 Model of pressure response . . . 44
3.2 Results and discussion . . . 44
3.2.1 Characterization of the dependence of conductivity on orientation of 3D print . . . 44
3.2.2 Characterization of the dependence of conductivity on removal of support material . . . 45
3.2.3 Characterization of the dependence of conductivity on contact resistance . . . 46
3.2.4 Characterization of the dependence of conductivity on water content . . . 48
3.2.5 Comparison between model and experimental data . . . 48
3.2.6 Multimodal sensitivity . . . 52
3.2.7 3D printed soft gripper with embedded sensors . . . 53
3.3 Conclusion and future work . . . 55

Chapter 4 3D printed resistive soft sensors . . . 58
4.1 Design and fabrication . . . 61
4.1.1 Uniaxial strain sensor and wire attachment to soft substrate . 62
4.1.2 Multilayer integrated strain and pressure sensor . . . 63
4.2 Analytical model . . . 64
4.2.1 Strain . . . 64
4.2.2 Pressure . . . 65
4.3 Experimental characterization . . . 66
4.3.1 Temporal response . . . 67
4.4 Complex, non-planar bodies . . . 69
4.5 Conclusion and future work . . . 70

Chapter 5 Soft robot perception using embedded soft sensors and recurrent neural networks . . . 73
5.1 Materials and methods . . . 81
5.1.1 Fabrication of the sensors . . . 82
5.1.2 Fabrication of the actuators . . . 86
5.1.3 Experimental setup . . . 86

5.1.4 Sampling for kinematics and force modeling 88
5.1.5 Long short-term memory for non-linear, time-varying material characteristics 89
5.2 Results 90
5.2.1 Kinematic modeling 90
5.2.2 Force modeling 94
5.2.3 Graceful degradation 96
5.2.4 Multi-degree-of-freedom system 99
5.3 Conclusion and future work 99

Chapter 6 Learning variabilities in materials and manufacturing for the control of soft robots 3D printed from TPU 103
6.1 Customized soft robots enabled by 3D printing 104

Chapter 7 Classification of components of affective touch using rapidly manufacturable, soft, sensor skins 107
7.1 Design and fabrication of soft sensors 110
7.1.1 Design 110
7.1.2 Fabrication 112
7.1.3 Data acquisition 113
7.2 Architecture of neural network 114
7.3 Towards a framework for interpreting affective touch with soft sensors 114
7.4 Experimental setup 115
7.4.1 Structure of our affective touch data 115
7.4.2 Structure of LSTM 118
7.4.3 Classification accuracy on the 2×2 sensor array 118
7.4.4 Margin of return as related to scalability and density of sensor array 119
7.4.5 Impact of soft vs. rigid substrate on soft sensor 119
7.4.6 Graceful degradation 120
7.5 Results 120
7.5.1 Classification accuracy on the 2×2 sensor array 120
7.5.2 Margin of return as related to scalability and density of sensor array 121
7.5.3 Impact of soft vs. rigid substrate on soft sensor 121
7.5.4 Graceful degradation 122
7.6 Conclusion and future work 122

Chapter 8 Electronic skins and machine learning for intelligent soft robots 125
8.1 Applications of e-skins 126
8.1.1 Shape sensing 126
8.1.2 Toward feedback control of soft robots 129
8.1.3 Manipulation 130

8.1.4 Exploration 131
8.1.5 Reaction 133

Chapter 9 Conclusions 135
9.0.1 Open questions and future directions 136
9.0.2 Outlook 139

Bibliography 140

ACKNOWLEDGEMENTS

First, thanks to my advisor Mike for giving me the opportunity to work in the Bioinspired Robotics and Design Lab. It's been a fantastic experience learning not only the perspective with which to ask and dive into research questions, but also many aspects of life, professionalism, and career. Thank you for the resources, support, patience, and freedom that you provided to enable me to grow as an independent researcher.

Thanks to my committee members Henrik, Andrea, Mike, Sheng, and Tania for all of the time, advice, and feedback throughout the years. I'm fortunate to have had the opportunity to learn from each of you and absorb your various perspectives and directions. The interdisciplinary viewpoints that you provided have been incredibly valuable for identifying open challenges and potential solutions across many fields.

The grad school experience would not have been the same without all of the wonderful members in the Bioinspired Robotics and Design Lab. I am especially fortunate to have shared a larger-than-typical starting phd cohort in Mike's lab with Caleb, Will, Dylan, and Adriane, and am fortunate to now be joined by Michael, Saurabh, Jess, Paul, Emily, Iman, and Jiayao. There are too many additional lab members and alumni to list here and I consider this to be an excellent "problem" to have, so in lieu: a big thank you to everyone who has been a part of the lab, and extra thanks to everyone that I have had the fortune of working with personally. I thoroughly enjoyed all of our conversations, meals, game nights, and scavenger hunts for happy hours and I'm excited to see all of the great things you'll do.

Thanks a lot to my collaborators and the visitors to our lab. In particular, Yong-Lae and Thomas: transitioning from reading your papers, to meeting you at conferences, to working with you in person, has substantially shaped and broadened my research vision and skillset. Additionally, thank you to all the friends in the (soft) robotics community for the engaging discussions, adventures around the world, and helpful advice; you are all incredibly inspiring. Thanks to Jamie for welcoming me into her lab at EPFL as well as all of my mentors and teachers

at CMU, for giving this random kid a chance to play with robots and develop an interest.

Thanks to all my friends at UCSD, and from undergrad (hi CMU), various internships (hi burgers, Switzerland, NanoJapan), high school (hi Blair), and everywhere else. It's been such an enjoyable journey learning from each and every one of you and I'm excited to see where life takes you next. Especially thanks to cinderblocks and lomo for putting up with my endless rambling.

Thanks to all the staff at UC San Diego, especially Chris, Roxanne, Ioana, David, and David, for helping make things a lot easier at UCSD.

Finally, thanks so much to my parents, sister, and family for their unwavering support.

It feels strange to be completing this dissertation during COVID-19, but in a way, I think that will make the transition of this chapter of life even more memorable.

Chapter 2, in full, is a reprint of the material as it appears in **B. Shih**, D. Drotman, C. Christianson, Z. Huo, R. White, H. I. Christensen, and M. T. Tolley, "Custom soft robotic gripper sensor skins for haptic object visualization," in 2017 IEEE/RSJ International Conference on Intelligent Robots and Systems (**IROS17**), pp. 494-501, Sept 2017. The dissertation author was the primary investigator and author of this paper.

Chapter 3, in full, is a reprint of the material as it appears in **B. Shih**, C. Christianson, K. Gillespie, S. Lee, J. Mayeda, Z. Huo, and M. T. Tolley, "Design considerations for 3D printed, soft, multimaterial resistive sensors for soft robotics," **Frontiers in Robotics and AI**, 6, 30, Apr 2019. The dissertation author was the primary investigator and author of this paper.

Chapter 4, in full, is a reprint of the material as it appears in **B. Shih**, J. Mayeda, Z. Huo, C. Christianson, and M. T. Tolley, "3D printed resistive soft sensors," in 2018 IEEE-RAS International Conference on Soft Robotics (**ROSO18**), pp. 152-157, Apr 2018. The dissertation author was the primary investigator and author of this paper.

Chapter 5, in full, is a reprint of the material as it appears in T. G. Thuruthel*, **B. Shih***,

C. Laschi, and M. T. Tolley, "Soft robot perception using embedded soft sensors and recurrent neural networks,", **Science Robotics**, 4:26, eaav1488, Jan 2019. The dissertation author was the co-primary investigator and author of this paper.

Chapter 6, in part, is currently being prepared for submission for publication of the material. The dissertation author is the primary investigator and author of this paper.

Chapter 7, in full, is a reprint of the material as it appears in **B. Shih**, E. Lathrop, I. Adibnazari, R. Martin, Y.-L. Park, M. T. Tolley, "Classification of components of affective touch using rapidly manufacturable, soft, sensor skins", 2020 IEEE-RAS International Conference on Soft Robotics (**ROSO20**), pp. 182-187, Apr 2020. The dissertation author was the primary investigator and author of this paper.

Chapter 8, in full, is a reprint of the material as it appears in **B. Shih**, D. S. Shah, J. Li, T. G. Thuruthel, Y.-L. Park, F. Iida, Z. Bao, R. Kramer-Bottiglio, M. T. Tolley, "Electronic skins and machine learning for intelligent soft robots", **Science Robotics**, 5:41, eaaz9239, April 2020. The dissertation author was the primary author of this paper.

The work presented in this thesis was made possible through the financial support of the UC San Diego Irwin Jacobs School of Engineering Fellowship, UC San Diego Frontiers in Innovation Scholars Program, ARCS Foundation Scholarship, Dr. Tom McKenna through the Office of Naval Research, and BASF.

LIST OF FIGURES

Figure 1.1: Trends in the intersections between e-skins, soft robotics, and machine learning. (Left) A range of e-skins and soft sensors that increase in complexity, from bottom to top, by metrics including density, resolution, and fabrication [1–7]. (Middle) Soft robots and e-skins that merge actuation and sensing [8–20], from left to right and top to bottom. (Bottom) Soft robots that focused primarily on actuation [21–25], from left to right. Red boxes indicate work that has leveraged machine learning in the processing of their sensor information. 3

Figure 1.2: Sensor arrays enable e-skins to extract information about their environment. (A) Human skin with various receptors used to sense stimuli. (B) A scalable tactile glove containing a passive matrix of 548 force sensors for the collection of large datasets [26]. (C) 2D sensor array used to generate a profile of pressure intensity from experimental mapping of the pixel signals using an active matrix [27]. The icons at the bottom represent biological analogies: Merkel disks, Meissner corpuscle, and free nerves. (D) A 3D array of electronic sensors assembled from 2D electronics [28]. (E) Multimodal sensor array that can capture both pressure and temperature information [29]. 5

Figure 1.3: Machine learning techniques for processing raw sensory information, different levels of abstraction to aid in robot perception, and action planning. The level of abstraction depends on the task, and the most effective type of learning architecture depends on the quality and structure of the sensor signals. The level of abstraction depends on the task, and the most effective type of learning architecture depends on the quality and structure of the sensor signals. Higher-level processes can include parallel execution of lower-level processes. End-to-end architectures [e.g., [30]] without mid-level and low-level pipelines would likely be faster and more effective but are computationally expensive to develop. 9

Figure 2.1: Our proposed soft pneumatic gripper with internal sensing attached to a robot arm. a) Using the soft gripper and robot arm to pick up a light bulb. b) Light bulb that we used to generate the visualization. c) 3D haptic object visualization generated by our gripper, with our data plotted in a 2D view. We estimated where the gripper contacted the object via sensor reading and each color represents a different height. 14

Figure 2.2: Dexterous soft gripper capable of safely handling delicate objects under uncertainty. a) Side view of human hand grasping and twisting a round object, which inspired our design for in-hand manipulation. b) Visual model of actuator in resting state (left), and when chamber C is inflated (right). c) Soft gripper handling, manipulating, and rotating a light bulb. 17

Figure 2.3: Our proposed soft gripper design is capable of performing a range of complex manipulation tasks, including: a) unscrewing a bottle cap, b) rotating a screw driver, c) opening up its grasp area to manipulate a larger box, and d) grasping complex shapes such as a pair of glasses. 19
Figure 2.4: Schematic of the 2D analytical model of our actuator. a) Cross-sectional view. b) Side view, where the actuator is inflated, bent, and at equilibrium. 19
Figure 2.5: Schematic of our soft actuator module fabrication process, based on retractable-pin casting [31] – side view, with only two chambers shown. Steps: a) Fill outer chamber of the mold with silicone. b) Insert inner chamber of the mold into the silicone and outer chamber of the mold. c) After the silicone cures, remove the outer chamber of the mold. d) Next, remove the inner chamber of the mold, leaving behind chambers in the silicone. e) Insert tubing and seal the pneumatic chambers. 23
Figure 2.6: Schematic of sensor fabrication process. A conductive silicone is embedded within thin layers of non-conductive silicone. We control the thickness of the layers via spin coating and the trace patterns are made via masking. 23
Figure 2.7: Schematic and manufacturing process for the finger modules. a) Mold the actuator modules from silicone elastomer. b) Sensor skins are fabricated as flat sheets with trace patterns that match the geometry of the actuator. c) The skins are rolled up, sealed, and worn as modular sleeves on the actuator. d) Cured silicone actuator module after it has been removed from the mold. e) Flexible, silicone strain sensors which form a skin around the actuator module. f) Completed finger that integrates both actuator and sensor skin, where C_i are the pneumatic chambers, B_i are the flexible sensors that measure the actuator bend, and S is the strain sensor that measures contact at the fingertip. 25
Figure 2.8: Plot comparing analytical actuator model, experimental data, and linear fit for the bend angle of the finger modules. Solid lines show the linear model prediction. Dashed lines show the best-fit line to the data. Individual points represent the experimental data. The theoretical model is approximately accurate for pressures at which we actuate our fingers. We assume an input range of 10 psi and above because below that threshold, the pressure does not overcome the elastic restoring forces of the material and thus no inflation occurs. 26
Figure 2.9: Plot comparing analytical sensor model, experimental data, and linear fit for the change in resistance of the sensors. Solid lines show the linear model prediction. Dashed lines show the best-fit line for the data. Individual points represent the experimental data. 27

Figure 2.10: Setup used for 2D tactile object modeling. a) Side view schematic of how the fingers and object are positioned. We use a protractor as a ground truth for the angle of rotation. b) Our soft gripper is able to model various convex shapes, including square, circle, rectangle, oval, and convex shapes. For each shape, the left is the 2D acrylic piece we used in the modeling experiment and the right is the resulting visualization. We connected the contact points with dotted, straight lines for visualization purposes. c) Gripper in resting position. d) Gripper rotating the object. Protractor not shown. 28

Figure 3.1: Overall vision of the pipeline for our 3D printed sensors. a) Digitized CAD design with embedded, integrated sensing. b) Multimaterial 3D printer that simultaneously co-fabricates both actuators and sensors. c) Post-processing such as removing support material or wire connections. d) Immediately deployable for real-world applications. 37

Figure 3.2: 3D printed, resistive, soft sensors and the correspoding CAD drawings. a, d) Humanoid robot - front view. Enlarged drawings of the embedded heart- and brain-shaped sensors. b, e) Multilayer strain and pressure sensor - top view. c, f) Uniaxial strain sensor with mechanical strain relief and functional gradient to improve wire interface - isometric view. 38

Figure 3.3: Stages of the process for removing the support material. a) Newly printed block of material for characterization, with a matte surface finish. b) Block of material after we mechanically remove the support material. Some patches of support material can remain on the surface. c) Block of material after we wash it with distilled water and dry the sample. 40

Figure 3.4: Our method for wire attachment. a) Schematic for the wire attachment procedure - isometric view. We insert the wire at 1, and pass through in order of 1-2-3-4 to both distribute strain on the wire and to improve the electrical conductivity between the solid wire and the photopolymer trace. These numbers are only labeled on half of the sensor shown, for clarity. b) Completed, physical version of the wire attachment - top view. 41

Figure 3.5: a) setup to measure conductivity of blocks. b) setup to simultaneously measure strain and conductivity. 42

Figure 3.6: Plot of the impact of anisotropy on the 3D printed material. Number of samples n = 10. 45

Figure 3.7: Plot of how the resistance of the 3D printed materials changes depending on how much support material is on the surface. Each group of bars corresponds to the measurement along the various stages in the removal process of the support material (Fig. 3.3). Number of samples n = 10. 46

Figure 3.8: Plot of the dependence of the magnitude of conductivity based on contact resistance. We plot the magnitudes on a logarithmic scale to show the order of magnitude difference that the wire connection results in. Number of samples n = 3. 47

Figure 3.9: Plots of changes in mass and resistance due to desiccation. a) Percent change in mass. b) Percent change in resistance. Number of samples n = 6. 49
Figure 3.10: Normalized change in resistance vs. strain for the uniaxial strain sensor. Comparison of analytical model to experimental characterization. The mean is 108 MΩ at rest. Number of samples $n = 3$. 49
Figure 3.11: Comparison of analytical model to experimental characterization for the multilayer sensor. a) Normalized change in resistance vs. strain. The mean is 147 MΩ at rest. Number of samples $n = 3$. b) Normalized change in resistance vs. pressure. The mean is 560 MΩ at rest. 50
Figure 3.12: Plot showing the strain response of the multimodal sensor in multiple directions as we stretch it along the vertically-aligned direction. In this situation, the sensor is more sensitive to the serpentine pattern that is horizontally-aligned as opposed to the one that is vertically-aligned, whereas the circular sensor experiences a minimal change in its response relative to the other directions. 53
Figure 3.13: Pneumatic gripper with embedded strain sensors and the static sensor readings of the gripper corresponding to the configuration of the fingers while holding various objects. S1, S2, and S3 are the sensor readings from each of the three fingers. a) Plastic strawberry. b) Pencil. c) Can of spam. d) Toy peg. e) Plastic banana. f) 3D perspective of the scatter plot. g) 2D perspective of the scatter plot. 54
Figure 3.14: Dynamic sensor readings of the gripper as the fingers close, without an object. S1, S2, and S3 represent each of the sensor readings that the fingers in the gripper produced. 55

Figure 4.1: Our proposed 3D printed, resistive, soft sensors. a) 3D printed sensor embedded in a complex geometry, showing the versatility of this technique. b) Multilayer integrated strain and pressure sensor. c) Uniaxial strain sensor. 59
Figure 4.2: Design, fabrication, and testing procedure for our 3D printed sensors. a) Digitized CAD design of the uniaxial sensor. b) Multimaterial 3D printer that we used to print the sensors. c) Wire attachment process (Section 7.1.1A) for adhering the photopolymer traces to the external wires. d) Characterization of the strain measurements that the sensors can detect. We acquired the data using a mechanical testing machine (Instron). 61
Figure 4.3: CAD drawings of our sensors. a) Humanoid robot - front view. b) Multilayer strain and pressure sensor - top view. c) Uniaxial strain sensor with mechanical strain relief and functional gradient to improve wire interface - isometric view. 63

Figure 4.4: Our method for wire attachment. a) Schematic for the wire attachment procedure - isometric view. We insert the wire at 1, and pass through in order of 1-2-3-4 to distribute strain on the wire. The space between 1 and 2 is printed and filled using a dielectric photopolymer, which provides mechanical relief by holding the wire in place. At 3 and 4, we coat the wire and photopolymer interface with silver paste to increase electrical conductivity. These numbers are only labeled on half of the sensor shown here. A is a rigid photopolymer, B is a functional gradient, and C is a flexible photopolymer. b) Completed, physical version of the wire attachment - top view. 64
Figure 4.5: Normalized change in resistance vs. strain for the uniaxial strain sensor. Comparison of analytical model to experimental characterization. 67
Figure 4.6: Comparison of analytical model to experimental characterization for the multilayer sensor. a) Normalized change in resistance vs. strain. b) Normalized change in resistance vs. load. 68
Figure 4.7: Demonstration of the time response for the uniaxial sensor when strained multiple times by hand to approximately 110%. The change in resistance is measurable in real-time and distinguishable from the noise, although there is a small shift in the baseline of the sensor reading. 69
Figure 4.8: Demonstration of the 3D sensor shapes embedded within a humanoid that we fabricated with the multimaterial printer. The signals are currently decoupled in these plots, e.g. deforming the head does not affect the torso. a) Measurement of the brain-shaped sensor embedded within the head, as the head is deformed. b) Measurement of the heart-shaped sensor embedded within the torso, as the torso is deformed. 70

Figure 5.1: a) Side view of the CAD of the soft actuator with infrared-reflective balls for tracking the motion of the tip. Embedded sensors are used to estimate the coordinates of the tip and the forces applied by the actuator when in contact. The plots we present in this chapter describe the position of the marker at the tip relative to the marker at the base. b) Physical actuator with embedded soft sensors. 75
Figure 5.2: Overview of the modeling architecture and its parallel to the human perceptive system. 80
Figure 5.3: a) Schematic of the strain sensors embedded into the 1-DoF actuator and the 2-DoF-serial actuator. All three sensors are intentionally depicted with arbitrary lengths and shapes to highlight that the sensor geometry can be similar, but does not need to be precise. b) Schematic of the strain sensors embedded into the 2-DoF-parallel actuators. The three sensors have different sizes and positioning within the actuator to highlight that the sensor geometry can also vary dramatically. Note that the effective length of the sensors depends on the length of the center cut. 82
Figure 5.4: Schematic of sensor fabrication process. We embedded conductive silicone within non-conductive silicone and cut out arbitrarily shaped sensors. . . . 83

Figure 5.5: Schematic of the motion of the 2-DoF actuators. a) 2-DoF-parallel actuator, with two chambers in parallel along the axial length (left and right). Inflation of either chamber results in non-planar motion, as compared to the 1-DoF actuator. b) 2-DoF-serial actuator, with two chambers in series along the axial length (top and bottom). Inflation of either chamber results in planar motion. In both types of actuator, the two chambers are controlled with independent inputs. c) 2-DoF-parallel actuator with indicators for the left and right chambers. d) 2-DoF-serial actuator with indicators for the top and bottom chambers. 85
Figure 5.6: Schematic of the experimental setup. 87
Figure 5.7: Diagram showing how contact along the continuum of the actuator results in a deformation that propagates throughout the system. 88
Figure 5.8: Diagram of how we obtain the force measurement at the tip of the actuator using a load cell. 89
Figure 5.9: a) Difference in workspace, demonstrating how the sensor significantly affects the finger dynamics b) Drift effect prominent in the soft cPDMS sensor. The readings are shown for a cyclic activation of the actuator. . . . 90
Figure 5.10: Real-time performance. 92
Figure 5.12: a) Error plot for tracking with the soft cPDMS sensor b) Error plot for tracking with the commercial flex sensor. 92
Figure 5.11: a) Predicted motion of the tip of the finger with the cPDMS sensors. The case of applying contact around the center of the finger is shown. The tip was still free to move after the constraint was applied but the kinematics changed. b) Predicted motion of the tip of the finger with the cPDMS sensors. The case of applying contact around at the tip of the finger is shown. c) Predicted motion of the tip of the finger with the flex sensor. Both cases of contact— one at the tip, and the other near the center of the finger— are shown. The first constraint was at the tip and the second constraint was near the center of the finger. 93
Figure 5.13: a) Response of one among the three cPDMS sensor embedded in the soft finger to tip contact. The tip contact blocks the finger stopped it from moving in the positive X-axis direction b) Corresponding response of the flex sensor to tip contact 94
Figure 5.14: a) Scatter plot matrix of the cPDMS sensor during a contact experiment with the diagonals showing histogram of resistance values and off-diagonals showing the scatter plots of two sensors for each discrete time period. Linearly uncorrelated information is observed from the three cPDMS sensors during the contact tasks. Note that if there are no contacts all the three sensors will be linearly correlated. b) Scatter plot matrix showing linearly correlated information from the three flex sensors during the contact tasks. 94
Figure 5.15: Force prediction at the finger tip. The raw load cell readings are filtered with a simple moving average filter with a one second window. External hand contact without the load cell is also shown. 96

Figure 5.16: Test accuracy with virtual sensor removal. The performance is affected only a little when one of the sensor information is lost for the 'no contact' case. The accuracy is significantly affected even with one sensor removal for the 'with contact' case. 97
Figure 5.17: a) Division of labor among the sensors. For the case without contact, all the sensors have equal contribution to the underlying model. Hence, removing any one of them affects the prediction error slightly but equally in the workspace. For this case, removing the pressure information drastically reduces the accuracy, showing how motor action information is also important for accurate proprioception. b) Division of labor among the sensors once in contact. Here we can see clear division of labor among the sensors as there are no redundant sensors. Each sensor is 'specialized' to a particular kinematic case as can be seen from the error distribution in the workspace. Also, once in contact, the action inputs are not useful for proprioception. . 98
Figure 5.18: a) The performance of the learned model on the training data with and without pressure information b) The prediction errors on the test set deteriorate for the model without pressure information. 99

Figure 6.1: Envisioned behavior synchronization process for soft robotic actuators. 1,2) Initial user designs and manufactures a soft robotic actuator using her own materials and fabrication processes. 3) Initial user characterizes material properties and collects training data for her design. 4,5) The initial user uploads her material properties and trained model to a cloud network. 6,7) In other locations around the world, additional users receive identical digital copies of the initial user's design and fabricate their own copies. 8) The additional users download the material properties and trained model, which enables them to train their own model that remotely synchronizes the performance of their actuator to that of the initial user's. Subsequent data is fed back to the cloud for federated (collaborative) learning. 9) Users all around the world now have personalized controllers for performing identical tasks, despite variations in their individual materials, 3D printers, and manufacturing methods. 105

Figure 7.1: Concept figure for rapidly-manufacturable soft sensor skins that can detect and interpret physical contact for human-robot interaction. The soft sensors can classify various types of affective touches (e.g. pokes and rubs) on substrates with different stiffnesses including soft actuators, balloon animals, and stuffed animals. The sensors can provide collaborative, interactive robots and objects with a natural sense of touch and enable them to detect actions such as a pat on the back or head. 109

Figure 7.2: Designs of the various soft sensor arrays and the corresponding physical, soft sensors. a, b) Computer-aided design drawings for the 2x2 and 1x1 sensors. c, d) The sensors consist of microfluidic channels filled with liquid metal that are embedded within silicone rubber. e) Changes in the geometry of these sensors—which users can induce via contact, strain, or pressure—result in a change of the resistance. The changes in the resistance within a sensor array enable classification of different types of affective touch. 111
Figure 7.3: Information flow of the data acquisition circuit for a single sensor. a) Individual traces in the sensor array. b) Signal conditioning for the sensors, including a constant current source of 6 mA and amplifier with gain of 50 V/V. c) Data acquisition and serial communication. d) Machine learning for interpreting the signal measurements. e) User interaction and classification of affective touches. 113
Figure 7.4: Heuristics for the sensor readings of pokes and rubs. Each of the Q_n represents touch at one of the four quadrants. These signals serve as general expectations for what defines a poke vs. a rub. Actual signals for individual users may differ, hence the use of LSTM to learn additional features in the time-series data. 116
Figure 7.5: Visualization of the 10 types of touches that we classified. The circles correspond to pokes at the correpsonding location. The arrows represent the path and the direction of the rub. 117

Figure 8.1: E-skins that can sense their shape in 3D. Recent advances in shape-sensing e-skins use several sensing modalities. (A and B) Accelerometers and/or magnetometers on rigid PCBs can rotate relative to each other and reconstruct their shape at discrete points. (A) “3D capture sheet” [32]. (B) Hexagonal PCBs with integrated accelerometers [33]. (C and D) Continuously flexible devices can sense deformation throughout their surface and estimate their resulting shape. Data-driven methods were then used in these examples to estimate the continuous shape of the e-skin. (C) Fiber Bragg gratings in silicone [34]. (D) Plastic optical fibers in silicone foam [35]. 127

Figure 8.2: Closed-loop tasks where tactile sensing is essential. These tasks primarily differ depending on the system that determines the objective (denoted by the shaded boxes). The middle row consists of biological demonstrations of the tasks. The bottom row contains examples (69, 128, 129) of these capabilities in current rigid robots, which we expect to further improve in parallel with the integration of e-skins, soft robotics, and machine learning. Note that the presented division is not strict, and real-world tasks often involve a combination of all three elementary tasks. Yellow arrows indicate energy flow; blue arrows indicate information flow. (A) Manipulation involves altering the state of an external object to a desired set point using internal actuators. (B) Exploration involves motion of the body to account for uncertainties in the environment based on somatosensory feedback. (C) Reaction involves estimating and responding to environmental cues such that the body remains in a desired state. 132

Figure 9.1: Tactile sensing and proprioception will enable soft robots to operate effectively in numerous challenging domains. **(A)** Multimodal sensing would be useful during manipulation, for detecting gripper states, object properties, and events such as contact and slip. **(B)** E-skins with an integrated human-robot interface could enable seamless assistive wearable robots and intuitive teleoperation of anthropomorphic robots. **(C)** When paired with the appropriate actuators, shape sensing would enable closed-loop changes of shape. **(D)** Closed-loop control algorithms would enable soft robots equipped with e-skins to succeed when performing complex tasks, including in-arm manipulation. 135

LIST OF TABLES

Table 5.1: Training performance of the kinematic model. 91

VITA

2009-2013	B. S. in Electrical and Computer Engineering, Carnegie Mellon University
2013	M. S. in Electrical and Computer Engineering, Carnegie Mellon University
2015-2020	Ph. D. in Engineering Sciences (Mechanical Engineering), University of California San Diego

PUBLICATIONS

B. Shih, D. S. Shah, J. Li, T. G. Thuruthel, Y.-L. Park, F. Iida, Z. Bao, R. Kramer-Bottiglio, M. T. Tolley, "Electronic skins and machine learning for intelligent soft robots", **Science Robotics**, 5:41, eaaz9239, April 2020.

B. Shih, C. Christianson, K. Gillespie, S. Lee, J. Mayeda, Z. Huo, and M. T. Tolley, "Design considerations for 3D printed, soft, multimaterial resistive sensors for soft robotics," **Frontiers in Robotics and AI**, 6, 30, Apr 2019. **Special issue article in Current Advances in Soft Robotics: Best Papers from RoboSoft 2018.**

T. G. Thuruthel*, **B. Shih***, C. Laschi, and M. T. Tolley, "Soft robot perception using embedded soft sensors and recurrent neural networks,", **Science Robotics**, 4:26, eaav1488, Jan 2019. **Special issue article in Robot learning-Beyond imitation.** *equal contribution.

B. Shih, E. Lathrop, I. Adibnazari, R. Martin, Y.-L. Park, M. T. Tolley, "Classification of components of affective touch using rapidly manufacturable, soft, sensor skins", 2020 IEEE-RAS International Conference on Soft Robotics (**ROSO20**), pp. 182-187, Apr 2020.

B. Shih, J. Mayeda, Z. Huo, C. Christianson, and M. T. Tolley, "3D printed resistive soft sensors," in 2018 IEEE-RAS International Conference on Soft Robotics (**ROSO18**), pp. 152-157, Apr 2018.

B. Shih, D. Drotman, C. Christianson, Z. Huo, R. White, H. I. Christensen, and M. T. Tolley, "Custom soft robotic gripper sensor skins for haptic object visualization," in 2017 IEEE/RSJ International Conference on Intelligent Robots and Systems (**IROS17**), pp. 494-501, Sept 2017.

S. Jadhav, M. R. A. Majit, **B. Shih**, J. Schulze, and M. T. Tolley, "Variable stiffness actuator using fiber jamming for applications in soft robotics and wearable haptics", **Soft Robotics**, Nov 2020, in press.

M. Ishida, D. Drotman, **B. Shih**, M. Hermes, M. Luhar, and M. T. Tolley, "Morphing structure for changing hydrodynamic characteristics of a soft robot walking underwater," **IEEE Robotics and Automation Letters**, 4, 4, 4163-4169, Aug 2019 & presentation at 2019 IEEE/RSJ International Conference on Intelligent Robots and Systems (**IROS19**), Nov 2019.

Y.-S. Kim, J. Lu, **B. Shih**, A. Gharibans, Z. Zou, K. Matsuno, R. Aguilera, Y. Han, A. Meek, J. Xiao, M. T. Tolley, and T. P. Coleman, "Scalable manufacturing of solderable and stretchable physiologic sensing systems," **Advanced Materials**, vol. 29, no. 39, Jul 2017.

T. Kalisky, Y. Wang, **B. Shih**, D. Drotman, S. Jadhav, E. Aronoff-Spencer, and M. T. Tolley, "Differential pressure control of 3D printed soft fluidic actuators," in 2017 IEEE/RSJ International Conference on Intelligent Robots and Systems (**IROS17**), pp. 6207-6213, Sept 2017.

J. M. Florez, **B. Shih**, Y. Bai, and J. K. Paik, "Soft pneumatic actuators for legged locomotion," in 2014 IEEE International Conference on Robotics and Biomimetics (ROBIO14), pp. 27-34, Dec 2014.

ABSTRACT OF THE DISSERTATION

Informative Touch for Intelligent Soft Robots

by

Benjamin Shih

Doctor of Philosophy in Engineering Sciences (Mechanical Engineering)

University of California San Diego, 2020

Professor Michael T. Tolley, Chair

As robots grow increasingly prevalent in real-world environments, sensory systems capable of sensing complex deformations and environmental interactions are needed for robust control. Soft robotics has emerged as a field of study that seeks to replace rigid components in traditional robots with materials that are compliant. It has garnered interest for real-world applications due to intrinsic safety embedded at the material level, deformable materials capable of shape and behavioral changes, and conformable physical contact for manipulation. Yet, with the introduction of soft and stretchable materials to robotic systems comes a myriad of challenges for sensor integration, including multi-modal sensing capable of stretching, embedment of high-resolution but large-area sensor arrays, and sensor fusion with an increasing volume of data. This

dissertation describes the design, fabrication, and data processing of soft, tactile sensor skins, with the ultimate goal of enhancing future collaborative robots that will work alongside and physically interact with people with a human-like sense of touch.

This thesis focuses on how the integration of soft sensor skins and machine learning enables soft robots to perceive physical interaction for complex haptic tasks. Part 1 on Soft Sensors (Chapters 2, 3, and 4) presents the design and fabrication of various types of soft strain sensors, using compliant materials such as silicones and polymers. Fabrication methods include soft lithography and 3D printing. Performance of the sensors are characterized and modeled. Part 2 on Soft Robot Perception (Chapters 5 and 6) describes how machine learning can be used to augment the performance of soft sensors and actuators. The method demonstrates how recurrent neural networks can be used for graceful degradation and learned perception of external contacts and forces despite not having a priori information about the individual sensors. Part 3 on Social Touch for Physical Human-Robot Interaction (Chapters 7 and 8) analyzes the use of the liquid metal sensors as robotic skins for the classification of affective (social) touch and builds towards the development of a framework for representing physical contact, for use at the human-robot interaction layer of abstraction.

In recent years, the concept of soft-bodied robots has rapidly grown in popularity. Researchers have developed many interesting forms of actuation that more closely mimic the functionality and capabilities found in nature. The next step for the field is to develop biologically-inspired tactile sensing for soft-bodied robots that can safely interact with and explore their environments. In the short term, the field can focus on deployable, high-resolution sensor skins, algorithms for processing the dense sensor information, and reliable feedback control for soft robots. Building upon the fundamental work presented in this dissertation, the future consists of robots that can touch and feel with the sensitivity and perception of natural systems.

Chapter 1

Introduction

Summary This thesis focuses on how the integration of soft sensor skins and machine learning enables soft robots to perceive physical interaction for complex haptic tasks.

Skin plays an essential role for biological systems as a barrier between an organism's external environment and its internal components. Embedded within its layers is a dense network of mechanical, chemical, vibrational, temperature, and pain receptors, which work in coordination to enable somatosensation in skin. These capabilities would also be incredibly useful for robots. Electronic skin (e-skin) research was originally motivated, in part, by a desire to understand biological sensing, but the lessons learned can help improve the design of robotic systems. To sense, plan, and act, robots require a variety of sensors embedded throughout their bodies so that they can obtain information about their environment.

1.0.1 Soft robotics

The field of soft robotics [36] studies the use of flexible and compliant materials as components for building robots, instead of traditionally rigid components such as metals. Soft robots often draw inspiration from nature, which has evolved organisms that can operate in unstructured environments. In contrast, current robotic systems are usually confined to structured laboratories

or warehouse environments. In addition, natural environments typically contain several objects of varying material properties that further complicate tasks such as object interaction and locomotion.

The overlap between e-skins, soft robotics, and machine learning is continually growing, and recent advances are summarized in Fig. 1.1. Soft actuation has improved tremendously in capabilities (Fig. 1.1 bottom), and soft sensors and e-skins exhibit a wide range of complexities (Fig. 1.1 left).

Several recent advances have combined principles from each field, often physically manifesting in the form of sensorized fingers and grippers (Fig. 1.1 top). Future breakthroughs in the field may come from further integration of sensors and actuators as roboticists move toward designing systems that rival the abilities of biological organisms.

Several reviews have covered related topics on e-skins and perception in soft robots, including design and fabrication of e-skins [37, 38], wearable sensors [39], e-skins for interactive robots [40, 41], and future directions in sensing and perception for soft robots [42, 43]. This chapter examines recent developments in skin-based sensing for soft robots, covering hardware and fabrication techniques and machine learning techniques that translate robot perception into action planning. In the scope of this thesis, we consider a soft robot skin to be skin sensors directly mounted on the surface [e.g., [44]] or embedded in a thin layer beneath the surface of the body of a soft robot [e.g., [15]]. To highlight the opportunities at the intersection of e-skin and soft robotics research, we cover a variety of interdisciplinary topics including fabrication, learning, and control.

Compared with rigid robots, the high mechanical compliance of soft robots enables safer and more efficient human-robot interaction (HRI) because they can seamlessly interact with the human body [45]. Further advancement of soft robots requires high-performance electronics and sensors that can stretch continuously with their bodies. Recent research in artificial skin has mainly focused on making individual sensor devices with better performance, such as sensitivity, stretchability, and reliability over many use cycles (Fig. 1.2). To realize fully biomimetic skin for

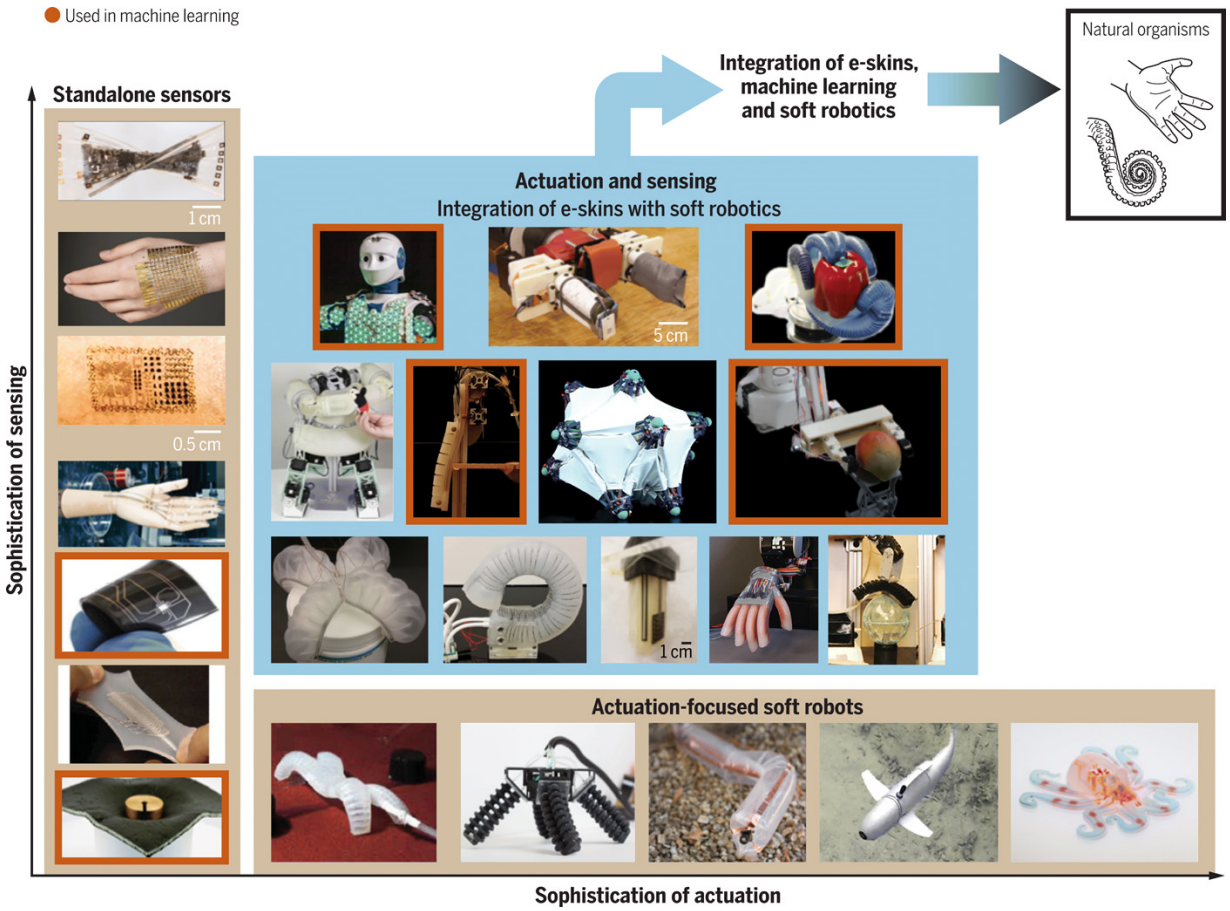


Figure 1.1: Trends in the intersections between e-skins, soft robotics, and machine learning. (Left) A range of e-skins and soft sensors that increase in complexity, from bottom to top, by metrics including density, resolution, and fabrication [1–7]. (Middle) Soft robots and e-skins that merge actuation and sensing [8–20], from left to right and top to bottom. (Bottom) Soft robots that focused primarily on actuation [21–25], from left to right. Red boxes indicate work that has leveraged machine learning in the processing of their sensor information.

soft robotics, artificial skin should contain sensor arrays that are stretchable, cover large areas with a high spatiotemporal resolution, and have multiple functions that mimic diverse receptors of the human skin (Fig. 1.2A). These features should enable robots to use data-driven methods to extract rich information about their environment.

1.0.2 Design and fabrication of integrated e-skins

Increasing sensor density and quantity normally requires a larger number of interconnecting wires. To reduce this burden, sensor arrays are normally designed in matrix form. For example, a recently developed tactile glove comprising 548 force sensors was constructed using readily available materials and simple fabrication tools (Fig. 1.2B) [26]. This sensor array recorded a large-scale dataset of tactile maps (about 135,000 frames), which was used to identify objects using convolutional neural networks. This work highlights the ability of large-scale datasets collected by a high-density sensor array to enable not only a sense of touch but also the intelligent extraction of information from touch. Increasing the sensor density simply by scaling down a passive matrix architecture will reduce the amplitude of analog signals while increasing cross-talk between interconnects. If multiple sensors are sampled simultaneously, each line will produce electromagnetic noise, which will corrupt the signals being carried on neigh- boring conductive traces. Furthermore, the large number of addressing lines will be difficult to manage as the number of sensors increases substantially. These problems can be addressed with an active matrix that pairs each sensor with a transistor to provide local signal amplification and allows sensors to take turns transmitting information [46–49].

Active matrices with multiplexed signal transduction typically consume less power than passive matrices because they require fewer sampling lines and do not need external circuitry [50]. However, stretchable e-skins could allow better coverage of curved robot surfaces while allowing sensing of complex texture information through detection of deformation and vibration, mimicking biological skin. Recent advancements in organic electronics by Wang et al. [51]

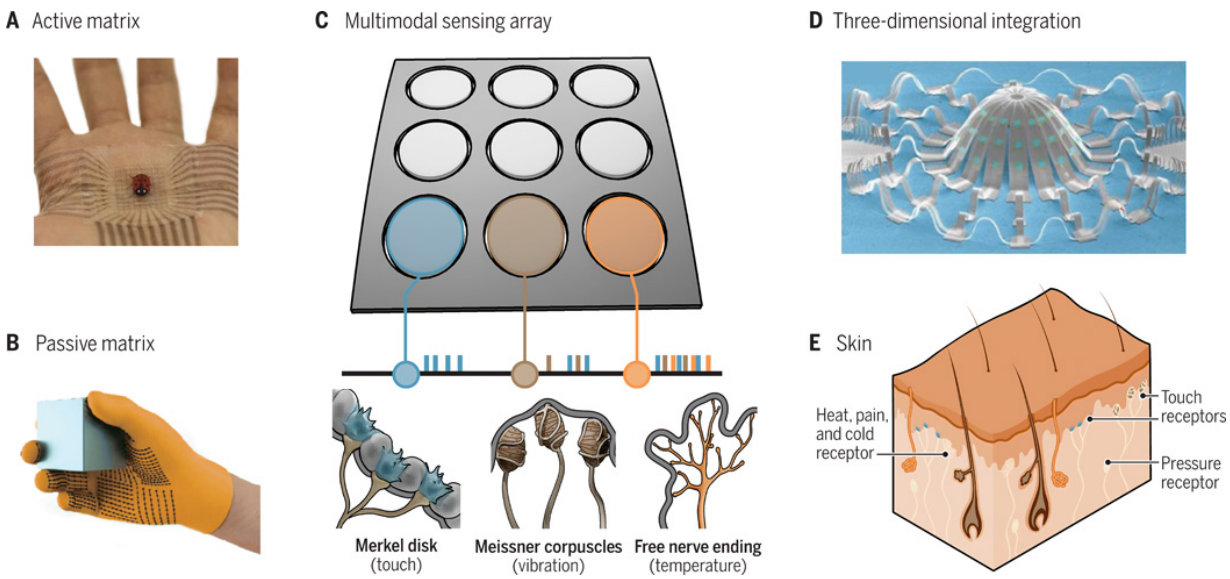


Figure 1.2: Sensor arrays enable e-skins to extract information about their environment. (A) Human skin with various receptors used to sense stimuli. (B) A scalable tactile glove containing a passive matrix of 548 force sensors for the collection of large datasets [26]. (C) 2D sensor array used to generate a profile of pressure intensity from experimental mapping of the pixel signals using an active matrix [27]. The icons at the bottom represent biological analogies: Merkel disks, Meissner corpuscle, and free nerves. (D) A 3D array of electronic sensors assembled from 2D electronics [28]. (E) Multimodal sensor array that can capture both pressure and temperature information [29].

led to the creation of an intrinsically stretchable transistor array with 347 transistors per square centimeter. Their proof-of-concept demonstration illustrated that such a conformable active matrix could accurately map the force applied on each sensor. These capabilities indicate that stretchable active matrices containing soft sensors and transistors are a promising step toward soft robotic skin with high resolution and high data fidelity.

Making multilayered sensor arrays in a three-dimensional (3D) lattice can further increase the sensor areal density and allow greater integration of different sensor modalities. Just as receptors in bio- logical skin are embedded at various depths, engineers can embed sensors that are sensitive to different stimuli in different spatial locations. For example, pressure, shear, and strain sensors can be distributed in different layers of the e-skin to achieve optimized sensitivity. Huang et al. [7] demonstrated that stretchable electronics integrated in 3D can be built with a

layer-by-layer method using transfer printing of predesigned stretchable circuits on elastomers with vertical interconnects. This stretchable human-machine interface had a four-layer design that offered multimodal sensing and had integrated circuits for wireless data transfer. Using strain engineering methods, 2D structures can also be assembled into 3D electronic systems with sensing capabilities. Semiconductor materials can play critical roles in this context, through demonstrations of complex, mechanically assembled 3D systems for light-imaging capabilities that can encompass measurements of the direction, intensity, and angular divergence properties of incident light.

3D printing has also been used to directly print sensors in soft robots to improve both exteroceptive and interoceptive capabilities [52]. This work highlights how a 3D integration framework enables a higher integration density on stretchable substrates than single-layer approaches and allows new functionalities that would be difficult to implement with conventional layer-by-layer designs.

Processing complex tactile information from a sensor array requires efficient signaling and sampling methods. In human skin, stimulation of the receptors is converted into a series of voltage pulses sent to the nerves. This inspired researchers to develop artificial receptors and afferent nerves to convert tactile information to digital pulses at the site of sensation [4, 53]. The signal could potentially be perceived by a user's nerves and brain, thus directly linking the human brain with soft robotic prosthetics. For example, Kim et al. recently developed a flexible artificial afferent nerve that can effectively collect pressure information from arrays of pressure sensors and convert them to action potentials to activate muscles [54].

Biological skin contains receptor networks that can detect various stimuli, such as vibration, humidity, and temperature. Several studies on e-skin sensor arrays focused on the classification of a single type of information, such as force, shape, or direction of motion. The next generation of e-skins should integrate multimodal sensor arrays to capture richer sensory information than their predecessors. Recently, Lee et al. reported a neuromimetic architecture that

enabled simultaneous transmission of both tactile and thermotactile information (Fig. 1.2E) [29]. The pressure- and temperature-sensitive transducers can both be communicated through the pulse signatures by a single electrical conductor. As a biomimetic signaling method, this approach is promising for reducing wiring and computational requirements when a robot is covered with thousands of sensors. Multimodal sensing could also be achieved through integration of multiple stretchable optical fibers, which has been shown to be effective at localizing and estimating force in soft actuators [55].

Overall, many innovations are required for realizing high-density and multifunctional sensor arrays for soft robots. A close collaboration between roboticists and materials scientists is needed to develop high-performance stretchable conductors for electrodes and inter- connections and stretchable semiconductors for building active matrices and signal amplifiers. Different sensing modalities and integration architectures should also be explored. Lastly, hardware and algorithms for data processing should be considered during the design of sensory systems, and their performance should be evaluated on a holistic range of practical robotic tasks.

1.0.3 Skin-based sensing for soft robots

As sensors are increasingly integrated into soft robots, we can imagine a conceptual plane that categorizes research based on the sophistication of actuation and sensing independently (Fig. 1.1). Stand-alone sensors lie on the y axis; some consist of simpler strain sensors [the bottom three images in Fig. 1.1 left [1–3]], whereas others have more sophisticated sensing schemes, including distributed or multimodal sensing [the top four images in Fig. 1.1 left [4–7]]. The x axis, representing actuation-focused soft robots, shows examples of increasingly complex soft systems that can walk [21, 22], grow [23], swim [24], and operate autonomously on chemical fuel [25] (Fig. 1.1 bottom). Last, many recent works have begun exploring the intersection of the actuation and sensing (Fig. 1.1 middle). Several of them embedded strain sensors for state estimation or tactile sensing in a finger-like structure [8–17], whereas the others mounted their

skins externally [18–20]. As both areas progress, we envision further integration of increasingly sophisticated actuation and sensing, extending into the top-right quadrant of the conceptual plane.

Access to higher-resolution data about touch will increase the ability of soft robots to perceive the complex deformations that they experience during tasks, including locomotion and manipulation. Today's discrete sensors, which are built with high sensitivity and selectivity, can be tailored to sense deformation modes in a localized region or known environment with high confidence [19, 56]. However, this sensing paradigm is insufficient in dynamic or unknown environments where robots will experience substantial deformation because robots do not yet have the level of sophistication of human skin receptors or the human brain to collect a broad range of information. In addition, many robots are unable to process the volume of information to accurately determine the environment or the object being sensed. The transition from discrete to continuous sensing and the shift from structured to unconstrained environments both require e-skins that can rapidly collect and process large amounts of information. The added complexity from both transitions compounds the processing required to interpret the signals.

Several designs of skin-like sensors have been used in soft robotics. Many of these sensors contain conductive and stretchable materials to produce resistive or capacitive strain sensors [1, 15, 57, 58]. Other groups have used optical devices such as cameras and optical fibers to sense deformations within an actuator [35, 59, 60]. Several of these existing sensors are well suited for measuring characteristics such as strain, pressure, and bending but do not enable the high sensor densities or resolutions that have been demonstrated in e-skins. Soft robots would benefit from integration with e-skins, such as the skin-like sensor arrays that have been deployed in medical applications or directly on skin [5, 53, 61–63].

Currently, soft skin-like sensors have been deployed in several ways. Some groups used their sensors as wearables; Mengüc et al. used liquid metal sensors to measure human gaits [64] using a sensor fabrication process first presented by Park et al. [2]. The resistance of these sensors increases as the embedded microchannels inside the elastomer matrix are stretched because of the

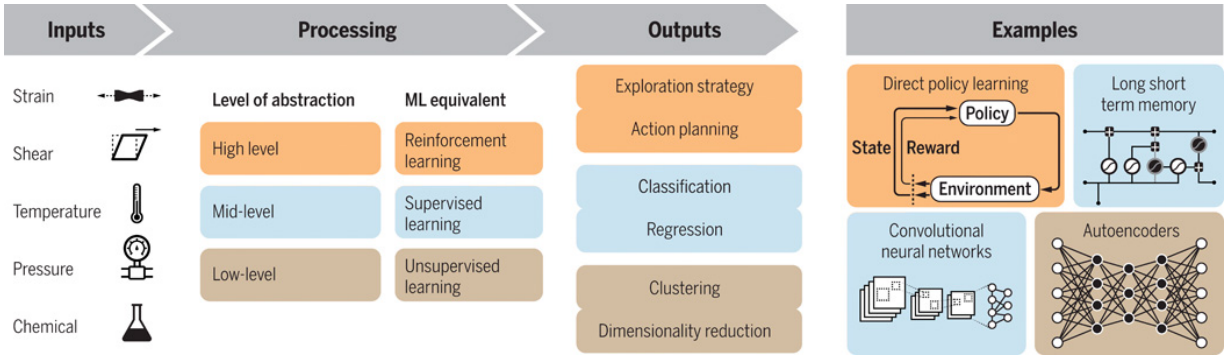


Figure 1.3: Machine learning techniques for processing raw sensory information, different levels of abstraction to aid in robot perception, and action planning. The level of abstraction depends on the task, and the most effective type of learning architecture depends on the quality and structure of the sensor signals. The level of abstraction depends on the task, and the most effective type of learning architecture depends on the quality and structure of the sensor signals. Higher-level processes can include parallel execution of lower-level processes. End-to-end architectures [e.g., [30]] without mid-level and low-level pipelines would likely be faster and more effective but are computationally expensive to develop.

increased length and decreased area of their bulk liquid-metal channels. Others incorporated their sensors with robots: Boutry et al. paired a shear force sensor with a robot arm to allow robotic hand control [65]. Booth et al. demonstrated reconfigurable, actuatable e-skins that could control the motion of deformable inanimate objects from their surface [20]. Zhao et al. embedded optical sensors within soft pneumatic fingers, which they then integrated with a Baxter robot [16]. As skin-based sensing capabilities continue to improve, the goal is to develop capabilities that match or outperform biological systems (top right corner of Fig. 1.1).

1.0.4 Machine learning for soft e-skins

As e-skins increase in resolution, their signals could be processed to detect higher-order deformation modes and higher-level notions about the environment, such as material type. However, obtaining this information requires algorithms that can extract useful information from large quantities of data. To handle the vast amount of data that e-skins can provide, machine learning is emerging as a versatile tool for making sense of large quantities of data (Fig. 1.3).

For example, Piacenza et al. obtained high-resolution data from a robotic fingertip and used ridge regression to process this data to estimate the locations of indentations [66]. Similarly, Larson et al. used convolutional neural networks to learn deformations on a sensor array that can interpret human touch in soft interfaces [67]. At the level of abstraction of the entire robotic system, Van Meerbeek et al. tested various learning algorithms to estimate the twist and bend angles in sensorized foam, finding that k-nearest neighbors (kNN) outperformed other common algorithms, including support vector machines (SVM) and multilayer perceptrons [35]. In addition, researchers have also focused on recurrent neural networks, which have been shown to be advantageous for learning patterns in time series data [8, 11, 68, 69].

Because of the complexity of the mapping between raw sensory information and relevant functional abstractions, information theory and machine learning will play a large role in bringing tactile sensing to human-like performance levels. In particular, the subfield of reinforcement learning (RL) will be important for developing closed-loop control for tactile feedback. Suitable algorithms and architectures for analogous tasks in soft robotics can be developed by learning from biological processes. For example, in computer vision and machine learning, the hierarchical nature of visual processing (corresponding to compositional functions) [70] has recently enabled deep neural networks to achieve human-like performance across a variety of visual processing tasks [71]. Processing signals from arrays of tactile sensors may benefit from similar techniques, as sets of sensor readings have information encoded in spatial relationships that can be naturally represented using matrices.

Tactile exploration can benefit from recent developments in learning-based simultaneous localization and mapping algorithms. Notably, Mirowski et al. used an asynchronous advantage actor-critic algorithm for navigating in a complex environment and additionally solved auxiliary prediction tasks that made the RL problem faster and more data efficient [72]. Chen et al. showed a direct policy learning algorithm with spatial memory and bootstrapped with human-mediated imitation learning without explicit task rewards [73]. In the absence of continuous reward

functions, actor-critic algorithms are preferred because they require fewer samples.

Similarly, tactile manipulation tasks can use insights from learning- based manipulation controllers. A general trend observed in such works is the success of model-based RL [74] or learning by demonstration [75], approaches that leverage techniques from control theory or human knowledge, respectively. There has been a successful solution for the direct learning of control policies for dexterous manipulation, but it relied on the availability of an accurate simulation environment [76]. Until robot simulators can model soft-body dynamics that reliably transfer to real robot hardware, such approaches are difficult to apply to soft robots and deformable objects. For specific simple tasks, it might be easier to find a direct policy than to fit a general-purpose model of the system dynamics [77].

Chapter 2

Custom soft robotic gripper sensor skins for haptic object visualization

Tactile sensing is an important capability for robots that assist or interact with humans or fragile objects in uncertain environments. An ongoing challenge for soft robots has been incorporating sensors that can recognize complex motions. We present sensor skins that enable haptic object visualization when integrated on a soft robotic gripper that can twist an object. First, we investigate how the design of the actuator modules impact bend angle and motion. Each soft finger is molded using a silicone elastomer, and consists of three pneumatic chambers which can be inflated independently to achieve a range of complex motions. Three fingers are combined to form a soft robotic gripper. Then, we manufacture and attach modular, flexible sensory skins on each finger to measure deformation and contact. These sensor measurements are used in conjunction with an analytical model to construct 2D and 3D tactile object models. Our results are a step towards soft robot grippers capable of a complex range of motions and proprioception, which will help future robots better understand the environments with which they interact, and have the potential to increase physical safety in human-robot interaction.

Robots are becoming increasingly prevalent in our society in forms where they are

assisting or interacting with humans in a variety of environments, and thus they must have the ability to sense and detect objects by touch. An ongoing challenge for soft robots has been incorporating flexible sensors that can recognize complex motions and close the loop for tactile sensing. We present sensor skins that enable haptic object visualization when integrated on a soft robotic gripper that can twist an object. First, we investigate how the design of the actuator modules impact bend angle and motion. Each soft finger is molded using a silicone elastomer, and consists of three pneumatic chambers which can be inflated independently to achieve a range of complex motions. Three fingers are combined to form a soft robotic gripper. Then, we manufacture and attach modular, flexible sensory skins on each finger to measure deformation and contact. These sensor measurements are used in conjunction with an analytical model to construct 2D and 3D tactile object models. Our results are a step towards soft robot grippers capable of a complex range of motions and proprioception, which will help future robots better understand the environments with which they interact, and has the potential to increase physical safety in human-robot interaction. Please see the accompanying video for additional details.

In the absence of visual information, humans can readily identify unknown objects through touch alone. However, the same task is a major challenge for typical robotic systems, although it would be useful in many situations including industrial automation, and human-robot interaction. In particular, rigid grippers require special care and dexterity to manipulate delicate objects, especially unknown ones, without damage. By contrast, robotic grippers that are soft, composed of compliant materials like silicone elastomers, are suitable candidates for tactile interaction with fragile objects or even humans. Furthermore, adding sensing to these soft robotic grippers can enable new capabilities such as haptic identification and modeling.

The human ability to rotate an object in-hand is an important capability, and key for haptic object recognition. As more robots enter and co-exist in a world where objects are designed for humans, in-hand manipulation becomes an increasingly important ability for robots to mimic. However, to our knowledge, this capability has not yet been replicated in a soft robot gripper with

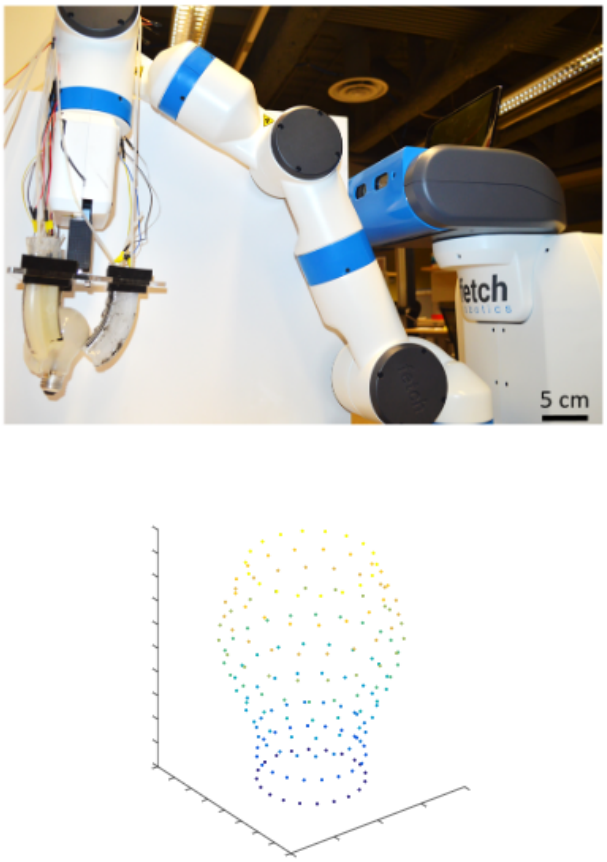


Figure 2.1: Our proposed soft pneumatic gripper with internal sensing attached to a robot arm. a) Using the soft gripper and robot arm to pick up a light bulb. b) Light bulb that we used to generate the visualization. c) 3D haptic object visualization generated by our gripper, with our data plotted in a 2D view. We estimated where the gripper contacted the object via sensor reading and each color represents a different height.

integrated sensing.

We developed soft robotic fingers that can sense their deflections during actuation, sense fingertip contact, and build 3D outline models of unknown objects. We improve upon existing approaches by synthesizing hardware and software components and creating soft, twisting fingers with internal sensing to estimate unknown object outlines using touch. Finally, we put our soft gripper onto a commercial robot arm (Fetch, Fetch Robotics Inc.) to demonstrate its capability to build 3D tactile object models.

In this chapter, we present:

- An approach for designing, fabricating, and using flexible, modular skins with custom geometries and sensor layouts for proprioception and exteroception.
- Sensorized soft pneumatic fingers capable of twisting. When multiple fingers are combined into a gripper, we can rotate objects in-hand when they are fixed along a central axis.
- A method for using haptic information obtained from these soft pneumatic fingers to collect point clouds for objects.

By altering the fundamental assumption that a robot consists of a kinematic chain of rigid links, we sacrifice characteristics such as precisely predictable dynamics and strength in exchange for compliance and the ability to handle fragile objects from a materials standpoint. Recent review papers [36, 78–80] have discussed how robot designers can replace traditionally rigid robot components with compliant materials. Doing so improves locomotion in rough terrain [22] and enables safe physical contact in human-robot interaction [81]. These new design principles have the potential to unlock a technological change in the way we design robots.

Unlike rigid grippers, soft manipulators are capable of conforming to objects of different shapes and sizes, typically with minimal changes in hardware and software. Zhao et al. developed a robot gripper with soft fingers using waveguide sensors that can pick up both hard and soft objects and feel their textures [16]. Homberg et al. clustered sensor readings in their gripper to identify correspondences to finger configurations, and used this information to classify unknown objects [82]. Deimel and Brock created a soft hand made primarily from silicone [83]. On a mm scale, Suzumori et al. developed flexible microactuators capable of a twisting action to loosen and tighten small screws [84].

Current soft grippers rely primarily on external sensing to estimate location in space. In contrast, biological fingers rely on a combination of internal and external sensing, such as using both vision and touch for localization and object recognition [85]. Many different types of sensors are available for detecting contact [86]. Multiple groups have created actuators that can sense,

grasp, and touch using liquid metal strain sensors [13, 14]. Using a similar manufacturing process, Muth et al. embedded conductive material using 3D printers to deposit traces within highly stretchable elastomers [58]. Kim et al. 3D printed pockets of air that sensed contact through deviations in pressure [87].

Fingers with tactile-based internal sensing can be used to identify unknown objects through touch. Okamura et al. [88] analyzed how rigid robotic fingers with soft, force-sensing fingertips can be used to explore unknown objects via dexterous manipulation. An example of soft haptics is Sonar and Paik's pneumatic haptic feedback device where they embedded sensitive piezoceramic sensors into thin silicone layers [89]. In addition, research using rigid grippers has also studied methods for classifying objects from touch [90–92], while other work has studied how to combine tactile sensing with in-hand manipulation [93] and define types of in-hand manipulation [94].

2.1 Design

2.1.1 Actuator module design

Soft pneumatic actuators operate by applying air pressure inside of a sealed chamber, resulting in motion. Typically, some asymmetry in the structure, material, or actuation of these chambers directs the motion. We present a simple actuator module composed of three sealed chambers oriented longitudinally, with independent control of the pressure in each chamber, modeled on a previous design by Suzumori et al. [84] and other three chamber designs [22, 95]. Each chamber expands radially and longitudinally when inflated and the outer edge of the chamber lengthens. The central portion of the actuator acts as a constraint on the chamber, and thus the longitudinal motion of the chamber results in bending (Fig. 2.2). We can achieve a wide range of positions by inflating combinations of the three chambers – the workspace resulting from inflation of multiple chambers is a set of nested hemispheres. Inflating multiple chambers simultaneously

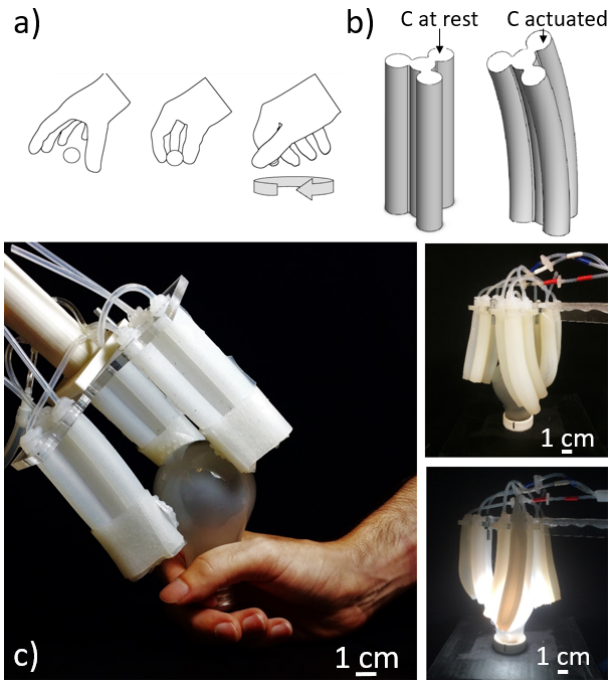


Figure 2.2: Dexterous soft gripper capable of safely handling delicate objects under uncertainty. a) Side view of human hand grasping and twisting a round object, which inspired our design for in-hand manipulation. b) Visual model of actuator in resting state (left), and when chamber C is inflated (right). c) Soft gripper handling, manipulating, and rotating a light bulb.

enables a twisting motion.

2.1.2 Sensor design

We next augmented our actuator modules with sensing capabilities. Previously, sensors have been directly adhered to or embedded within the actuator modules [13, 14, 16]. However, users or designers may want to change the arrangement of sensors on the skin for customizability and adaptability [96]. In addition, the lifetime of the sensors often differs greatly from the lifetime of the actuators because the actuators tend to form hernias over time. Other groups have addressed this challenge by reinforcing with fibers [83] or fabricating with foam [97]. Our approach was to design a modular, reusable sensor skin that would be customizable and scalable to arbitrary surfaces.

For the sensor skins described in this chapter, we placed one stretch sensor longitudinally along the outside of each of the pneumatic chambers of the actuator to measure bending and one strain sensor in the space between two chambers at the fingertip to detect contact.

2.1.3 Gripper design

The gripper is composed of three soft actuator modules mounted to a laser cut acrylic frame. The three actuator modules are situated so that they are radially symmetric around a central axis represented by the palm of the gripper. By executing the proper sequence of pneumatic actuation, the gripper can manipulate a variety of objects (Fig. 2.3).

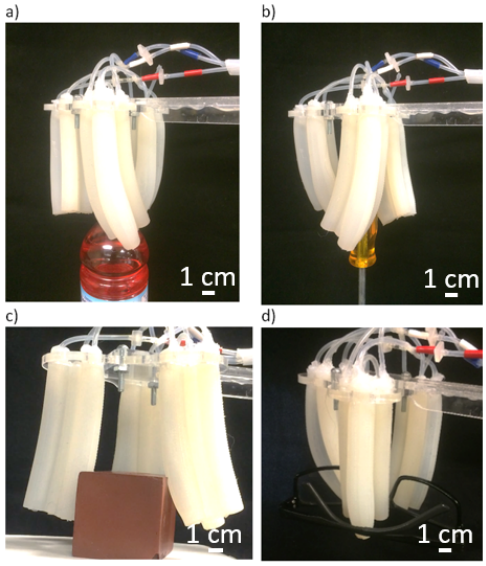


Figure 2.3: Our proposed soft gripper design is capable of performing a range of complex manipulation tasks, including: a) unscrewing a bottle cap, b) rotating a screw driver, c) opening up its grasp area to manipulate a larger box, and d) grasping complex shapes such as a pair of glasses.

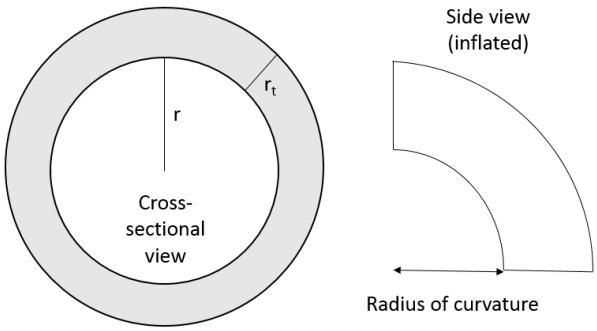


Figure 2.4: Schematic of the 2D analytical model of our actuator. a) Cross-sectional view. b) Side view, where the actuator is inflated, bent, and at equilibrium.

2.2 Analytical model

2.2.1 2D actuator model

Our 2D model uses a force balance between expansion and elastic compression forces at steady state, as described by Farrow et al. [14]. In this model, we assume that: 1) when a single chamber inflates, only the outer edge of the chamber extends; 2) the actuator deforms

uniformly and thus maintains constant curvature; 3) the actuator is radially symmetric (Fig. 2.4); 4) pressure on the end caps is a negligible fringe effect; 5) radial expansion is negligible compared to longitudinal expansion; and 6) the actuator is hanging vertically.

Our model studies the actuator curvature in 2D only because we only need to know the in-plane bending of the actuator for haptic modeling. Previous work has explored modeling three-chambered actuators in 3D [84], but for chambers with different geometry and scale. Translating these models to 3D for our actuators lies outside the scope of this chapter.

The expansion force can be computed as:

$$\begin{aligned} F_{expand} &= \int_0^{2\pi} \int_r^{r+r_t} P r dr d\theta \\ &= P\pi(2rr_t + r_t^2) \end{aligned} \tag{2.1}$$

where r is the radius of the internal chamber, r_t is the thickness of the actuator walls, and P is the internal pressure of the chamber.

Using Hooke's Law for elastic materials, we computed the compression force as:

$$\begin{aligned} F_{contract} &= k\Delta x \rightarrow \frac{EA_0}{L_0}\Delta L \\ &= \int \frac{E}{L}\Delta L(r,\theta) dA \end{aligned} \tag{2.2}$$

where E is the Young's modulus of the material of the actuator, A_0 is the initial cross-sectional area, L_0 is the initial length of the actuator, and ΔL is the extension of the actuator which can be described here as a function of r and θ.

From the side-view geometry, $\Delta L(r,\theta)$ can be written as $2r\frac{L}{C}$. These forces are balanced at equilibrium and thus by substituting and setting $F_{expand} = F_{contract}$, we can solve for both the curvature κ and radius of curvature K of the actuator:

$$\begin{aligned} \kappa &= \frac{4E(3rr_t + 3r^2 + r_t^2)}{3P(2r + r_t)} \\ K &= \frac{1}{\kappa} \\ &= \frac{3P(2r + r_t)}{4E(3rr_t + 3r^2 + r_t^2)} \end{aligned} \tag{2.3}$$

Taking mass effect into account:

$$\begin{aligned} F_{mass} &= \int g\rho\, A\Delta h \cos\theta d\theta = mg\sin\theta \\ F_{mass} + F_{contract} &= F_{expand} \end{aligned} \tag{2.4}$$

From the above equation, the relationship for bend angle vs. pressure is:

$$P = \frac{2E}{L}(r + r_t)\theta + mgsin\theta \tag{2.5}$$

2.2.2 Sensor model

We modeled the strain of the sensor by analyzing the relationship between the resistance and the extended length of the sensor. In this model, we assume that: 1) the sensor experiences no deformations other than lengthwise extension from length l to $l + \Delta l$; 2) negligible fringe and edge effects of the sensor; and 3) the conductive material inside the sensor is incompressible and thus maintains a constant volume.

We start with the general formula for resistance, $R = \frac{\rho l}{A}$. Since the sensor has constant volume, we can calculate the cross sectional area after stretching as:

$$A_{stretched} = \frac{l}{l + \Delta l} A \tag{2.6}$$

Plugging the stretched length into the general resistance equation, we obtain:

$$R = \frac{2\rho}{A}\left(\frac{\Delta l^2}{l} + 2\Delta l + l\right) \tag{2.7}$$

The factor 2 in front of ρ is due to the parallel construction of two identical sensors. Thus, we obtained a second order polynomial relationship between resistance and the change in length.

2.3 Fabrication

2.3.1 Fabrication of actuator module

We fabricated the actuators using a five step procedure: 1) filled the mold with silicone (Fig. 2.5a), 2) inserted the inner chamber rods (Fig. 2.5b), 3) left the actuator to cure (Fig. 2.5c), 4) removed the actuator from the mold (Fig. 2.5d), and 5) sealed the actuator openings with tubing and silicone epoxy (Fig. 2.5e).

Using a photopolymer resin (Veroclear, Stratasys Objet350 Connex3), we 3D printed actuator molds which consisted of five pieces that encapsulate and shape the silicone during the curing process. We found that the use of translucent molds made with a high precision 3D printer significantly improved fabrication yields as compared to the use of opaque molds printed on desktop fused deposition modeling printers, as it allowed us to easily resolve molding problems like leaks or bubbles. The silicone was a commercial, two-part elastomer compound (Dragon Skin 20, Smooth-On Inc.).

2.3.2 Fabrication of sensor skin

We made sensors with conductive-polydimethylsiloxane (cPDMS) traces (Fig. 2.6). First, we dispersed multiwall carbon nanotubes (MWCNT) (30-50 nm diameter, Cheap Tubes, Inc.)

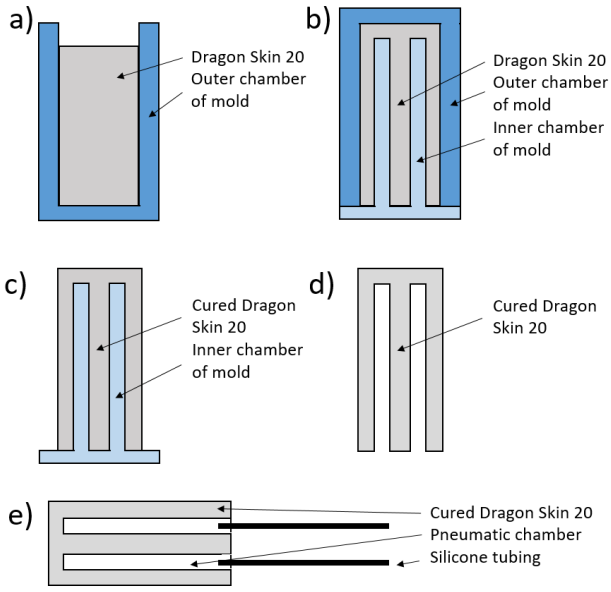


Figure 2.5: Schematic of our soft actuator module fabrication process, based on retractable-pin casting [31] – side view, with only two chambers shown. Steps: a) Fill outer chamber of the mold with silicone. b) Insert inner chamber of the mold into the silicone and outer chamber of the mold. c) After the silicone cures, remove the outer chamber of the mold. d) Next, remove the inner chamber of the mold, leaving behind chambers in the silicone. e) Insert tubing and seal the pneumatic chambers.

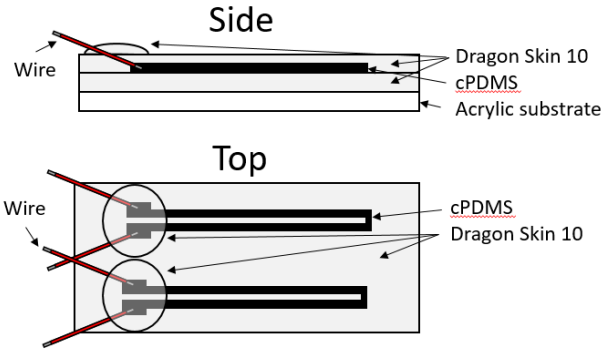


Figure 2.6: Schematic of sensor fabrication process. A conductive silicone is embedded within thin layers of non-conductive silicone. We control the thickness of the layers via spin coating and the trace patterns are made via masking.

in toluene by mixing with a stir bar for two hours. We then added PDMS base (Sylgard 184, 3M) to achieve 12% MWCNT loading by weight, which is expected to result in a conductivity of approximately 6 S/m [98]. We continued to stir the cPDMS overnight at 90 ^{o}C to allow the remaining toluene to evaporate. We then spin-coated a thin (approximately 0.05 mm thick) layer of silicone elastomer (Dragon Skin 10, Smooth-On Inc) onto a rigid substrate to form the lower layer of the sensing skin. We used Dragon Skin 10 as it has a lower shore value than the actuator material, reducing the effect of the sensors on the overall stiffness of the actuator modules. We patterned a mask for the trace using silicone adhesive transfer tape via a digital laser machining system. Then, we removed one of the carrier layers of the tape, exposing one side of the adhesive, and affixed the adhesive to the layer of silicone elastomer. We next used a doctor blade to apply cPDMS to the mask, resulting in a trace thickness of approximately 100 μm. We then removed the second carrier layer, applied wire leads to the conductive traces, and encapsulated the traces with a final layer of silicone elastomer.

2.3.3 Assembly of finger module

We formed our soft fingers by wrapping each actuator with a sensor skin (Fig. 2.7). We assume that there is no slipping between the skin and fingers due to the high coefficient of friction between the silicone elastomers. Each finger on the gripper has three degrees of freedom, which enable both bending and twisting. Three strain sensors in total are located on each of the outer inflating chambers. This positioning allows measurement of the actuator's bend in each direction. In addition, the fingertip strain sensor detects contact. The fingers are controlled using an open source fluidic control board [99]. We explore the advantages of a system that has both of these properties by conducting tactile object modeling experiments on various shapes to compare the visualization results (Section 4.3-B, 4.3-C).

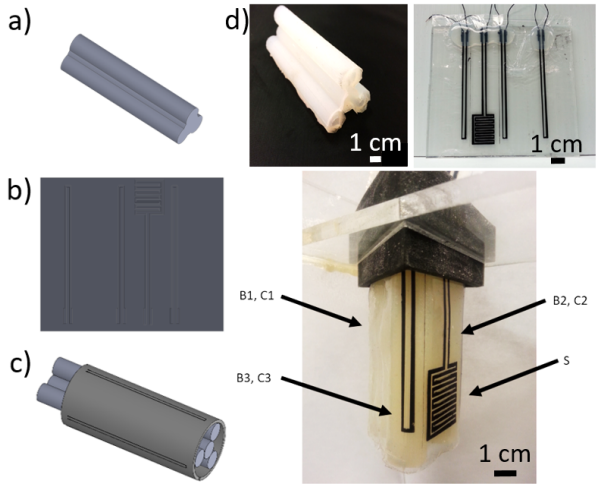


Figure 2.7: Schematic and manufacturing process for the finger modules. a) Mold the actuator modules from silicone elastomer. b) Sensor skins are fabricated as flat sheets with trace patterns that match the geometry of the actuator. c) The skins are rolled up, sealed, and worn as modular sleeves on the actuator. d) Cured silicone actuator module after it has been removed from the mold. e) Flexible, silicone strain sensors which form a skin around the actuator module. f) Completed finger that integrates both actuator and sensor skin, where C_i are the pneumatic chambers, B_i are the flexible sensors that measure the actuator bend, and S is the strain sensor that measures contact at the fingertip.

2.4 Results

2.4.1 Experimental validation

In order to explore the design space of actuator chamber sizes and the resulting pressures required for actuation, we tested two actuator designs with inner diameters of 5.08 mm (0.2 in) and 6.35 mm (0.25 in). We validated our model by comparing our bend angle measurements as a function of pressure (Fig. 2.8) and measured the bend angles by recording the angle of the end effector with respect to the horizon [22]. By observation from equation 2.5, the magnitude of mg is negligible compared to the magnitude of $\frac{2E}{L}(r+r_t)$. Thus, using a linear fit is reasonable for data analysis. The slope of θ vs. P in $\frac{degree}{psi}$ is:

$$\frac{L}{2E(r+r_t)} = 2.7579 \tag{2.8}$$

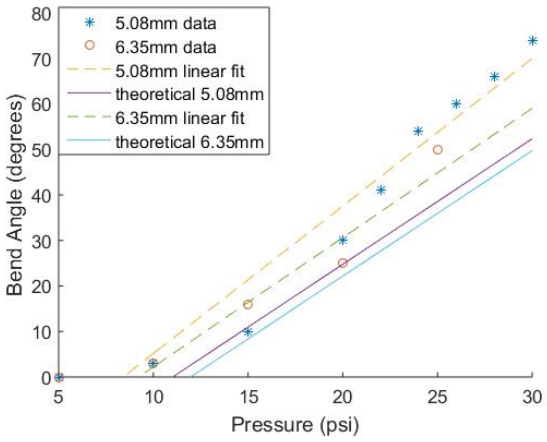


Figure 2.8: Plot comparing analytical actuator model, experimental data, and linear fit for the bend angle of the finger modules. Solid lines show the linear model prediction. Dashed lines show the best-fit line to the data. Individual points represent the experimental data. The theoretical model is approximately accurate for pressures at which we actuate our fingers. We assume an input range of 10 psi and above because below that threshold, the pressure does not overcome the elastic restoring forces of the material and thus no inflation occurs.

Using the linear fit generated from experimental data, the slope is 3.2386 $\frac{degree}{psi}$ for the 5.08 mm chamber size, and 2.8406 $\frac{degree}{psi}$ for the 6.35 mm chamber size.

To validate our sensor model, we measured the resistance vs. change in length relationship for multiple sensors (Fig. 2.9). From equation 2.7, we know that the ideal behavior of R vs. Δl should be a second order polynomial. However, since the stretched length of the sensor is very small, the second order term Δl^2 has a small effect and thus the first order term Δl dominates. The predicted slope, which is calculated by $\frac{4\rho}{A}$, is 1958 $\frac{ohm}{m}$. From the linear fit of the data, the slope is 2038 $\frac{ohm}{m}$. Since the values are similar, we can conclude that a linear model for the sensor is reasonable.

We demonstrated our sensor skin for our specific soft robotic gripper, but this skin approach could be usable for other grippers as well. Several factors can result in differences

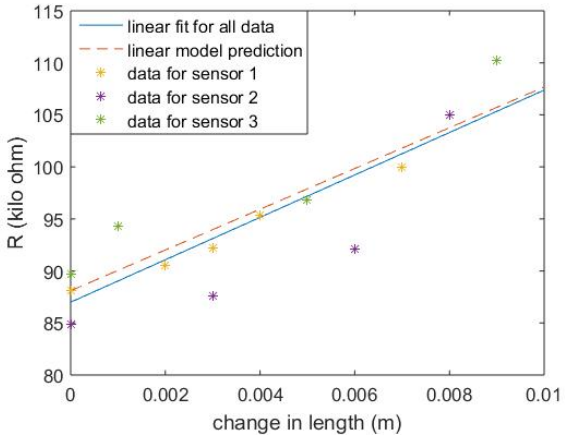


Figure 2.9: Plot comparing analytical sensor model, experimental data, and linear fit for the change in resistance of the sensors. Solid lines show the linear model prediction. Dashed lines show the best-fit line for the data. Individual points represent the experimental data.

between our theoretical and experimental results. The major factor is from the uncertainty of the Young's modulus of the actuators. The actual Young's modulus should be lower than the theoretical one because of the other hollow chambers in the actuator. Since the volume fraction of the hollow chamber is approximately 20% to 30% of the total volume of the actuator, the larger slope of the θ vs. P fit is reasonable. In addition, some inhomogeneities may be introduced during the manufacturing process and to the abrupt material strain as the finger begins inflating. Nevertheless, the finger modules and sensors provided measurements sufficient for haptic modeling.

2.4.2 2D tactile object modeling

The ability to predict the pose of our actuator enables us to visualize an object's shape by obtaining its 2D outline. To assist with detecting contact on the fingertip, we incorporated a strain sensor pattern on the skin that fits in between chambers C2 and C3 (Fig. 2.7). This sensor stretches only when the fingertip comes into contact with an object, giving us a signal to identify touch. In addition, the fingertip helped our fingers recognize sharp corners that could fit in between chambers C2 and C3 and would not otherwise be detectable.

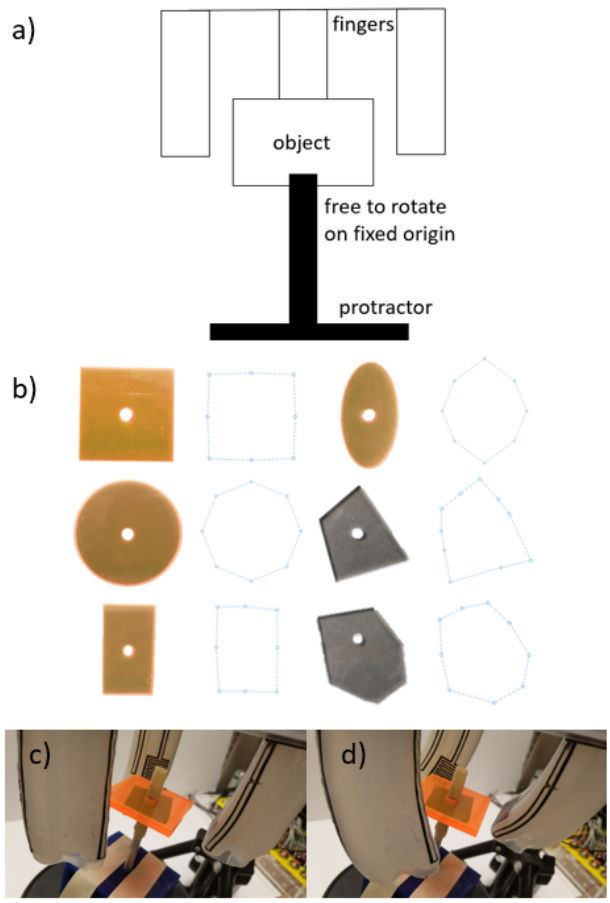


Figure 2.10: Setup used for 2D tactile object modeling. a) Side view schematic of how the fingers and object are positioned. We use a protractor as a ground truth for the angle of rotation. b) Our soft gripper is able to model various convex shapes, including square, circle, rectangle, oval, and convex shapes. For each shape, the left is the 2D acrylic piece we used in the modeling experiment and the right is the resulting visualization. We connected the contact points with dotted, straight lines for visualization purposes. c) Gripper in resting position. d) Gripper rotating the object. Protractor not shown.

We then used the resistance value of the one corresponding bend sensor (B1 in Fig. 2.7) and the sensor model to determine the position of the tip of the finger. We also manually recorded the angle of rotation that the object has moved via visual ground truth. Finally, we plotted these (r, θ) points to generate the 2D tactile object model. We summarized this process in the inner while loop of Algorithm 1.

For the 2D demonstration, we constrained the objects in these visualizations to a fixed central axis and selected points of contact relative to a ground truth to visualize both edges and corners (Fig. 2.10).

2.4.3 3D tactile object modeling

3D visualizations can be generated from multiple 2D outlines by varying the z-axis positioning at which the gripper comes into contact with the objects. We summarized the 3D twisting and measuring procedure in Algorithm 1 and demonstrated this algorithm by attaching our soft gripper to a robot arm (Fig. 2.1a). The pneumatics and wires are connected to an open source fluidic control board [99]. Fig. 2.1b shows a resulting visualization where we fixed the light bulb to a stationary axis of rotation.

Algorithm 1 3D Tactile Object Modeling

while *height of object has not been traversed* **do**

  while *object has not been fully rotated* **do**

    Actuate the fingers until each fingertip pressure sensor comes into contact with the object.

    Measure the strain sensor value of a single fingertip.

    Compute and record the displacement distance and corresponding ground truth angle at which we obtain the measurement.

    Rotate the object by twisting with all of the actuators.

  end

  Increment the position of the gripper along the object's z-axis.

end

Model the object outline by plotting each 2D layer with its corresponding z-axis height.

Our results from the 2D and 3D haptic object visualization are a first step towards using haptics to map and learn about objects by touch. The capabilities of our current gripper demonstrate that soft fingers with custom sensor skins are a feasible approach. The object models generated by the gripper produce outlines that visually resemble the original shapes. We could potentially use these results for classifying shapes [100]. However, some limitations include being able to recognize the slope of the surface, nonlinear interpolation between contact points, and convex objects. We require additional improvements and quantification to perform tasks like in-hand manipulation or understand the friction and contact properties of unfamiliar objects.

2.5 Conclusion and future work

This chapter presents soft sensor skins integrated with a soft pneumatic gripper. The gripper uses tactile sensing and twist objects to obtain a three dimensional tactile feedback-based model of an object. These fingers can deal with unknown, delicate objects without damaging them,

as demonstrated by their ability to visualize a light bulb (Fig. 2.1). Internal sensing addresses the forward kinematics problem in soft robotics of not precisely knowing where the end effectors are. The experiments in this chapter demonstrated the grippers's ability to model objects through touch.

Future work could include augmenting our gripper's capability to understand unknown objects. Our model is limited by the size of the fingers of the gripper because the geometry of the fingers fundamentally limits the resolution of the resulting visualization. We have left a full model and characterization of the 3D workspace of each finger and twisting capabilities of the gripper to future work. In addition, more intelligent, in-hand manipulation algorithms that enable our gripper to maintain its grasp on an object throughout manipulation would eliminate the need for a fixed axis of rotation. For these more advanced manipulations, we could integrate additional fingers and multiple sensor readings in varying contact sequences, rather than simply using a single sensor to detect contact for visualization. We could potentially account for some slipping in the grasping, which can result in a different number of data points despite similar cross-section sizes in an object. We also plan to quantify and experiment with a broader set of objects. One current limitation to full autonomy and in-hand manipulation is our need for a ground truth measurement to identify how much the gripper has rotated the object, which could be addressed using an external camera. We could also enhance our tactile object modeling with higher-resolution sensors on the fingertips to improve our knowledge of sloped surfaces and gather rich tactile-based datasets for grasping. Lastly, communication between the microprocessor controlling our soft gripper and the Robot Operating System (ROS) on-board the robot arm is necessary for a fully autonomous system.

Chapter 2, in full, is a reprint of the material as it appears in **B. Shih**, D. Drotman, C. Christianson, Z. Huo, R. White, H. I. Christensen, and M. T. Tolley, "Custom soft robotic gripper sensor skins for haptic object visualization," in 2017 IEEE/RSJ International Conference on

Intelligent Robots and Systems (**IROS17**), pp. 494-501, Sept 2017. The dissertation author was the primary investigator and author of this paper.

Chapter 3

Design considerations for 3D printed, soft, multimaterial resistive sensors for soft robotics

Sensor design for soft robots is a challenging problem because of the wide range of design parameters (e.g. geometry, material, actuation type, etc.) critical to their function. While conventional rigid sensors work effectively for soft robotics in specific situations, sensors that are directly integrated into the bodies of soft robots could help improve both their exteroceptive and interoceptive capabilities. To address this challenge, we designed sensors that can be co-fabricated with soft robot bodies using commercial 3D printers, without additional modification. We describe an approach to the design and fabrication of compliant, resistive soft sensors using a Connex3 Objet350 multimaterial printer and investigated an analytical comparison to sensors of similar geometries. The sensors consist of layers of commercial photopolymers with varying conductivities. We characterized the conductivity of TangoPlus, TangoBlackPlus, VeroClear, and Support705 materials under various conditions and demonstrate applications in which we can take advantage of these embedded sensors.

3D printing has enabled many new design and fabrication approaches for robotics [101]. In parallel, a new perspective on the role that materials play in robotic design has altered the building blocks and tools with which we create our robotic systems. The ability to print soft and rigid materials simultaneously using a single machine has expanded the realm of possibilities for fabricating robots, including systems that are biomimetic [102–104] and ones that have improved resistance to impact through functional gradients [105].

In the long term, one goal of 3D printing is the ability to print an entire robot in one go and have it walk itself out of the machine upon completion [106]. Recent work has demonstrated this "get up and walk away" concept. Felton et. al. describe a method for building self-folding machines using laminate structures that fold themselves up in multiple stages and can walk away after receiving electronics and a battery [107]. Similar in overall concept, MacCurdy et. al. used a multimaterial 3D printer to print fluid-filled bellows directly integrated into the transmission of their locomotive robot, which can also walk immediately after attaching a motor and battery without additional mechanical modifications [108]. However, neither of these robots possess sensing capabilities for feedback control and learning. In addition, robots that can get up and walk away entirely on their own require a built-in, on-board energy source. The previous robots have batteries added after printing, whereas robots like the EcoBots have a stomach for real digestion that enables them to sustain themselves [109].

Soft robotics is one field that has benefited significantly from 3D printing [36]. Robot designers can print both the molds for making soft robots [110] as well as the soft robots directly [105]. However, a major challenge with soft robots is the development of effective sensors. Soft robots are not constrained to prismatic or revolute motions, and obtaining sensory feedback on these motions requires different types of sensors than those used for rigid robots. In addition, soft robots may require sensors that can be placed on complex surface geometries or embedded within the body.

Much of the soft robot development today has focused on actuation [111–114]. Sensor

design for soft robots is complicated because flexible, compliant robots often have non-planar, complex surfaces that are difficult to cover and sensorize with traditional manufacturing techniques. Proper selection from among the wide range of design parameters (e.g. geometry, material, actuation type, etc.) is critical to the function of soft robots. Conventional rigid sensors can be effective for soft robots with constrained motions [16, 115, 116]. However, the general case of a soft robot with a high number of degrees of freedom requires capabilities such as out-of-plane twisting. Sensors that are directly integrated into the bodies of soft robots and co-fabricated could help improve both their exteroception and interoception capabilities. We want to move towards highly integrated structural and sensing components as we see in biological human bodies, which may not be possible with discrete, rigid sensors.

Recently, interest in 3D printing soft robots has grown significantly. Previously, research groups have printed various actuators [22, 117] and bodies [105, 108, 118] for soft manipulation and locomotion. Alongside the development of soft robot actuators, many groups have become interested in incorporating sensors and closing the control loop for feedback on the robot's interactions with its environment. Felt et. al. designed an inductance-based sensing system to measure and control bellowed continuum joints, by wrapping coils of wires and measuring changes in inductance [119]. We [15] and others [13, 14], have embedded soft sensors for measuring bending into the layers of pneumatic fingers, which enabled the fingers to estimate the shapes of various objects using tactile sensing [13–16]. Homberg et. al. clustered sensor readings from their fingers to identify correspondences to gripper configurations and to classify grasped objects [82], Kim et. al. 3D printed pneumatic pouches and connected them to pressure sensors to sense when the pouches came into contact with external objects [87], and Pearson et. al. demonstrated tactile sensing in both compliant, 3D structures and soft, 3D printed actuators [120].

Many groups have also begun experimenting with various fabrication techniques for soft sensors, particularly in the form of skin-like structures [121–124]. Muth et. al. customized a printer for sensor fabrication which embeds conductive material into a partially-cured silicone

elastomer substrate that then fully cures and solidifies [58]. Frutiger et. al. and White et. al have also 3D printed conductive materials for sensors [125, 126]. Inspired by mechanoreceptors found within skin, Lipomi et. al. and Tee et. al. developed skin-like sensors that can detect strain and pressure [4, 127], and Yin et. al. fabricated a robotic skin that senses shear force [128]. Multiple groups have explored using deep learning to understand deformations and changes in a soft robot using embedded, soft sensors [8, 11, 129]. However, the integration of these skins into real-world robot systems for sensing remains an open problem [130]. Having a separate skin also requires the robot designer to affix the sensing elements in a separate manufacturing step, limiting the ability to sensorize the complex, dynamic bodies of soft robots.

In this chapter, we present:

- A method for printing multiple, soft materials simultaneously to produce a resistive sensing element using a commercial 3D printer, which enables users to incorporate arbitrary sensor geometries into their soft robots.
- Design considerations for creating sensors based on 3D printable conductive materials.
- A demonstration for how we can embed soft, complex-shaped sensors into compliant grippers.

A surprising aspect of what we present is that many researchers are thinking about how to make soft robots with embedded liquid metals, whereas commercially available systems today already allow us to directly print general conductive traces. We hypothesize that current commercial systems already allow for the fabrication of soft actuators with embedded sensors. Not only can existing systems already perform the manufacturing, but this approach also enables designs that would otherwise be very challenging for existing fabrication techniques, e.g. multilayer sensor or complex structures within a 3D body. With traditional lithographic approaches, it is not obvious how to fabricate such designs.

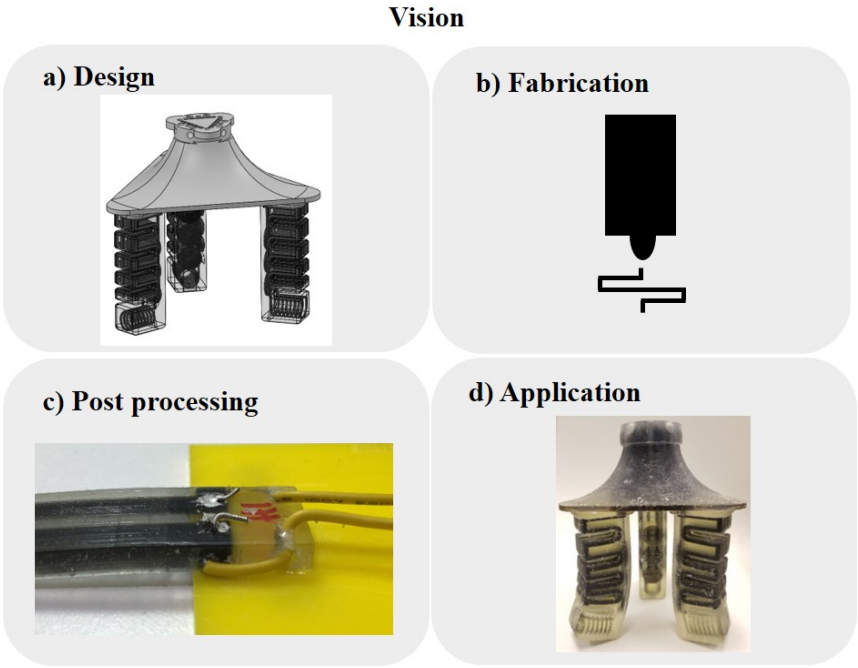


Figure 3.1: Overall vision of the pipeline for our 3D printed sensors. a) Digitized CAD design with embedded, integrated sensing. b) Multimaterial 3D printer that simultaneously co-fabricates both actuators and sensors. c) Post-processing such as removing support material or wire connections. d) Immediately deployable for real-world applications.

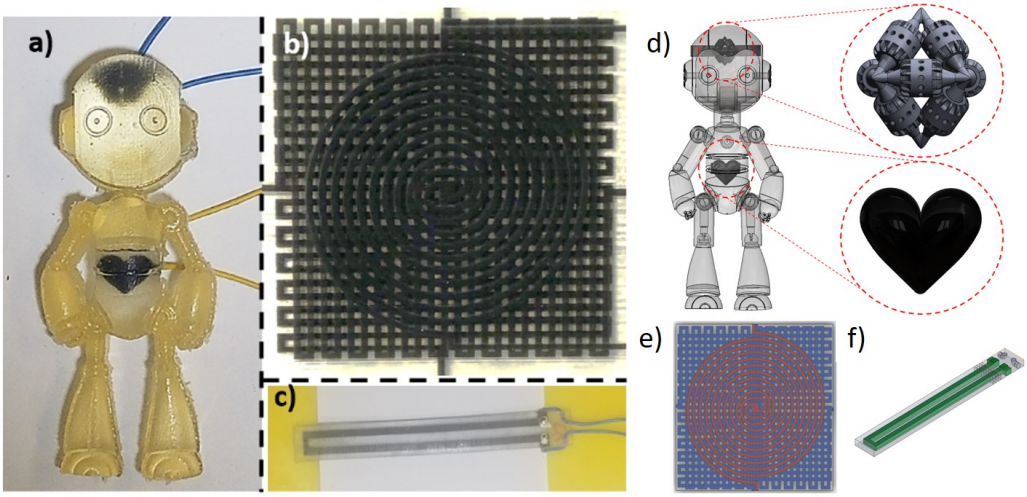


Figure 3.2: 3D printed, resistive, soft sensors and the correspoding CAD drawings. a, d) Humanoid robot - front view. Enlarged drawings of the embedded heart- and brain-shaped sensors. b, e) Multilayer strain and pressure sensor - top view. c, f) Uniaxial strain sensor with mechanical strain relief and functional gradient to improve wire interface - isometric view.

In Section 3.1, we explain the materials and methods that we used for the experiments. In Section 3.2, we present and discuss the results, including the types of sensors that we printed and parameters that contributed to their conductivity, model of the sensitivity to strain, and experimental characterization of the sensors. Lastly, in Section 3.3, we discuss conclusions and future work.

3.1 Materials and methods

3.1.1 Design and fabrication of the resistive sensors

Many challenges exist with the integration of sensors into the body of soft robots. Current techniques are often unable to accommodate the elastic, large deformations of soft robots (i.e. the stretching and bending) that arise in applications such as wearable computing and smart textiles [131].

We can overcome many of these challenges using a commercially available 3D printer

(Stratasys Objet350 Connex3) that has the ability to mix conductive and dielectric materials. Many groups have produced actuatable soft robots with this tool: [22,87,102,103,105,108,117,118,132]. We investigated whether this printer can also directly embed sensors into soft robot systems.

Materials that the printer can produce include a flexible, translucent photopolymer (TangoPlus FLX930); a flexible, black photopolymer (TangoBlackPlus FLX980); a rigid, clear photopolymer (VeroClear RGD810); and a flexible, low-yield polymer (SUP705) as support material. The black resin contains carbon particles [133], which provide a small but measurable conductivity, and can serve as conductive traces for sensors. We created the geometry of the sensors using computer-aided design (CAD) software, fabricated our designs using the 3D printer, and secured the wires using silver paste and mechanical strain reliefs (Fig. 4.2). Fig. 3.2 and Fig. 3.3 show the sensor-only designs and the test samples, respectively, that we characterized in this chapter.

The commercial material has comparable mechanical strain-to-failure properties as skin: it is reported to have 70-120% elongation at break [134]. During our tests (Section 3.2) we observed strain-to-failure of approximately 20%. However, even this reduced value may be sufficient for most applications. For comparison, most types of human skin fail after exceeding 15% strain [135]. The physiological limitation is measured to be at most 45% in areas such as the fully flexed knee or elbow [135, 136]. Thus, even with relatively low strain-to-failure, the commercial material may still be useful in creating bioinspired and biomimetic designs.

3.1.2 Removal of support material

The printer allows the user to choose between surface finishes that are either glossy or matte, where matte is achieved by coating the entire print in support material. We printed the test blocks with matte coatings to maintain a uniform surface finish. The dimensions of the test blocks were 10x10x50 mm, with 10x10x3 mm tabs for the measurement clamps (Fig. 3.3). The process we use to remove the support material occurs in multiple stages (Fig. 3.3). Because the

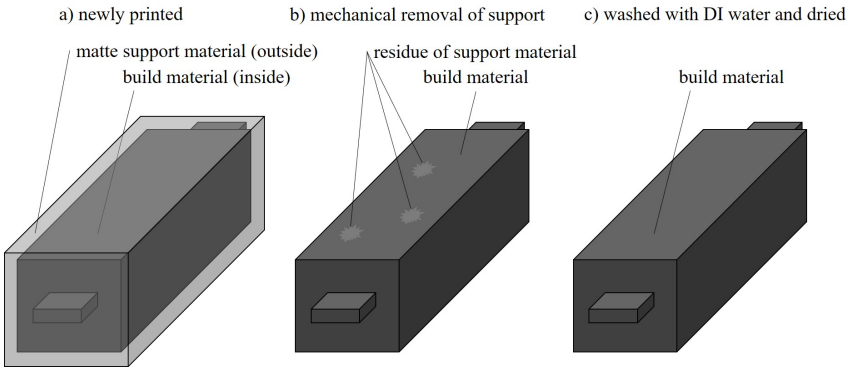


Figure 3.3: Stages of the process for removing the support material. a) Newly printed block of material for characterization, with a matte surface finish. b) Block of material after we mechanically remove the support material. Some patches of support material can remain on the surface. c) Block of material after we wash it with distilled water and dry the sample.

support material appears to contribute to the conductivity (further evaluated in Section 3.2.4), it is important to thoroughly clean the surface of the material or enclose it within a different material. In this process (Fig. 3.3a), a fresh block of material comes off the 3D printer with a matte surface finish and is coated in support material. Fig. 3.3b depicts the block of material after the support is mechanically scraped off the surface of the block by hand. Finally, as shown in Fig. 3.3c, this process ends with the careful cleaning of any remaining support material on the surface of the block, by washing the block with distilled water and drying it.

3.1.3 Mechanical strain relief

As noted in previous work [64, 132], attaching solid-core wires to soft materials can be difficult and result in an unstable connection because the wire can tear the soft material or gradually shift around. Thus, our solution for effective electrical connections is to combine: 1) soft insertion points for mechanically securing the wires, and 2) additional mechanical relief using an extra loop of wire to wrap around, which reduce the tearing of the electrodes when the sensor experiences strain.

For this sensor design, we included soft holes within the rigid material to function as

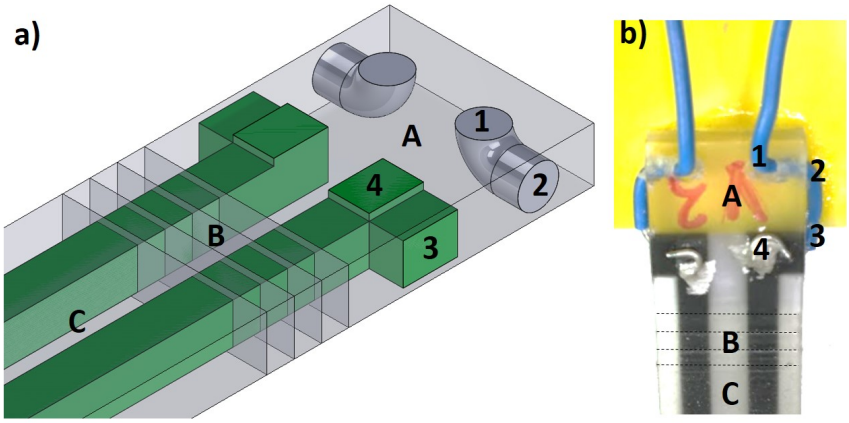


Figure 3.4: Our method for wire attachment. a) Schematic for the wire attachment procedure - isometric view. We insert the wire at 1, and pass through in order of 1-2-3-4 to both distribute strain on the wire and to improve the electrical conductivity between the solid wire and the photopolymer trace. These numbers are only labeled on half of the sensor shown, for clarity. b) Completed, physical version of the wire attachment - top view.

a mounting point. The hole in Fig. 4.4 connecting the points labeled 1 and 2 is filled during the printing process using the dielectric photopolymer (TangoPlus, FLX930), which provides mechanical relief by restricting the motion of the wire. At 3 and 4, we push the bare wire through the black elastomer and coat the wire and photopolymer interface with silver paste to increase electrical conductivity. In Fig. 4.4, A represents a rigid photopolymer (VeroClear RGD810, Stratasys), B represents a functional stiffness gradient (consisting of TangoPlus and VeroClear: FLX9050, FLX9070, and FLX9095, Stratasys), and C represents a flexible photopolymer (TangoPlus FLX930, Stratasys).

3.1.4 Experimental setup for measurement and characterization

We connected the sensors to an inductance, capacitance, and resistance (LCR) meter (Keysight, E4980AL), which provides high precision measurements. We smoothed the sensor readings with an 8 point averaging filter on the LCR meter.

We prescribed the strain using a mechanical testing machine (Instron 5965) (Fig. 3.5a, 4.5, 4.6a). For the multilayer sensor, we tested the pressure by placing a range of standard masses

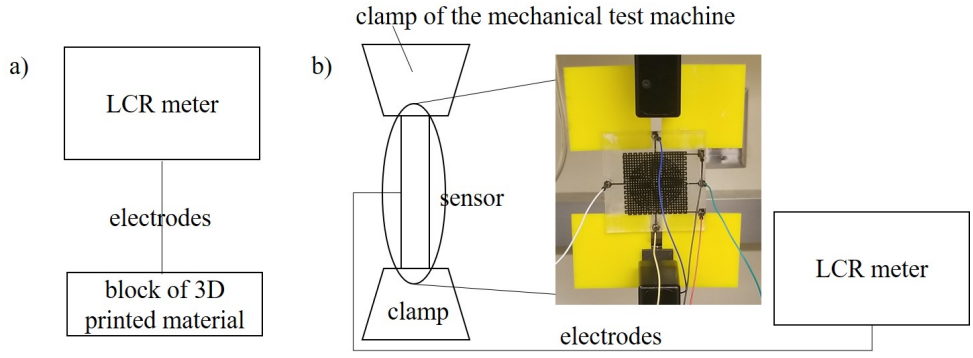


Figure 3.5: a) setup to measure conductivity of blocks. b) setup to simultaneously measure strain and conductivity.

on top of the pressure sensor, which we converted to a pressure using the relationship ($P = \frac{mg}{A}$) (Fig. 4.6b).

3.1.5 Removal of water content by desiccation

Because of the constituent components in the 3D printer material (further explanation in Section 3.2.4), we investigated how much of an impact water content had on mass and conductivity. In the desiccation process, we placed the test blocks in an air-tight, sealed container with packets of silica desiccant (Dry & Dry). Throughout multiple one hour periods, we removed the blocks and reported the conductivity.

3.1.6 Preferential strain response of the multi-dimensional sensor

We looked at the sensitivity of the multi-directional sensor by connecting it to the LCR meter while simultaneously stretching the sensor in the Instron. The parameters of the Instron include a strain rate of 0.0025 mm/mm/s (0.25% strain per second) and an auto-stop at 15% extension. Fig. 3.5b shows the setup for simultaneously stretching the material while measuring the conductivity.

3.1.7 Model of strain response

For elastomer-like materials, the overall length of the channel increases while the cross-sectional area of the channel decreases when the channel of the sensor experiences axial deformation, leading to an increase in the resistance of the channel ([2]). Here, we are ignoring the microscale, bond-level effects ([137]) and assuming the change is dominated by macroscopic geometric change.

Assuming rectangular traces, we can represent the resistance of an undeformed sensor as:

$$R_0 = \frac{\rho L}{wh} \tag{3.1}$$

where R_0 is the resistance in the undeformed state, ρ is the electrical resistivity of the photopolymer, L is the length of the conductive channel, and w and h are the width and height of the cross-section of the conductive material, respectively.

The change in resistance of the stretched material is:

$$\begin{aligned} \Delta R &= R - R_0 \\ &= \rho \frac{L + \Delta L}{(w + \Delta w)(h + \Delta h)} - \rho \frac{L}{wh} \end{aligned} \tag{3.2}$$

where R is the resistance when the sensor stretches by ΔL.

Next, we can replace Δw with $-\nu\varepsilon w$ and Δh with $-\nu\varepsilon h$, and substitute $\varepsilon = \frac{\Delta L}{L}$ to obtain:

$$\frac{\Delta R}{R_0} = \varepsilon \left[\frac{(1+2\nu) - \nu^2\varepsilon}{(1-\nu\varepsilon)^2} \right] \tag{3.3}$$

where ε is the strain and ν is the Poisson's ratio.

The Poisson's ratio for this photopolymer material is approximately $\nu = 0.49$ ([138]), which enables us to further simplify equation 4.3 to:

$$\frac{\Delta R}{R_0} = \frac{\varepsilon(8.25-\varepsilon)}{(2.04-\varepsilon)^2} \tag{3.4}$$

3.1.8 Model of pressure response

We modeled the relationship between the change in resistance and contact pressure using linear elastic fracture mechanics ([139]). Once again, assuming rectangular traces, we can represent the normalized change in resistance as:

$$\frac{\Delta R}{R_0} = \frac{1}{1-2(1-\nu^2)wP/(Eh)} - 1 \tag{3.5}$$

where P is the pressure on the sensor and E is the elastic modulus of the material.

3.2 Results and discussion

3.2.1 Characterization of the dependence of conductivity on orientation of 3D print

Previous work has shown that 3D printers exhibit anisotropic properties depending on the orientation of the print [140]. Thus, we characterized the dependence of the conductivity on the orientation of 3D print. We tested samples of each of the TangoPlus, TangoBlackPlus, and VeroClear materials.

Our results (Fig. 3.6) show that there is a difference in resistance measurements between TangoBlackPlus and TangoPlus in the x-axis and z-axis directions of the 3D print. However, in the y-axis direction, the conductivity changes minimally between the two materials. In all three directions of the coordinate frame, there is a substantial difference between the readings for the

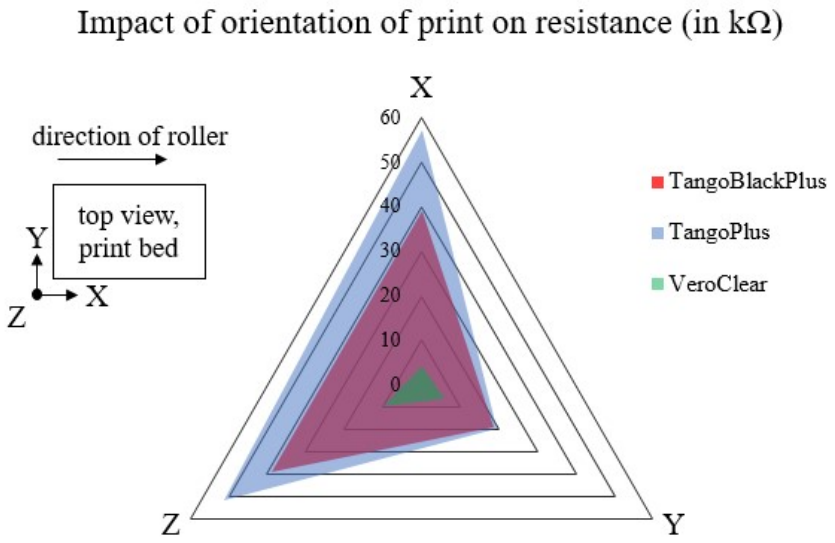


Figure 3.6: Plot of the impact of anisotropy on the 3D printed material. Number of samples n = 10.

VeroClear and for the other materials.

This phenomenon may be due to the spacing of the print heads. The commercial 3D printer moves along the x-axis of the bed and sputters droplets of uncured ink onto the print bed. The printer cures each layer of ink with a UV light before incrementing the positioning of the z-axis and moving to the subsequent layer. In addition, the roller component of the 3D printer, which smooths each layer of ink, also acts along the x-axis. This asymmetry in the plot could be due to increased overlapping of the ink in the x direction relative to the y direction. For the remainder of the experiments, we consider only the conductivity of the in-plane x-direction.

3.2.2 Characterization of the dependence of conductivity on removal of support material

To characterize the dependence of conductivity on the amount of support material coating the surface of the blocks of material, we measured the resistance of the materials at various points throughout the process of removing the support material.

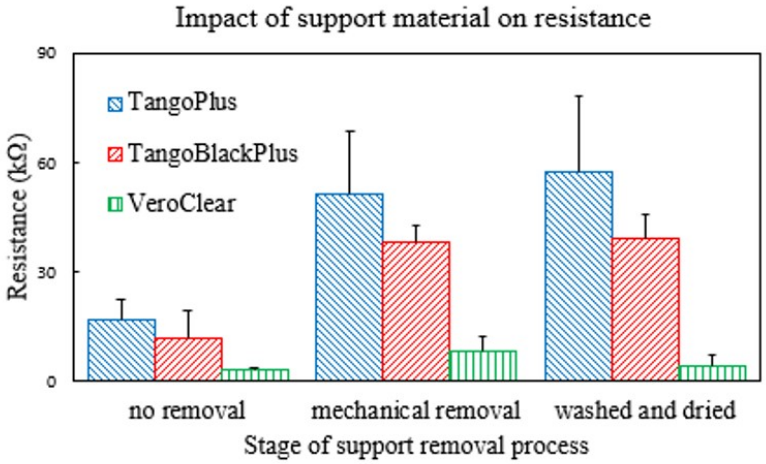


Figure 3.7: Plot of how the resistance of the 3D printed materials changes depending on how much support material is on the surface. Each group of bars corresponds to the measurement along the various stages in the removal process of the support material (Fig. 3.3). Number of samples n = 10.

We observed that the resistance of the TangoBlackPlus and TangoPlus samples increased, meaning the conductivity of the samples decreased overall (Fig. 3.7). This observation suggests that the support material contributed towards the conductivity measurement of each material, and indicated that the surface of various materials need to be thoroughly cleaned of support material.

In addition, the data show that the VeroClear material actually exhibited the most conductivity. While this result is interesting, we cannot directly integrate it into soft sensors or soft-bodied robots because of its intrinsic rigid mechanical properties. However, the relatively-lower resistance of VeroClear may be useful for other applications.

3.2.3 Characterization of the dependence of conductivity on contact resistance

While measuring the materials and designing the mechanical strain relief, we observed that the contact resistance due to the rigid wire and soft material appeared to play a significant role in the measurement of the conductivity. Thus, we characterized the dependence of conductivity

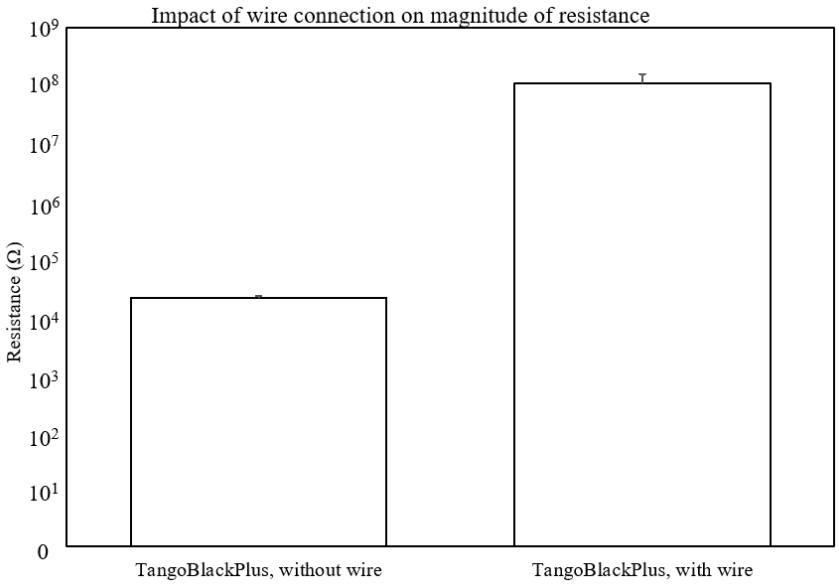


Figure 3.8: Plot of the dependence of the magnitude of conductivity based on contact resistance. We plot the magnitudes on a logarithmic scale to show the order of magnitude difference that the wire connection results in. Number of samples n = 3.

on the contact resistance by comparing the material with and without wires (clamping onto the material directly with the LCR probes). Fig. 3.8 shows the results of the comparison of the resistance pre- and post- wire attachment. Because the system is soft, it deforms upon clamping. We avoided directly clamping to the soft material by attaching a wire. The resistance measured when clamping directly to the material is less than that measured when a wire is connected to the material with silver paste at the interface because of contact resistance that the wiring introduced.

When the material comes directly into contact with the clamps for measurement, it gradually tears due to a stress concentration at the interface of contact. The mechanical breakdown of the material reinforces the need for a soft-rigid wire interface. By adding wires to the samples, we could reduce variance in the LCR measurements by providing a fixed point of attachment to the soft material. A single, physical point of contact also helped with the consistency of the measurements by reducing the mechanical wear of the LCR electrodes on the samples. Additionally, the mechanically strain relief (Section 3.1.3) further helps with reducing the movement of the wires.

There may be two scales of physical behavior that influence the reading that the LCR meter produces: 1. the physical, geometric deformation of the material at the macro-scale, and 2. the micro-scale separation of the particles in the soft material as the chemical bonds between the particles begin to separate and the material begins to tear [137].

3.2.4 Characterization of the dependence of conductivity on water content

The datasheets for the 3D printed materials indicate that they contain hydrophilic, organic compounds [133, 141–143]. In addition, we noticed that the cleanliness of the surface of the materials, particularly the removal of the support material, had an impact on the measurement of conductivity. These observations indicated that the support material was contributing to the conductivity, possibly because of the ability of the material to absorb and hold onto water.

To further understand how the water content impacts the conductivity of the material, we tested the effects of desiccating the materials. We reduced the water content in the blocks using silica desiccants, and measured the changes in mass due to water content as well as the resulting change in conductivity (Fig. 3.9). This procedure is further described in Section 3.1.5.

The mass of the blocks decreased due to the desiccation, which we attribute to the loss of water content. The desiccation process resulted in an overall decrease of -1.00%. The average resistance of the samples from the desiccation process increased by 84.78%, indicating that the samples became less conductive than before the desiccation process and that the presence of moisture can impact the sensor readings.

3.2.5 Comparison between model and experimental data

We compared the analytical models of the uniaxial and multilayer sensors (Section 4.2) with the measurements from our experimental tests. We characterized our sensors using an LCR meter. We required sensitive measurement equipment because the conductive photopolymer has a

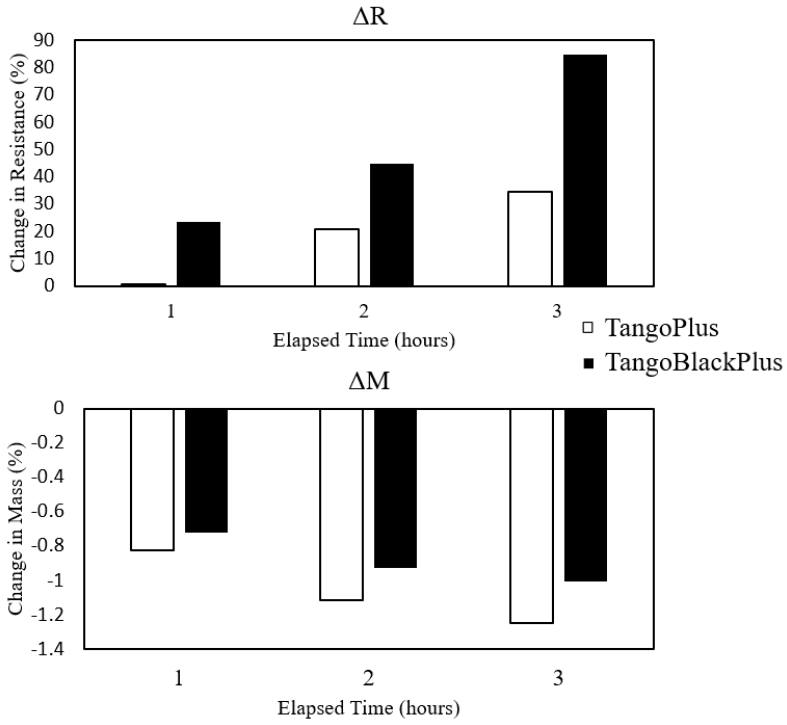


Figure 3.9: Plots of changes in mass and resistance due to desiccation. a) Percent change in mass. b) Percent change in resistance. Number of samples n = 6.

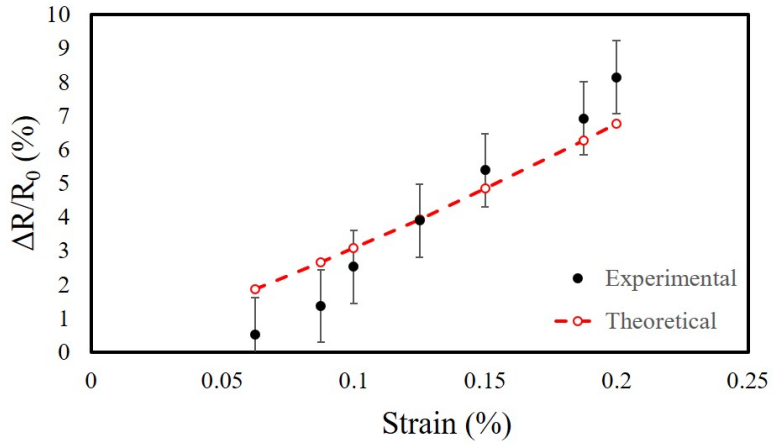


Figure 3.10: Normalized change in resistance vs. strain for the uniaxial strain sensor. Comparison of analytical model to experimental characterization. The mean is 108 MΩ at rest. Number of samples $n = 3$.

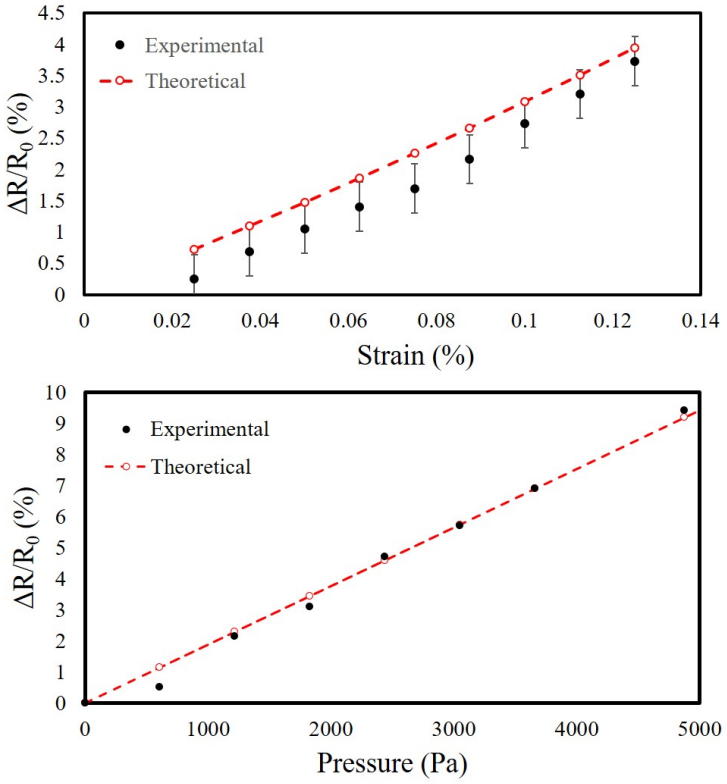


Figure 3.11: Comparison of analytical model to experimental characterization for the multilayer sensor. a) Normalized change in resistance vs. strain. The mean is 147 MΩ at rest. Number of samples $n = 3$. b) Normalized change in resistance vs. pressure. The mean is 560 MΩ at rest.

carbon black percentage of $< 0.1\%$ by mass [133], resulting in resistances with large magnitudes (in the MΩ range). We filtered the sensor readings with a 32 point averaging window on the LCR meter. Fig. 4.5 shows the normalized change in resistance vs. strain for the uniaxial strain sensor, Fig. 4.6a shows the normalized change in resistance vs. strain along one of the two axes of strain for the multilayer sensor, and Fig. 4.6b shows the normalized change in resistance vs. pressure for the multilayer sensor.

To better visualize the trends, we introduced a single constant scale factor of $S_{strain} = 14.25$ for both strain sensors (Eq. 4.6) and another of $S_{pressure} = 3850$ for the pressure sensor (Eq. 4.7), resulting in the theoretical plots in Figs. 4.5, 4.6. For the scale factor for strain, we selected its value by simultaneously minimizing the residuals for both the uniaxial and multilayer sensors. The scale factors are included to demonstrate that despite the differences in magnitude, the trend of the measurements behaves similarly to predictions of the sensors with similar geometry of the traces despite differences in the materials for fabricating the sensors.

$$\frac{\Delta R}{R_0} = S_{strain}\varepsilon\frac{(8.25-\varepsilon)}{(2.04-\varepsilon)^2} \tag{3.6}$$

$$\frac{\Delta R}{R_0} = S_{pressure}\left[\frac{1}{1-2(1-\nu^2)wP/(Eh)} - 1\right] \tag{3.7}$$

One potential reason for the difference in scale is that the resistivity may not be constant as we had previously assumed. During stretching, the geometry of the sensor changes, which can be described with Poisson's ratio. This change in geometry alters the resulting resistance of the trace. However, since our traces are polymers, strain will cause some carbon particles to get closer together while others will separate, depending on the initial distribution of the polymer network within the dielectric [144]. This would impact electron mobility, and thus the assumption

of constant resistivity might not be valid and requires further investigation.

3.2.6 Multimodal sensitivity

Analysis of the strain response of the multi-layer sensor helped identify that the patterning of the traces make a difference in the measurement, and demonstrated that the LCR meter could discern between the different directions of strain.

When stretching in the vertically-aligned direction, we observed that the vertically-aligned sensor increased in resistance whereas the horizontally-aligned and pressure sensors decreased in resistance (Fig. 3.12). The trend that we observed is consistent with what we expected from Poisson's ratio. However, the magnitudes are not: the vertically-aligned traces experienced less relative change than the horizontally-aligned traces did. This effect could potentially be because the change in resistance is bigger when you compress the material together than when you stretch it apart, as compared to liquid materials such as eGaIn. Modeling this material as a conductor of changing volume is not accurate, but rather the material is more sensitive to compression than extension as shown from these results.

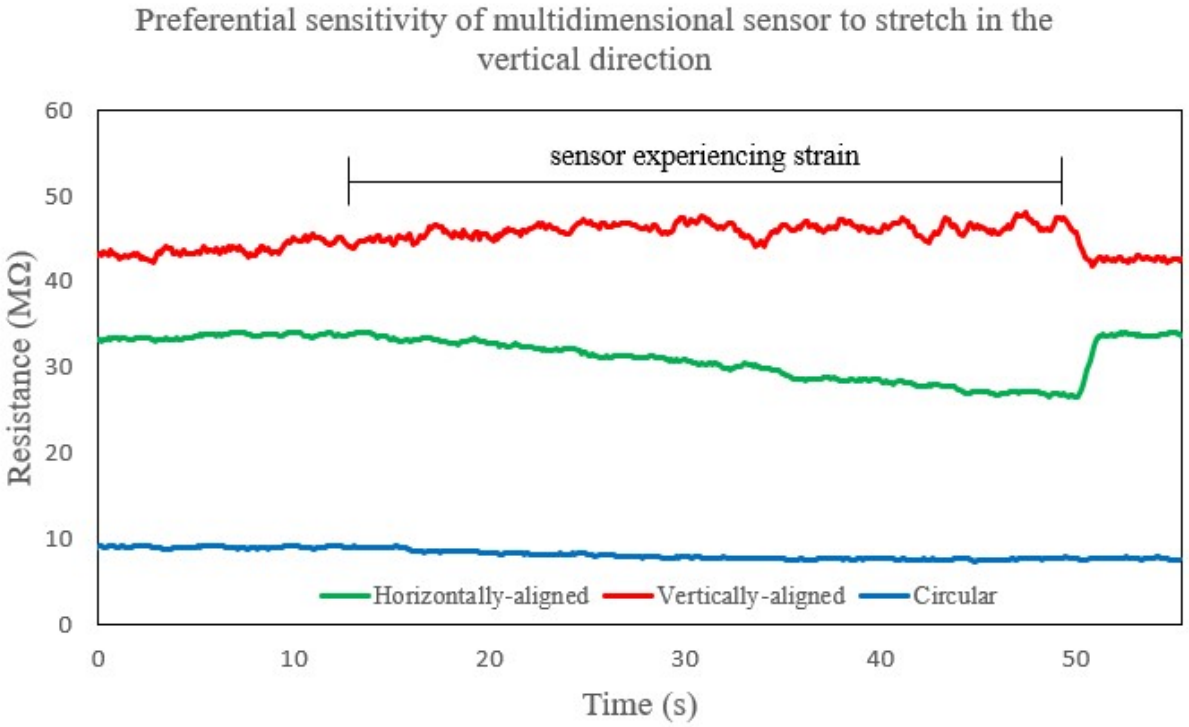


Figure 3.12: Plot showing the strain response of the multimodal sensor in multiple directions as we stretch it along the vertically-aligned direction. In this situation, the sensor is more sensitive to the serpentine pattern that is horizontally-aligned as opposed to the one that is vertically-aligned, whereas the circular sensor experiences a minimal change in its response relative to the other directions.

3.2.7 3D printed soft gripper with embedded sensors

We demonstrated the use of this fabrication process to print a soft gripper with embedded sensors by integrating the sensing capabilities directly into a pneumatic gripper (Fig. 3.13). In addition, we measured the static sensor readings as the gripper held onto various objects, which we selected from the YCB dataset [145] (Fig. 3.13). We also measured the dynamic response of the sensors as we actuated the fingers simultaneously (Fig. 3.14).

As a proof of concept demonstration, we measured the sensor readings for the various gripper configurations associated with grasping different objects. Each finger is pneumatically actuated, like previously presented pneunets [146], and we denoted the corresponding sensors

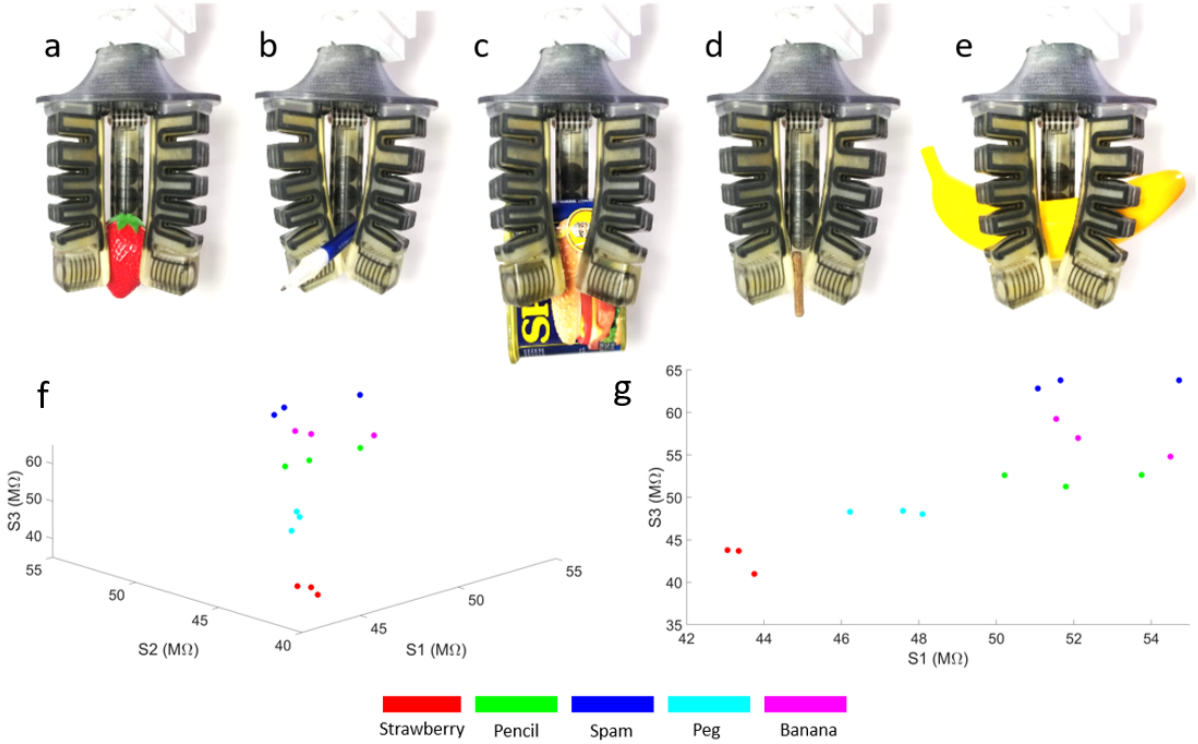


Figure 3.13: Pneumatic gripper with embedded strain sensors and the static sensor readings of the gripper corresponding to the configuration of the fingers while holding various objects. S1, S2, and S3 are the sensor readings from each of the three fingers. a) Plastic strawberry. b) Pencil. c) Can of spam. d) Toy peg. e) Plastic banana. f) 3D perspective of the scatter plot. g) 2D perspective of the scatter plot.

as S1, S2, and S3. We defined holding as the grasp position associated with the configuration of each finger as it conforms around the objects (Fig. 3.13) and repeated each grasp 3 times. Previous work has shown that these configurations can be used to identify or classify these object-associated grasps [82]. The embedded sensors could be beneficial for detecting touch or helping with state estimation for the gripper, and clusters formed from multiple grasps could be amenable to classification.

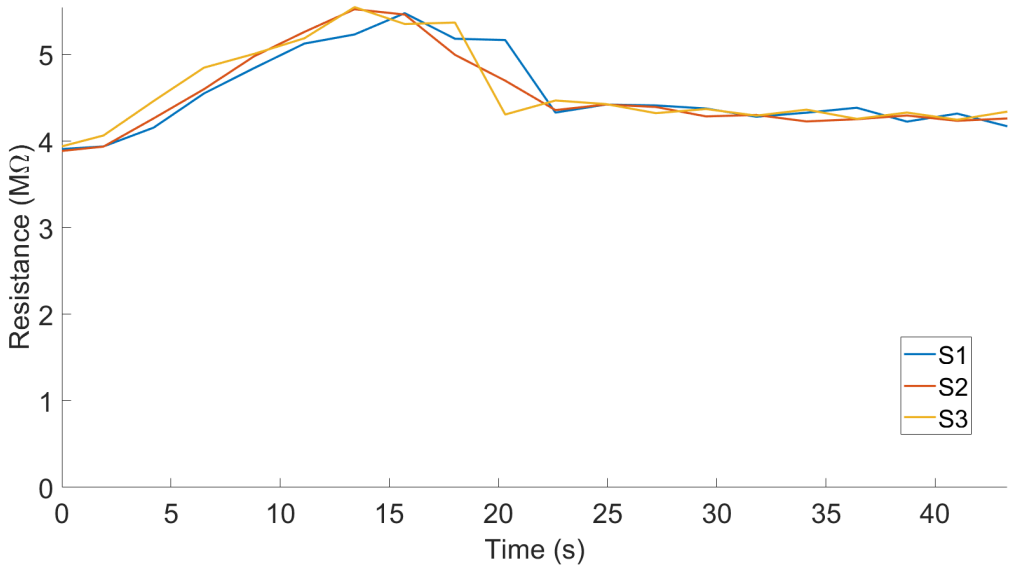


Figure 3.14: Dynamic sensor readings of the gripper as the fingers close, without an object. S1, S2, and S3 represent each of the sensor readings that the fingers in the gripper produced.

3.3 Conclusion and future work

This chapter presents the concept of 3D printing resistive sensors using a commercially available printer and material. We characterized the dependence of the 3D printed material's conductivity on a variety of factors and introduce guidelines on how to improve the fabrication method for similar types of sensors. In addition, we studied the mechanical strain response and model the sensors that we fabricated using this process.

The current iteration of the 3D printed material is promising, but there are some limitations to consider when working with it. To begin with, the company did not intentionally design the material as a conductor, and thus the resistance has a large magnitude. Measurement of the sensor values requires high-sensitivity electronics and the high impedance and limited conductivity could limit sensitivity. The readings also experience drift and oscillations due to the macro- and micro-scale deformations of the material. In addition, this photopolymer material experiences limited strain compared to materials for 'traditional' soft sensors like silicone elastomers, which could limit its use for soft robots.

Future work includes studying the other modes of sensors that this method may enable, such as printing capacitive and inductive sensors. Finding a method to reduce the drift of the readings over time would help improve the potential for deploying this material for real-world applications. In addition, knowledge of the mechanical and chemical properties of the materials can inform and optimize the design of 3D printed sensors for future applications. The ability to embed sensors into soft robots using accessible, commercial 3D printers would one day play a role in printing an entire robot along with all of its components.

This work is a step towards the direct printing of sensorized soft robots using commercially available systems. Simultaneously, embedded printing of sensors is a powerful process that could enable and enhance seamless integration of sensors into soft robots, but there does not yet exist a suitable, commercially available, easy-to-use platform that allows users to simultaneously print soft actuators and sensors. Because we expect the availability of conductive, commercial 3D printed materials to increase in the future, our focus for the future can shift to further exploring applications that this approach enables. As 3D printing technology improves and decreases in cost, multimaterial and conductive printing will grow increasingly ubiquitous and accessible, further enabling novel methods for integrating sensors into complex bodies.

Multimaterial digital manufacturing has the potential to enable robot designs with not only varying mechanical properties, but also varying electrical properties. This capability enables a whole new design space of sensors embedded in the bodies of soft robots. However, there are currently several practical challenges to applying this method, including interfacing and characterization of material properties. In this chapter, we explored some of the above challenges and demonstrated how we can fabricate soft, fully 3D printable machines with embedded sensing.

Chapter 3, in full, is a reprint of the material as it appears in **B. Shih**, C. Christianson, K. Gillespie, S. Lee, J. Mayeda, Z. Huo, and M. T. Tolley, "Design considerations for 3D printed, soft, multimaterial resistive sensors for soft robotics," **Frontiers in Robotics and AI**, 6, 30, Apr

2019. The dissertation author was the primary investigator and author of this paper.

Chapter 4

3D printed resistive soft sensors

Sensor design for soft robots is a challenging problem because of the myriad of geometries, materials, and motions that play a role in helping these robots function. While conventional rigid sensors are effective in specific situations, sensors that are directly integrated into the bodies of soft robots could help improve both their exteroception and interoception capabilities. Our goal is to design sensors that can be co-fabricated with soft robot bodies using commercial 3D printers, without additional modification. We describe an approach to the design and fabrication of compliant, resistive soft sensors, and present characterizations for linear, planar, and 3D sensors. The sensors consist of layers of a nonconductive and conductive commercial photopolymer that the printer cures with UV light. We demonstrate the capabilities of our method by embedding heart- and brain-shaped sensors within a non-planar, humanoid shape, which enables the humanoid to detect contact with its environment.

3D printing has enabled many new design and fabrication approaches for robotics [101]. In parallel, a new perspective on the role that materials play in design has altered the building blocks and tools with which we create our robots. The ability to print soft and rigid materials simultaneously using a single machine has expanded the realm of possibilities for fabricating robots, including systems that are biomimetic [102] and ones that have improved resistance to

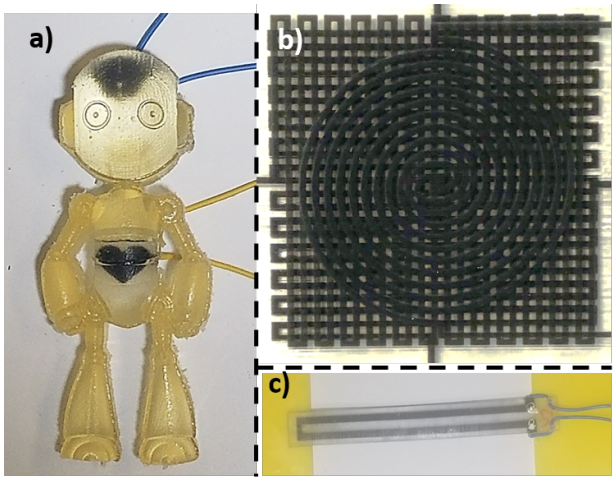


Figure 4.1: Our proposed 3D printed, resistive, soft sensors. a) 3D printed sensor embedded in a complex geometry, showing the versatility of this technique. b) Multilayer integrated strain and pressure sensor. c) Uniaxial strain sensor.

impact through functional gradients [105].

In the long term, one goal of 3D printing is the ability to print an entire robot in a single instance and have it walk itself out of the machine upon completion [106]. Recent work has demonstrated the "get up and walk away" concept. Felton et. al. describe a method for building self-folding machines using laminate structures that fold themselves up in multiple stages and can walk away after receiving electronics and battery [107]. Similar in overall concept, MacCurdy et. al. used a multimaterial 3D printer to print fluid-filled bellows directly integrated into the transmission of their locomotive robot, which can also walk immediately after attaching a motor and battery without additional mechanical modifications [108].

Soft robotics is one field which has benefitted substantially from 3D printing [36]. Robot designers can print both the molds for making soft robots [110] as well as the robots directly [105]. One challenge with soft robots is the development of effective sensors. Soft robots are not constrained to prismatic or revolute motions, and obtaining sensory feedback on these motions requires different types of sensors than those used for rigid robots. In addition, soft robots may require sensors that can be placed on complex surface geometries or embedded within the body.

In this chapter, we present:

- A method for simultaneously printing conductive and dielectric materials to produce a resistive element.
- An approach for interfacing electrical wires with soft photopolymers.
- How this fabrication process could be used for sensorizing complex, 3D, non-planar bodies.

We fabricated soft, resistive sensors using a commercial 3D printer. We described the types of sensors that we printed, modeled the predicted change in resistance, and experimentally characterized the sensors we fabricated. Lastly, we demonstrated the capabilities of the non-planar, complex geometry sensors which were embedded into the body of a miniature, soft humanoid.

Recently, interest in 3D printing soft robots has grown significantly. Previously, groups have printed various actuators [22, 117] and bodies [105, 108, 118] for soft manipulation and locomotion. Alongside the development of soft robot actuators, many groups have become interested in incorporating sensors and closing the control loop for feedback on the robot's interactions with its environment. Felt et. al. designed an inductance-based sensing system to measure and control bellowed continuum joints, by wrapping coils of wires and measuring changes in inductance [119]. Farrow and Correll, Bilodeau et. al, and Shih et. al. embedded soft bend sensors into the layers of pneumatic fingers, which enabled their fingers to estimate the shapes of various objects using tactile sensing [13–15]. Homberg et. al. clustered sensor readings from their fingers to identify correspondences to gripper configurations and classify other objects [82]. Kim et. al. 3D printed pneumatic pouches and connected them to pressure sensors to sense when the pouch came into contact with external objects [87].

Many groups have also begun experimenting with various fabrication techniques for soft sensors, particularly in the form of skins [121]. Muth et. al. customized a printer for sensor fabrication, which embeds their conductive material while their elastomer substrate has not yet cured [58]. Inspired by mechanoreceptors found within skin, Lipomi et. al. and Tee et. al. developed skin-like sensors that can detect strain and pressure [4, 127], and Yin et. al. fabricated a

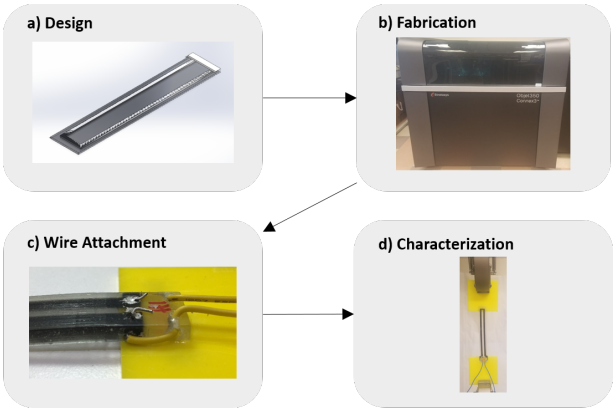


Figure 4.2: Design, fabrication, and testing procedure for our 3D printed sensors. a) Digitized CAD design of the uniaxial sensor. b) Multimaterial 3D printer that we used to print the sensors. c) Wire attachment process (Section 7.1.1A) for adhering the photopolymer traces to the external wires. d) Characterization of the strain measurements that the sensors can detect. We acquired the data using a mechanical testing machine (Instron).

skin that senses shear force [128]. However, the integration of these skins for sensing in real-world robot systems remains an open problem [130]. Having a separate skin also requires the robot designer to affix the sensing elements in a separate manufacturing step, limiting the ability to sensorize the complex, dynamic bodies of soft robots.

4.1 Design and fabrication

Soft robots face many challenges with existing methods for integrating sensors into their bodies. Existing techniques are often unable to accommodate the elastic deformations of soft robots, such as the stretching and bending that arise in wearable computing and smart textiles [131].

We can overcome many of these challenges by using a commercially available 3D printer (Stratasys Objet350 Connex3) that has the ability to mix conductive and dielectric materials. Many groups have already produced actuatable soft robots with this tool [22, 87, 102, 105, 108, 117, 118]. In this chapter, we will demonstrate that this printer can also directly embed sensors into soft robot systems.

One of the materials that the printer can produce is a translucent photopolymer (TangoPlus FLX930, Stratasys) and another is a black photopolymer (TangoBlackPlus FLX980, Stratasys). The black resin contains carbon particles [133], which provide a small but measurable conductivity, and can thus serve as conductive traces for sensors. The translucent photopolymer does not contain the carbon particles and thus can be used as a dielectric.

The three sensors we present here are a uniaxial strain sensor, a multilayer strain and pressure sensor, and a 3D humanoid with complex sensor geometries (Fig. 4.1). We created the sensors using computer-aided design (CAD) software, fabricated our designs using the 3D printer, and secured the wires using silver paste and mechanical strain reliefs (Fig. 4.2).

The commercial material also has similar mechanical strain-to-failure properties as skin. It nominally has 170-220% elongation at break [134], but during our tests (Section 4.3) we observed strain-to-failure of approximately 20%. We compared the mechanical properties of the photopolymer to those of human skin, and found in previous work that most parts of human skin fail after exceeding 15% strain. The physiological limitation is measured to be at most 45% in areas such as the fully flexed knee or elbow [135, 136]. Thus, even with relatively low strain-to-failure, the commercial material may still be useful in creating bioinspired and biomimetic designs.

With this approach, it becomes much easier to perform tasks such as sensorizing complex 3D geometries or placing sensors within the internal structure of a soft robot. Integrating sensors into soft, complex, 3D geometries that are deformable is a difficult problem given traditional techniques, so our objective is to address this challenge with multimaterial 3D printing.

4.1.1 Uniaxial strain sensor and wire attachment to soft substrate

We quantified the effect of strain on the traces made from conductive photopolymer by starting with a uniaxial sensor. This design enabled us to test how strain affects resistance and to explore methods for adhering the rigid wires to the soft traces (Fig. 4.3c).

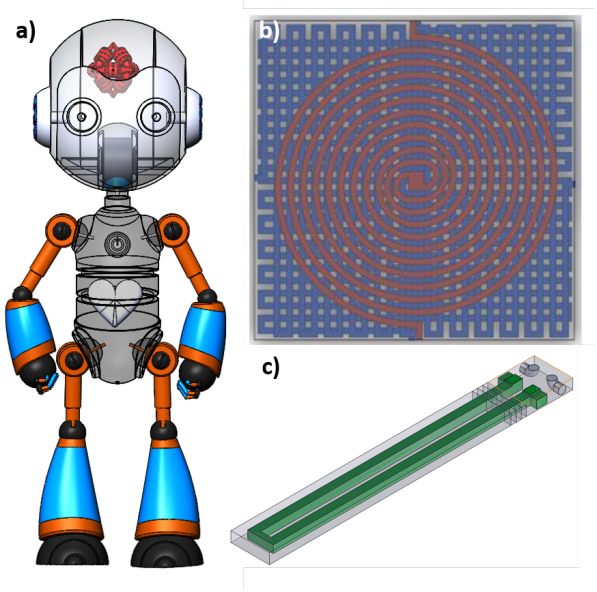


Figure 4.3: CAD drawings of our sensors. a) Humanoid robot - front view. b) Multilayer strain and pressure sensor - top view. c) Uniaxial strain sensor with mechanical strain relief and functional gradient to improve wire interface - isometric view.

When attaching solid-core wires to the soft material, our solution for effective connections at the electrical and mechanical interface was 1) soft insertion points for mechanically securing the wires and 2) a stiffness graded wire attachment point (Fig. 4.4) [105].

For this sensor design, we included soft holes within the rigid material for the mounting point. The holes in Fig. 4.4 labeled 1, 2, 3, and 4 served as mechanical strain relief, and the silver paste at the interface of holes 3-4 improved the electrical conductivity between the solid wire and the photopolymer trace.

4.1.2 Multilayer integrated strain and pressure sensor

Next, we demonstrated our ability to print embedded, multimodal sensors by fabricating an integrated strain and pressure sensor [2] (Fig. 4.3b).

The multilayer sensor consists of three layers of conductive traces embedded within a dielectric: two perpendicular serpentine traces which measure strain in the xy-plane (along the page, in Fig. 4.3b) and one circular trace that measures pressure along the z-axis (in and out of

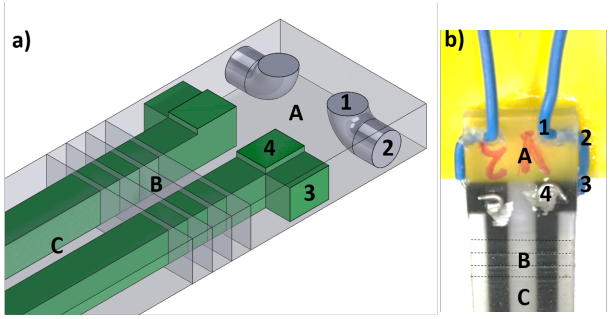


Figure 4.4: Our method for wire attachment. a) Schematic for the wire attachment procedure - isometric view. We insert the wire at 1, and pass through in order of 1-2-3-4 to distribute strain on the wire. The space between 1 and 2 is printed and filled using a dielectric photopolymer, which provides mechanical relief by holding the wire in place. At 3 and 4, we coat the wire and photopolymer interface with silver paste to increase electrical conductivity. These numbers are only labeled on half of the sensor shown here. A is a rigid photopolymer, B is a functional gradient, and C is a flexible photopolymer. b) Completed, physical version of the wire attachment - top view.

the page, in Fig. 4.3b).

4.2 Analytical model

4.2.1 Strain

For elastomer-like materials, the overall length of the channel increases while the cross-sectional area of the channel decreases when the channel of the sensor experiences axial deformation, leading to an increase in the resistance of the channel [2].

Assuming rectangular traces, we can represent the resistance of an undeformed sensor as:

$$R_0 = \frac{\rho L}{wh} \tag{4.1}$$

where R_0 is the resistance in the undeformed state, ρ is the electrical resistivity of the photopolymer, L is the length of the conductive channel, and w and h are the width and height of the cross-section of the conductive material, respectively.

The change in resistance of the material upon stretching can be represented as:

$$\begin{aligned}\Delta R &= R - R_0 \\ &= \rho \frac{L + \Delta L}{(w + \Delta w)(h + \Delta h)} - \rho \frac{L}{wh}\end{aligned} \tag{4.2}$$

where R is the resistance when the sensor stretches by ΔL.

Next, we can replace Δw with $-\nu\varepsilon w$ and Δh with $-\nu\varepsilon h$, and substitute $\varepsilon = \frac{\Delta L}{L}$ to obtain:

$$\frac{\Delta R}{R_0} = \varepsilon \left[\frac{(1 + 2\nu) - \nu^2 \varepsilon}{(1 - \nu\varepsilon)^2} \right] \tag{4.3}$$

where ε is the strain and ν is the Poisson's ratio of the material.

Based on a Neo-Hookean model, the Poisson's ratio for this photopolymer material is approximately $\nu = 0.49$ [138], which enables us to further simplify equation 4.3 to:

$$\frac{\Delta R}{R_0} = \frac{\varepsilon(8.2466 - \varepsilon)}{(2.0408 - \varepsilon)^2} \tag{4.4}$$

4.2.2 Pressure

We can model the theoretical relationship between the change in resistance and contact pressure by using linear elastic fracture mechanics [139]. Once again assuming rectangular traces, we can represent the normalized change in resistance as:

$$\frac{\Delta R}{R_0} = \frac{1}{1 - 2(1 - \nu^2) wP/(Eh)} - 1 \tag{4.5}$$

where P is the pressure on the sensor and E is the elastic modulus of the material.

4.3 Experimental characterization

In this section, we compare the analytical models of the uniaxial and multilayer sensors (Section 4.2) with the measurements from our experimental tests. We characterized our sensors using an inductance, capacitance, and resistance (LCR) meter (Agilent E4980AL). We required sensitive measurement equipment because the conductive photopolymer has a carbon black percentage of $< 0.1\%$ by mass [133], resulting in resistances with large magnitudes (in the MΩ range). We smoothed the sensor readings with a 32 point averaging filter on the LCR meter.

We tested strain in both the uniaxial and multilayer sensor by stretching the material. For the multilayer sensor, we tested the pressure by placing a range of masses on top of the pressure sensor (Fig. 4.6b). To convert between load and pressure, we multiplied the mass by gravity on earth to obtain the normal force on the pressure sensor, and then divided by the contact area of the mass ($P = \frac{mg}{A}$).

Fig. 4.5 shows the normalized change in resistance vs. strain for the uniaxial strain sensor, Fig. 4.6a shows the normalized change in resistance vs. strain along one of the two axes of strain for the multilayer sensor, and Fig. 4.6b shows the normalized change in resistance vs. load for the pressure component of the multilayer sensor.

To better visualize the trends, we introduced constant scale factors of $S_{strain} = 20$ for both strain sensors (Eq. 4.6) and $S_{pressure} = 4000$ for the pressure sensor (Eq. 4.7).

$$\frac{\Delta R}{R_0} = S_{strain}\varepsilon\frac{(8.2466-\varepsilon)}{(2.0408-\varepsilon)^2} \tag{4.6}$$

$$\frac{\Delta R}{R_0} = S_{pressure}\left[\frac{1}{1-2(1-\nu^2)wP/(Eh)} - 1\right] \tag{4.7}$$

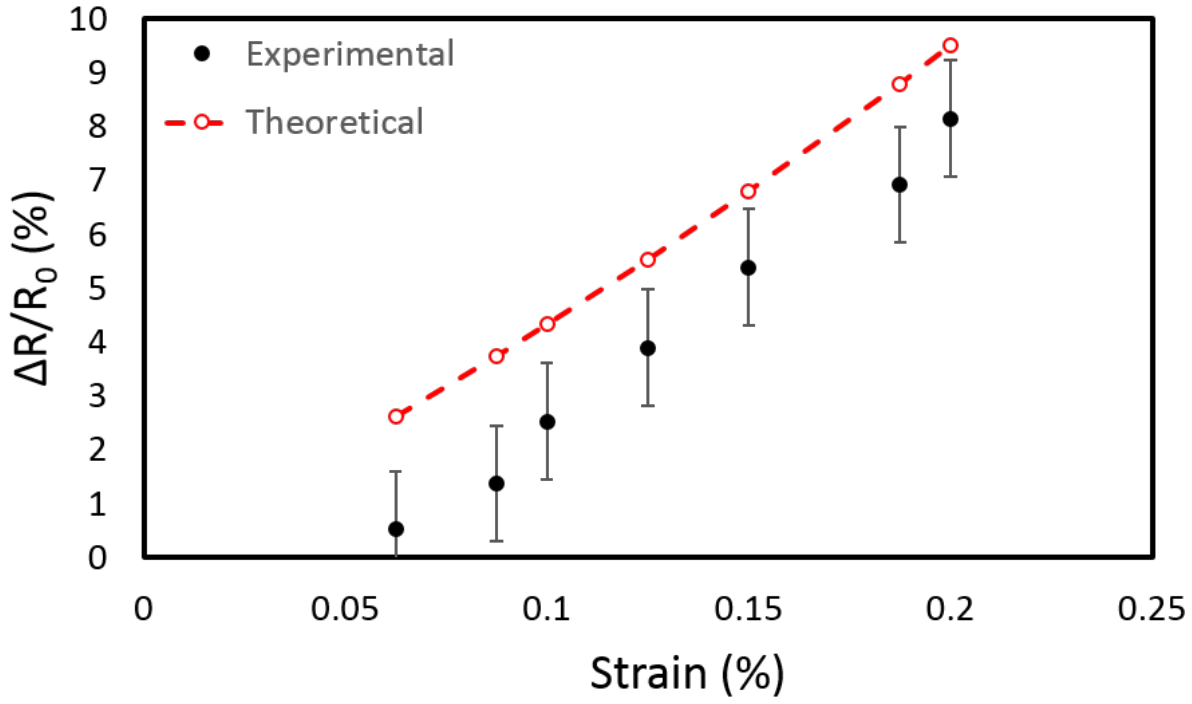


Figure 4.5: Normalized change in resistance vs. strain for the uniaxial strain sensor. Comparison of analytical model to experimental characterization.

One potential reason for the difference in scale is the resistivity may not be constant as we had previously assumed. During stretching, the geometry of the sensor changes, which can be described with Poisson's ratio. This change in geometry alters the resulting resistance of the trace. However, since our traces are polymers, strain will cause some carbon particles to get closer together while others will separate, depending on the initial distribution of the polymer network within the dielectric. This would impact electron mobility, and thus the assumption of constant resistivity might not be valid and requires further investigation.

4.3.1 Temporal response

One important element of sensing for real-world robots is temporal response. Many soft materials exhibit creep or hysteresis due to material-related properties such as elastic restoring force or Mullin's effect [2, 13–15, 110].

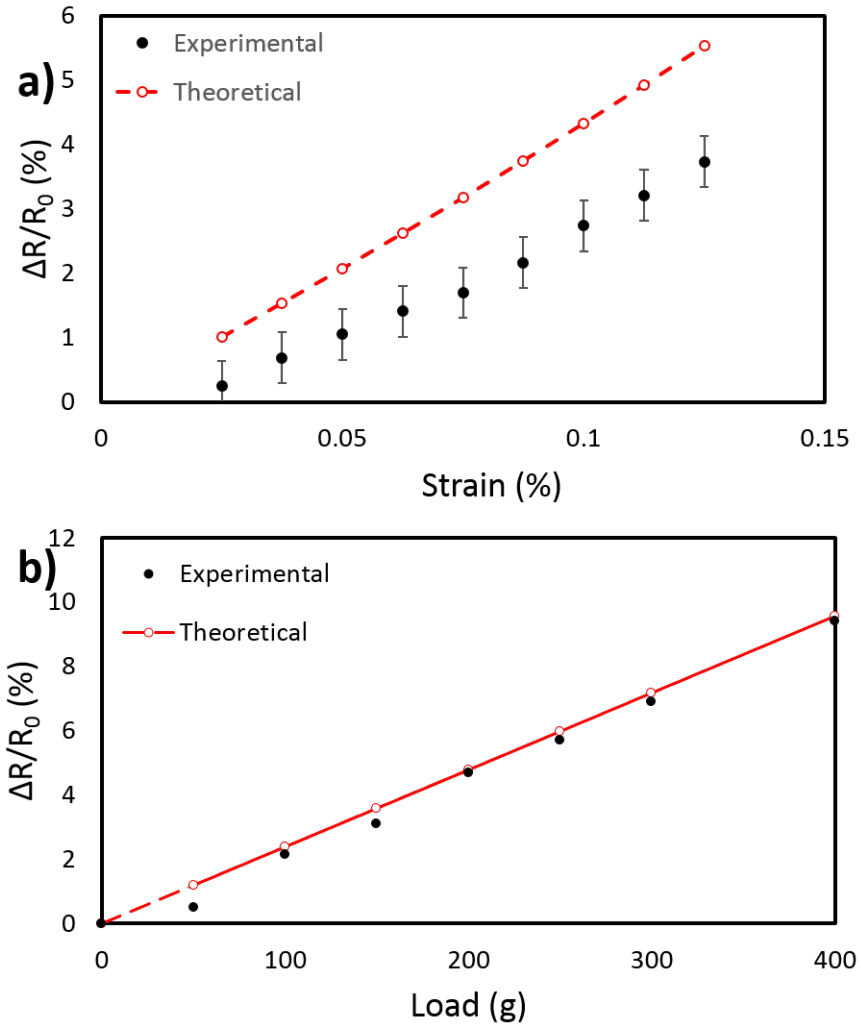


Figure 4.6: Comparison of analytical model to experimental characterization for the multilayer sensor. a) Normalized change in resistance vs. strain. b) Normalized change in resistance vs. load.

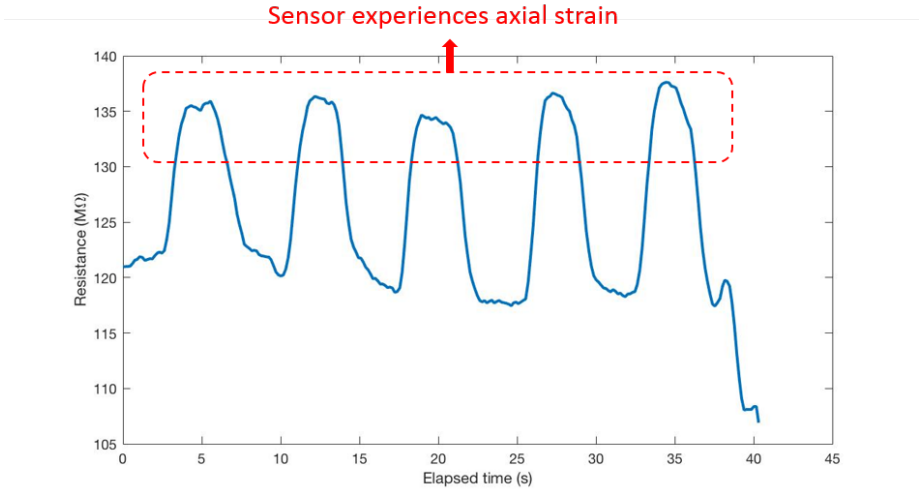


Figure 4.7: Demonstration of the time response for the uniaxial sensor when strained multiple times by hand to approximately 110%. The change in resistance is measurable in real-time and distinguishable from the noise, although there is a small shift in the baseline of the sensor reading.

Our sensors experienced some noise and shifting baseline. However, we can still distinguish between and threshold the signal because there is an approximately 10% difference between the resting and deformed states, which is higher than the background noise (Fig. 4.7).

4.4 Complex, non-planar bodies

In the previous sections, we first wanted to use 3D printing to reproduce planar sensors similar to the ones found in [2, 13–15] and show that they would work. Then, to show that we can make 3D objects that would be impossible with those planar methods, we printed sensors that have complex geometries within robot bodies that are also complex.

As a demonstration, we designed (Fig. 4.3a) and 3D printed (Fig. 4.1a) a humanoid with heart- and brain-shaped resistive sensors. The process was similar to that of the planar cases: we 3D printed the body with embedded sensors, attached the wires, pressed the head and torso individually, and measured the sensor readings. The outputs presented in Fig. 4.8 are an example of how multimaterial printing can be used to simultaneously fabricate complex external bodies

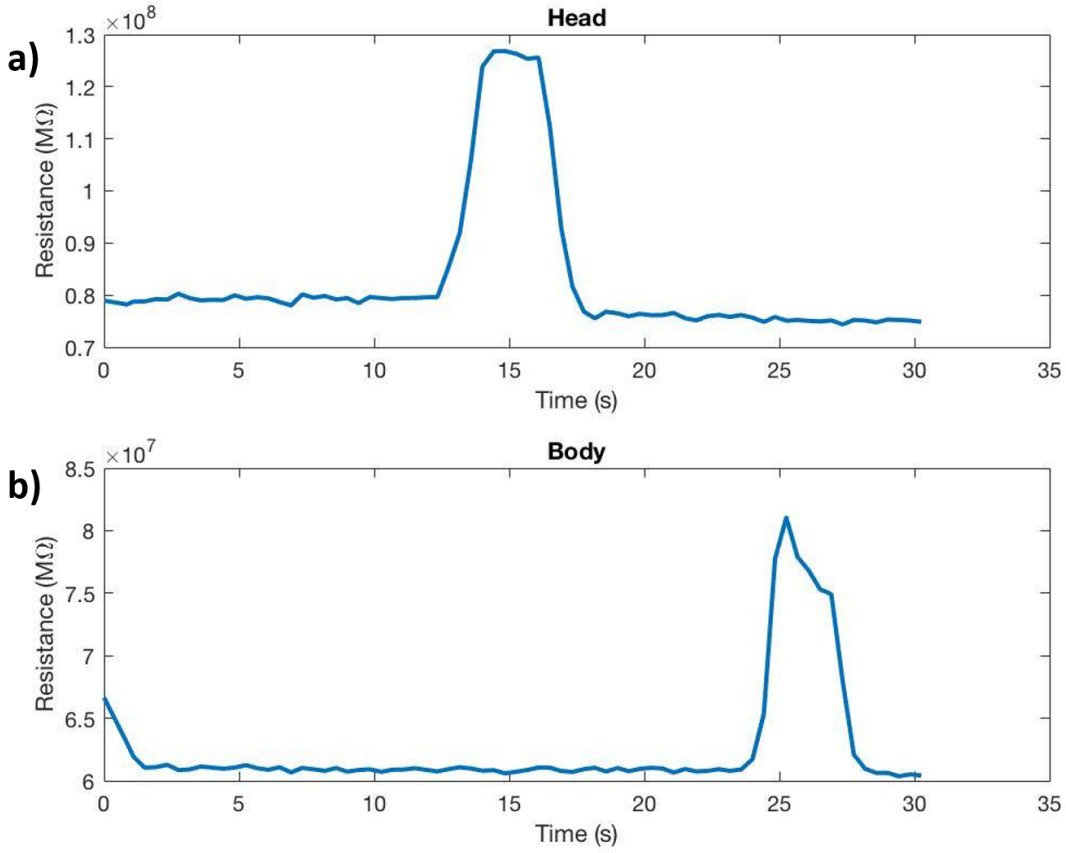


Figure 4.8: Demonstration of the 3D sensor shapes embedded within a humanoid that we fabricated with the multimaterial printer. The signals are currently decoupled in these plots, e.g. deforming the head does not affect the torso. a) Measurement of the brain-shaped sensor embedded within the head, as the head is deformed. b) Measurement of the heart-shaped sensor embedded within the torso, as the torso is deformed.

alongside complex sensor geometries.

4.5 Conclusion and future work

We prototyped soft, 3D printed resistive sensors which can sense various modalities including strain and pressure. The sensors are easily customizable using CAD software and can also be embedded into custom, complex, 3D geometries. This property enables roboticists to directly integrate sensors into the body of a 3D printed soft robot. Characterizations of the sensing

modalities demonstrate the predictable response and validate the potential use of these sensors in soft robots.

While the current version of these 3D printed sensors offers reasonable response times and readings, there are many potential areas for improvement. One challenge is to decouple the inputs to the sensors. There are multiple inputs and a single output, so we have an underdetermined systems of equations for resolving the input. We can address this challenge in part by selecting the proper locations for sensor placement Although 3D printing our sensors helped improve consistency in the fabrication process, we still observed some variance in the resistance readings across sensors. The most likely source of the inconsistencies is the interface between the wire and conductive photopolymer, because the mechanical and electrical attachment are still performed by hand. Increased conductivity of the photopolymer material would help dramatically. There may also be some variance that can be attributed to anisotropy due to the print direction of the sensors because the resistivity may depend on the distribution of the conductive particles within the polymer. Another challenge we face with these sensors is hysteresis. Despite the time constant associated with the elastic restoring force in elastomer-like materials being smaller than in previous work [15], we still need to determine the time constant and how slow of a response we can tolerate. Another potential source of noise that we noticed is parasitic capacitance. While using the LCR meter, we observed that the capacitance of the resistive soft sensors can change with the proximity of surrounding objects. This may be addressable with electromagnetic shielding.

Despite the challenges that we encountered, this work is a step towards being able to directly print sensorized soft robots using commercial systems. As 3D printers advance in technical capabilities and decrease in cost, multimaterial and conductive printing will grow increasingly ubiquitous and accessible, further enabling novel methods for integrating sensors into complex bodies. We expect 3D printing to improve the future of sensing for soft robots.

Chapter 4, in full, is a reprint of the material as it appears in **B. Shih**, J. Mayeda, Z. Huo, C. Christianson, and M. T. Tolley, "3D printed resistive soft sensors," in 2018 IEEE-RAS International Conference on Soft Robotics (**ROSO18**), pp. 152-157, Apr 2018. The dissertation author was the primary investigator and author of this paper.

Chapter 5

Soft robot perception using embedded soft sensors and recurrent neural networks

Recent work has begun to explore the design of biologically inspired soft robots composed of soft, stretchable materials for applications including the handling of delicate materials and safe interaction with humans. However, the solid-state sensors traditionally used in robotics are unable to capture the high-dimensional deformations of soft systems. Embedded soft resistive sensors have the potential to address this challenge. However, both the soft sensors—and the encasing dynamical system—often exhibit nonlinear time-variant behavior, which makes them difficult to model. In addition, the problems of sensor design, placement, and fabrication require a great deal of human input and previous knowledge. Drawing inspiration from the human perceptive system, we created a synthetic analog. Our synthetic system builds models using a redundant and unstructured sensor topology embedded in a soft actuator, a vision-based motion capture system for ground truth, and a general machine learning approach. This allows us to model an unknown soft actuated system. We demonstrate that the proposed approach is able to model the kinematics of a soft continuum actuator in real time while being robust to sensor nonlinearities and drift. In addition, we show how the same system can estimate the applied forces while interacting with

external objects. The role of action in perception is also presented. This approach enables the development of force and deformation models for soft robotic systems, which can be useful for a variety of applications, including human-robot interaction, soft orthotics, and wearable robotics.

Perception is an essential component of an intelligent autonomous system. It is one of the basic necessities for closed-loop control and representation of the environment. Robotic perception involves the kinematic estimation of the self, contact modeling, and mapping of the surroundings. With traditional rigid robotics, solutions to proprioception and tactile sensing involves highly specialized sensors precisely developed and arranged to ensure maximum state observability. This is feasible due to the availability of accurate models and reliable technological development. With the rise of soft robotics and the complexities involved with the modeling and development of soft robots [36, 78], we are presented with new challenges in perception . The high dimensionality of soft robots and soft sensors complicates the selection of the type, number, and placement of sensors. With the availability of analytical models, statistical metrics can be formulated for this problem [147]. However, the modeling of soft sensors is challenged by inconsistencies in their manufacturing and non-linearities in their dynamics [39, 42, 148].

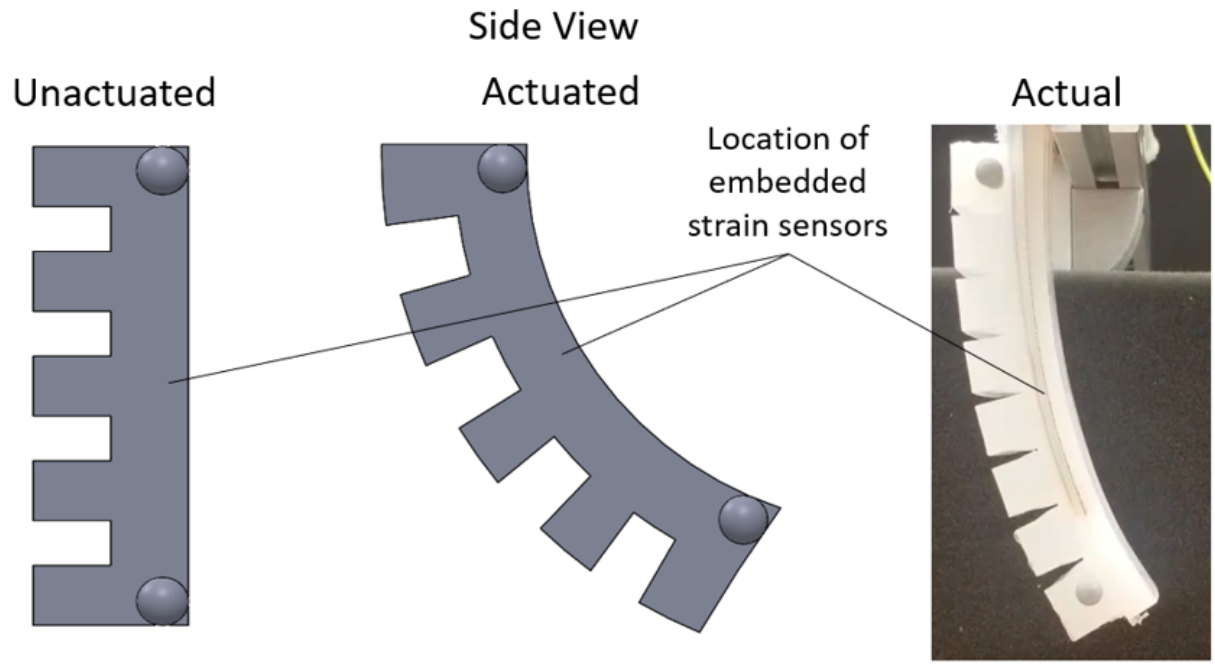


Figure 5.1: a) Side view of the CAD of the soft actuator with infrared-reflective balls for tracking the motion of the tip. Embedded sensors are used to estimate the coordinates of the tip and the forces applied by the actuator when in contact. The plots we present in this chapter describe the position of the marker at the tip relative to the marker at the base. b) Physical actuator with embedded soft sensors.

The development of technologies for sensing in soft robotics is a growing field with diverse potential solutions [42]. There are subtle differences between each of these technological solutions that give each unique advantages depending on the required task. An ideal soft sensor must provide state information along the body of a soft system with minimal effect on the dynamics of the system. Embedded sensing is the most viable solution for strain, stress, contact, and roughness estimation [16, 35, 64, 69, 91, 149, 150]. Unlike external sensing (e.g. vision), embedded soft strain sensors are not restricted by occlusion and coordinate transformation problems. In cases where the sensor must be embedded in the soft system, a requirement for high omni-directional compliance ensues. Conductive nanocomposites are one of the most commonly used material for soft strain sensors [151, 152]. However, the modeling of these embedded sensors is quite difficult due to high nonlinearities and creep [58, 153, 154], although precise manufacturing may

help alleviate the latter [151]. Another prominent strain sensor design is based on metals that are liquid at room temperature, encased in a non-conductive elastomer [139, 155]. Although they do not exhibit significant creep characteristics, these sensors are difficult to manufacture and are susceptible to leakage. Higher accuracy can be obtained with fiber Bragg gratings [156], stretchable optical waveguides [16] and magnetic sensors [157]. However, these options have reduced omni-directional compliance. For this work, we use strain sensors consisting of layers of polydimethylsiloxane (PDMS) impregnated with conductive carbon nanotubes (cPDMS). We chose this particular sensor design due to its ease of manufacture, and scalability in number. From the viewpoint of modeling, these sensors exhibit many of the the nonlinearities and creep phenomenon typically observed in other soft sensors. Hence, an approach viable for these sensors should be easily transferred to soft sensors with other designs (as discussed above).

Once a consistent sensor is embedded in a system of concern, the next step is to obtain meaningful information about the system states from the raw sensors readings. Unlike traditional sensing technologies, soft sensors conform to the structure of the surrounding dynamical system. Consequently, formulating kinematic and contact models based on these sensors requires an understanding of the sensor dynamics as well as the system dynamics. Due to their omni-directional compliance, these sensors could potentially have singular configurations (sensor values do not change at certain system configurations), and non-unique mappings (i.e. similar sensor readings for different system configurations). Furthermore, in the case of interactions with the surroundings, contact modeling is a highly complex mathematical problem, currently limited to theoretical studies [42]. Due to the complexity in modeling, most work has adopted empirical or semi-analytical approaches. A purely analytical framework would require advancements in technologies for precise and repeatable manufacturing of the sensors, as well as the dynamical system in question. This work circumvents these challenges by providing a general framework for automatically generating these models experimentally using machine learning algorithms. Recent work has also begun to explore the viability of using learning based approaches for model

synthesis [129, 158].

One of the biggest challenges in perception for soft robotics is multi-modal sensing, i.e. the capacity of a soft robot to perceive multiple physical parameters. For example, the ability of a soft manipulator to simultaneously estimate its kinematic configuration and the external forces applied to it. Previous works have proposed complex manufacturing and sensor design solutions for multi-modal sensing [132, 159, 160], however, these works are limited to proof-of-concept only and lack modeling processes of their embedded sensors. Moreover, they are designed based on prior knowledge about the type of contacts (typically only tip contacts), sensor properties, and applications. Interestingly, many sensory modalities like stress, strain and pressure can be theoretically observed with multiple strain sensors of the same kind [42]. Another overlooked phenomenon is the contribution of action to perception, an additional source of information utilized by humans [161]. Sensing in the presence of active (internal forces) and passive (due to external constraints) forces is a task that has not been investigated before in the context of soft robotics.

A compelling solution to the soft perception problem can be found in our own sensory system. The human proprioceptive system, in contrast to the traditional approach in robotics, is characterized by a highly redundant, diverse, and unstructured sensor architecture [162]. Either by design or due to fundamental limitations of biological systems, there is constant transformation in the sensory system caused by growth, damage, and fatigue. Hence the neuronal modeling centers are constantly adapting, using visual senses as teaching signals and frames of reference [163–165].

The highly redundant, randomized and scattered sensor distribution is a simple yet powerful solution to the problems of sensor placement, and determination of number and type of sensors. For soft sensors with higher compliance than the soft bodies they are sensing, an injudicious number of sensors can be embedded in the body being monitored with minimal perturbations to the system's dynamics. Previous work has investigated this concept by randomly placing commercial bend sensors and selecting the best combination for static modeling using

information theory [158]. The challenge in modeling unknown sensor and system dynamics can be solved with any machine learning approach as long as reliable training signals are available for developing the model. These ideas have been explored for object identification [15, 82], bend angle prediction [166], tactile gesture recognition [167], force sensing [129] and localization [129]

The three main areas of interest in soft robot perception are concerned with the estimation of body kinematics, external wrenches (i.e. applied combinations of forces and torques) and contact point estimation. Due to the strong coupling between the kinematics and statics of conventional soft robots, all these problems are interconnected [168]. The problem of kinematics estimation can be stated as follows: Given the current sensor deformation states $s_d(t)$ and the control input $\tau(t)$, the objective is to provide a model that predicts the position $y(t)$ of the system. The cardinality of the required sensor space increases with the number of contacts and the dynamic actuation range. For example, for a soft robot with a single actuated degree of freedom (DoF) and no contacts with the surrounding, a single deformation sensor is sufficient for static modeling. In this case, even local strain information along the length of the robot is sufficient for full observability. Additional sensors may be required for dynamic modeling as passive DoFs can get excited during motion. Once the robot comes in contact with the surroundings, the kinematics of a soft robot itself changes. Consequently, additional sensors are required to detect contact and to update the kinematic model accordingly.

External force sensing is a diversified problem with varying complexities and challenges depending on the system design. Broadly, they can be divided into direct and indirect estimation methods. Direct force sensing refers to approaches where the sensor is directly placed at the area of contact [155]. Hence, modeling direct force sensors becomes independent of the system in which they are embedded. However this approach imposes restrictions on the type and placement of sensors. Indirect force sensing infers contact forces based on information transmitted along the soft system; an approach that is more flexible in the type of sensors and their placement. This type of force sensing that uses configuration-level information without force sensors located proximal

to the end-effector is commonly referred to as 'intrinsic force sensing' [169]. Static models that predict the external wrenches applied to a continuum robot given the deformation sensor states s_d and tension sensor states s_t have been proposed for both estimation [170] and control [171]. The sensible wrench space depends on the configuration of the system and the cardinality of the tension sensors [169]. Khan et al. showed that with estimates of the compliance matrix, external forces could be measured indirectly using only strain sensors [172].

This chapter describes the use of a bio-inspired sensory architecture with a modeling recipe based on machine learning that can address many of the current challenges in soft robot perception (Figure 5.2). We demonstrate that this methodology can be used to perform model-free, real-time multimodal sensing: First, we demonstrate a kinematic state estimator that can detect external contacts and modify the kinematics accordingly; Second, we show how we can use the same sensor architecture for indirect external force sensing. Compared to the state of the art, we can relax numerous assumptions commonly made in previous efforts: 1) Our system has both active and passive elements and the modeling is done in continuous time without assumptions of static equilibrium; 2) We take into consideration the drift and hysteresis effects typically found in current soft sensors by representing our problem as a time sequence prediction problem; 3) The whole system can be made 'sensitive' without restrictions on the location and duration of contacts. Therefore, unlike previous works on direct force modeling system, we can develop a force sensing module that can be trained at regions anywhere along the robot. We propose a simple fabrication, integration and learning methodology for rapid prototyping. Additionally, we demonstrate how redundancy in the sensory system helps not only in multimodal sensing but also provides graceful degradation in response to sensor failure.

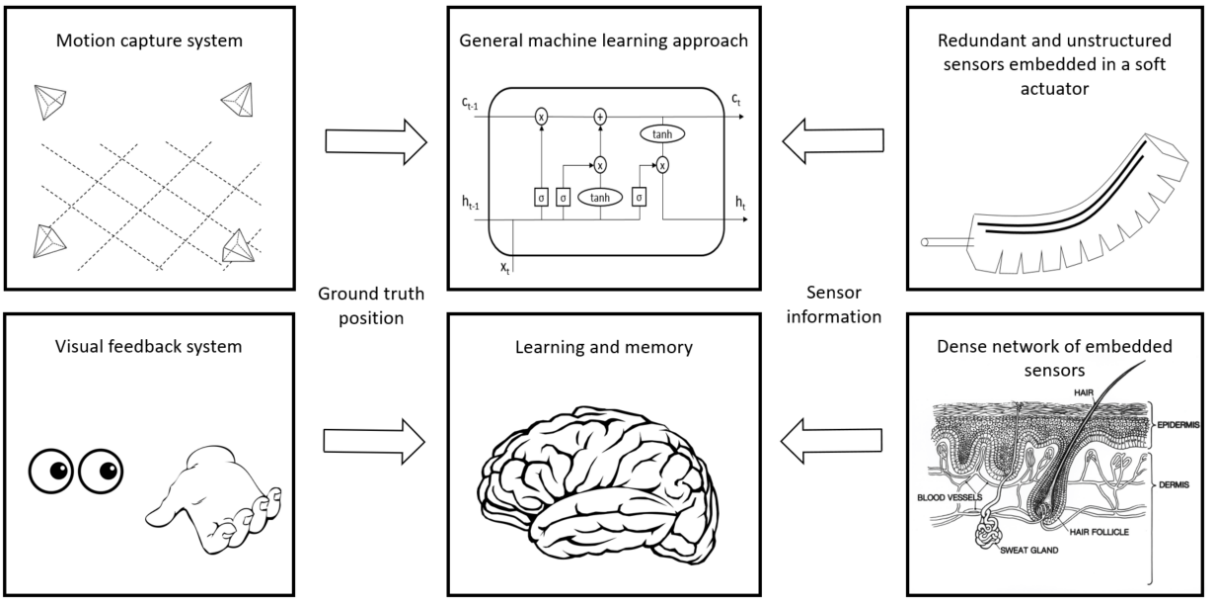


Figure 5.2: Overview of the modeling architecture and its parallel to the human perceptive system.

The next section presents the materials and methods used in this chapter. The performance of the kinematic model is presented first in the results section. With three partially independent cPDMS strain sensors, we train and test the model for three different conditions; (i) Free motion of the finger, (ii) External contact at the tip, and (iii) External contact at a fixed location along the continuum finger. The performance is benchmarked by applying the same learning approach to a finger embedded with a commercial flex sensors in the place of the soft cPDMS sensors. The subsequent section presents the results of the force estimation model. The experimental setup is not varied in this case except for adding a load cell to the external contact environment for obtaining the ground truth. The case of predicting forces applied at the tip is presented here. Finally, we present simulation studies that investigate how the redundant architecture can be exploited by the learned network to be more robust to noise even in the case of the complete loss of some sensors.

5.1 Materials and methods

The proposed approach is validated primarily on a pneumatically actuated planar soft finger with three embedded soft resistive strain sensor (Figure 5.1). The soft finger was composed of a series of channels and chambers surrounded by a soft elastomer. On pressurization, the finger deformed according to the internal stress distribution along the elastomer [21]. A single pneumatic actuator was used for driving the finger. Conductive carbon-nanotube-doped Polydimethylsiloxane (cPDMS), with a resistance that increases with strain, encased in a non-conductive elastomer, served as the soft strain sensor. The sensors were manually manufactured with varying lengths and implanted in the finger by randomly placing them roughly aligned with the length of the finger during the curing process of the finger. The main human knowledge required during sensor placement was to ensure that the sensors were not placed in a location that does not strain during actuation (e.g. along the neutral axis of bending). For the training and real-time testing period, the actuators were commanded to random reference pressures varying every second. A low-level proportional derivative (PD) controller tracked the reference pressure independently [117]. A motion capture system acted as our ground truth, tracking the motion of the tip of the finger during the training phase. For force modeling, a commercial, single-axis load cell provided the ground truth. A type of recurrent neural network called a long short term memory (LSTM) network was used for learning the time series mapping due its ability to train long time-lagged data [173]. The reference pressure inputs and the current impedance values of the three sensors were the only inputs to the network and the outputs were the Cartesian coordinates of the finger tip and the forces applied by the finger at the point of training. The LSTM network performs a mapping from $[s_d(t), \tau(t), c(t)] \rightarrow y(t)$ for kinematics estimation and a mapping from $[s_d(t), \tau(t), c(t)] \rightarrow F(t)$ for force estimation. Here, $s_d(t)$ is the sensor impedance readings consisting of the sensor resistance and reactance, $\tau(t)$ is the input pressure to the actuator, and $c(t)$ is the current state of the LSTM network. $p(t)$ is the kinematic parameter to be estimated (tip position for our case)

and $F(t)$ is the estimated force. Note that input components are the same for both the kinematics and force estimation. Therefore it is possible to perform both kinematic and force sensing at the same time

5.1.1 Fabrication of the sensors

Biological skin contains a dense, distributed network of a large variety of interspersed sensors [162]. In our system, we mimicked the biological anatomy with three soft cPDMS sensors. The sensors were placed arbitrarily along the length of the finger when the finger was being cured (Figure 5.3).

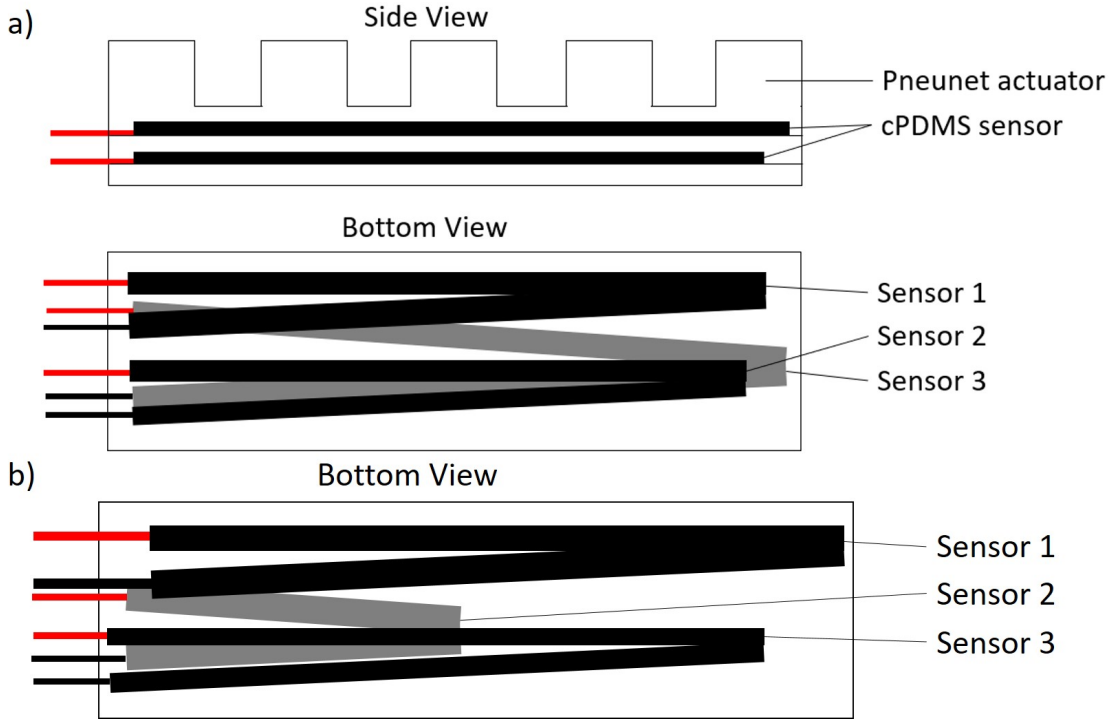


Figure 5.3: a) Schematic of the strain sensors embedded into the 1-DoF actuator and the 2-DoF-serial actuator. All three sensors are intentionally depicted with arbitrary lengths and shapes to highlight that the sensor geometry can be similar, but does not need to be precise. b) Schematic of the strain sensors embedded into the 2-DoF-parallel actuators. The three sensors have different sizes and positioning within the actuator to highlight that the sensor geometry can also vary dramatically. Note that the effective length of the sensors depends on the length of the center cut.

We made the soft sensors from patterned conductive-polydimethylsiloxane (cPDMS) traces (Fig. 5.4). First, we dispersed multiwall carbon nanotubes (MWCNT) (30-50 nm diameter, Cheap Tubes, Inc.) in PDMS base (Sylgard 184, 3M) to achieve 14% MWCNT loading by mass by mixing in a Speed Mixer for 20 minutes. We poured a thin layer of silicone elastomer (Dragon Skin 10, Smooth-On Inc.) onto a rigid substrate to form the lower layer of the sensing skin. We thoroughly coated the cPDMS onto the surface of the base silicone layer to ensure that there were no gaps. Then, we placed silicone-insulated wires with exposed leads onto the uncured cPDMS and poured a second layer of silicone elastomer on top to seal the conductive material inside. The cPDMS layer and the second layer of silicone elastomer was then cured at room temperature for about 6 hours.

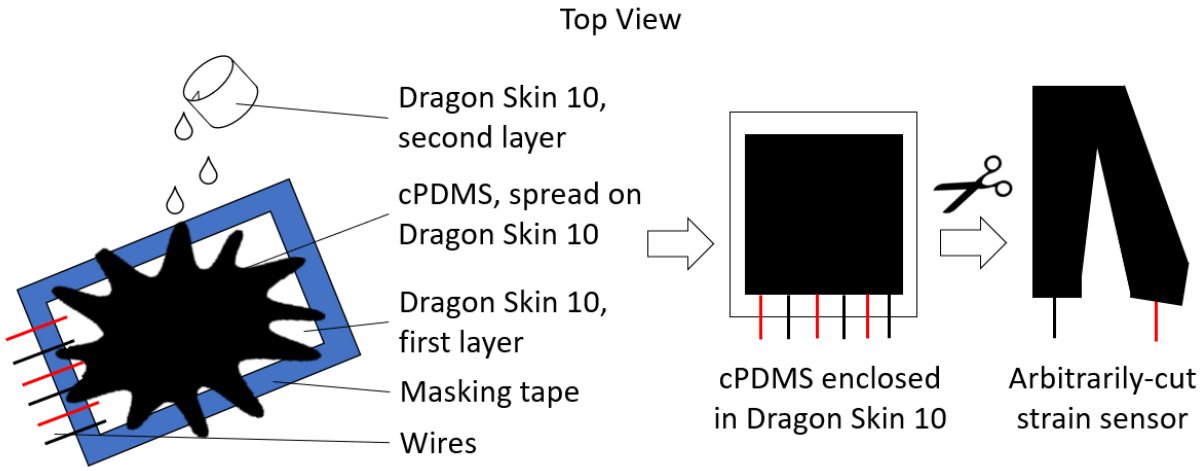


Figure 5.4: Schematic of sensor fabrication process. We embedded conductive silicone within non-conductive silicone and cut out arbitrarily shaped sensors.

From this sheet of cPDMS sensors, we then cut out the desired geometry of the sensor manually. The resulting thickness was approximately 3 mm. The ability to learn the material properties enables us to trade off precision in the fabrication for time and pay less attention to uniform thickness or orientation of the sensors within the finger. This makes the sensor fabrication process more general and scalable than previous approaches to fabricating cPDMS sensors [15] as we can avoid the step of sensor masking.

In the Results Section, the Sections on Kinematic Modeling, Force Modeling, and Graceful Degradation were done with a 1-DoF actuator which has a single pneumatic chamber. The Section on Multi-Degree of Freedom System was done with both a 2-DoF-parallel actuator (Fig. 5.5a) and a 2-DoF-serial actuator (Fig. 5.5b), both of which had two pneumatic chambers but inflated in different ways due to the alignment of the chambers. In the 1-DoF actuator and the 2-DoF-serial actuator, all three sensors had dimensions of approximately 110 mm x 25 mm x 3 mm, with intentional, minor differences in each sensor. In the 2-DoF actuator, the three sensors had dimensions of: 70 mm $\times$ 20 mm $\times$ 4 mm, 120 mm $\times$ 26 mm $\times$ 4 mm, and 103 mm $\times$ 27 mm $\times$ 4 mm.

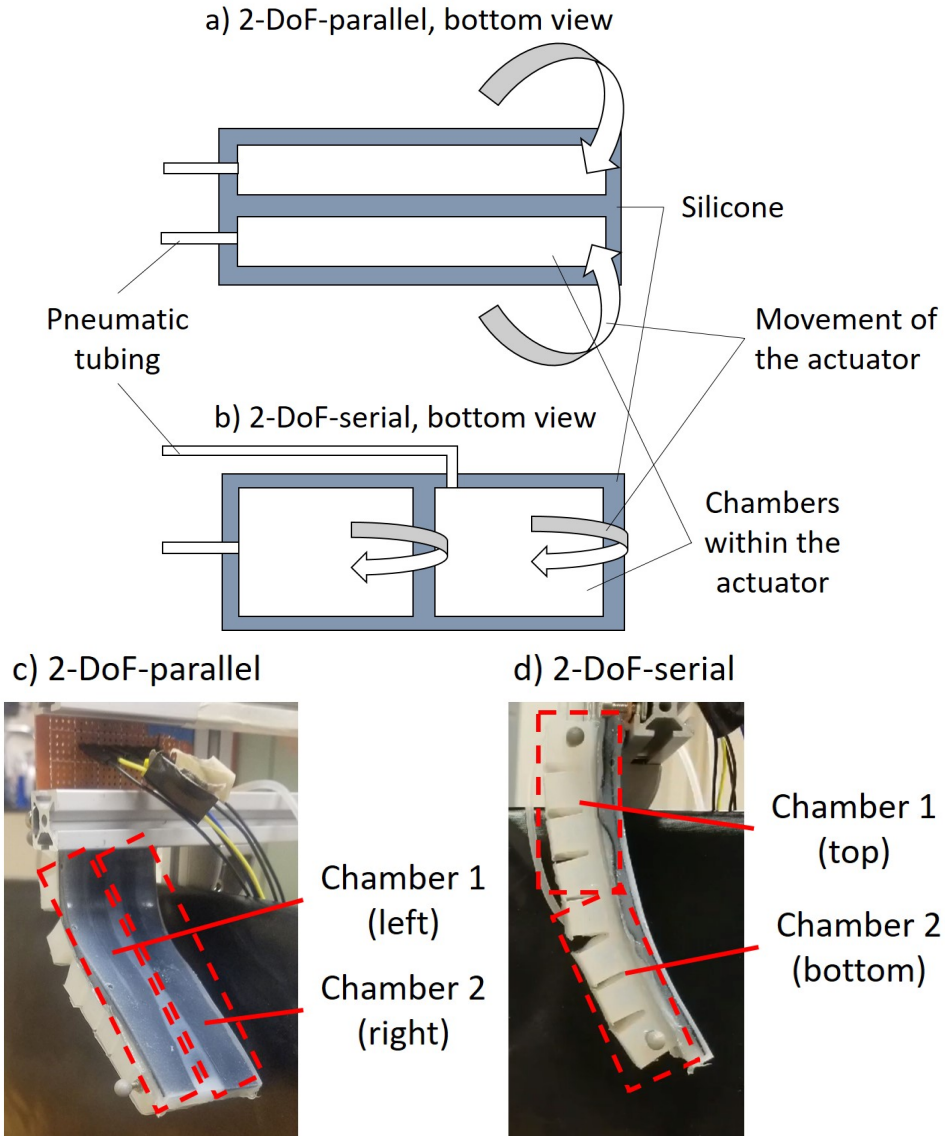


Figure 5.5: Schematic of the motion of the 2-DoF actuators. a) 2-DoF-parallel actuator, with two chambers in parallel along the axial length (left and right). Inflation of either chamber results in non-planar motion, as compared to the 1-DoF actuator. b) 2-DoF-serial actuator, with two chambers in series along the axial length (top and bottom). Inflation of either chamber results in planar motion. In both types of actuator, the two chambers are controlled with independent inputs. c) 2-DoF-parallel actuator with indicators for the left and right chambers. d) 2-DoF-serial actuator with indicators for the top and bottom chambers.

5.1.2 Fabrication of the actuators

We fabricated the actuators by casting silicone (Dragon Skin 20, Smooth-On Inc.) with 3D printed molds (Veroclear, Stratasys Objet350 Connex3) [15]. After molding the chambers of the actuator, we embedded and bonded the sensors to the bottom of the actuator, and sealed off the chambers by submerging in additional silicone. With the chambers fully sealed, we then inserted silicone tubing to enable inflation of the chambers. The wires for the sensors were then soldered to a PCB which provided mechanical stability for the connections and header pins to connect the electronics. The overall dimensions of the actuator are 120 mm x 35 mm x 25 mm.

5.1.3 Experimental setup

Our analog to the visual feedback used by many animals is a motion capture system (OptiTrack Prime 13, NaturalPoint Inc.). We used two OptiTrack cameras to provide ground truth validation for the position of the finger in the real world. We placed infrared tracking balls for the motion capture system at the base and tip of our pneumatic actuator with embedded sensors. All the coordinates of the finger tip was measured with respect to the base coordinates. We mounted the actuator onto the front of a metal stand (80/20, McMaster-Carr), such that two reflective markers affixed to the base and tip of the actuator were visible from the front (Figure 5.1). For the force sampling we used a compression load cell (FX1901, TE Connectivity).

Then, we connected the finger to a volumetric control system designed to apply commanded pressures to the internal chamber of the actuator [117]. A randomly generated sequence of pressure inputs was sent serially to the control board, which regulates the pressure inside the finger using a low-level PD controller running at 1000 Hz. The pseudo-random sequence was in the form of square wave with a range varying from 0-3.5 bars and a time period of 1 second. The learned model uses these reference pressure values along the actual sensor readings for kinematics and force predictions. We assumed that the actual pressure values inside the finger were similar

to the reference value. For real-time testing of the learned model, a new random sequence was send to the volumetric control system.

The sensors were connected to a LCR meter (Keysight, E4980AL), which provided high precision measurements. The measurements were made using AC signals of 300 kHz. Both the resistance and reactance of the sensor was measured and used for prediction. As the meter only had a single input, we first connected the embedded sensors to a multiplexer circuit. The three sensor measurements were obtained at 10 Hz. The marker coordinates and force readings were also resampled to 10 Hz. A schematic of the whole setup is shown in Figure 5.6.

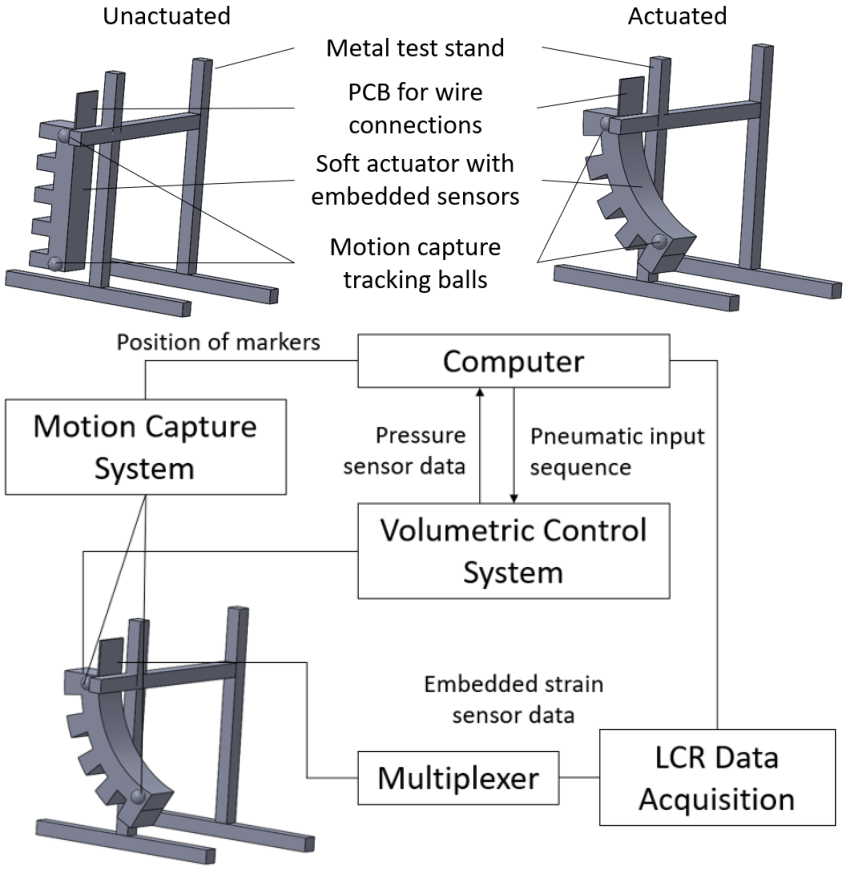


Figure 5.6: Schematic of the experimental setup.

5.1.4 Sampling for kinematics and force modeling

The samples for learning the kinematic model and the force model were obtained using the same setup. For the kinematic model, the marker information from the motion capture system and the corresponding sensor data was required for different kinematic configurations. To obtain this, the finger was occasionally brought in contact with a fixed line contact at two different locations (Fig. 5.7). Since the external contact was fixed, the finger was still completely free to move in the other direction. The contacts were designed to touch the finger at the tip and at a point near the center of the continuum finger. The timing, duration, and location of the external contact was randomized to avoid biases. The sampling was continuous and the data was not shuffled for learning. This is important to keep the temporal information intact. For force modeling, the external contact at the tip was integrated with a load cell (see figure 5.8).

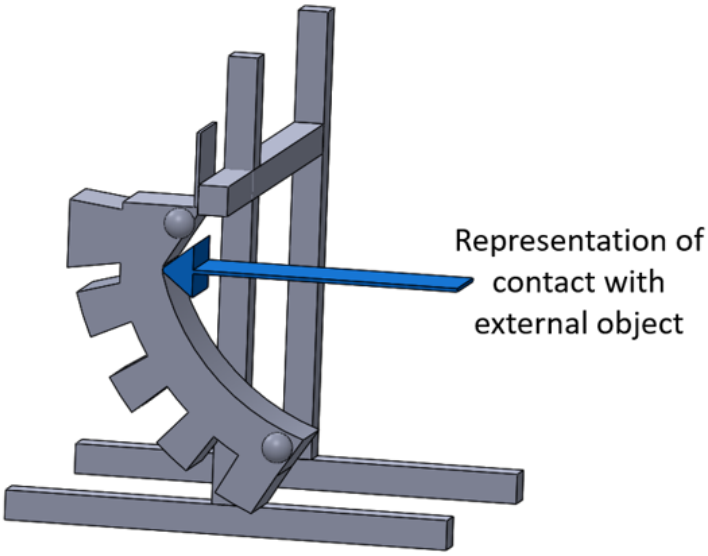


Figure 5.7: Diagram showing how contact along the continuum of the actuator results in a deformation that propagates throughout the system.

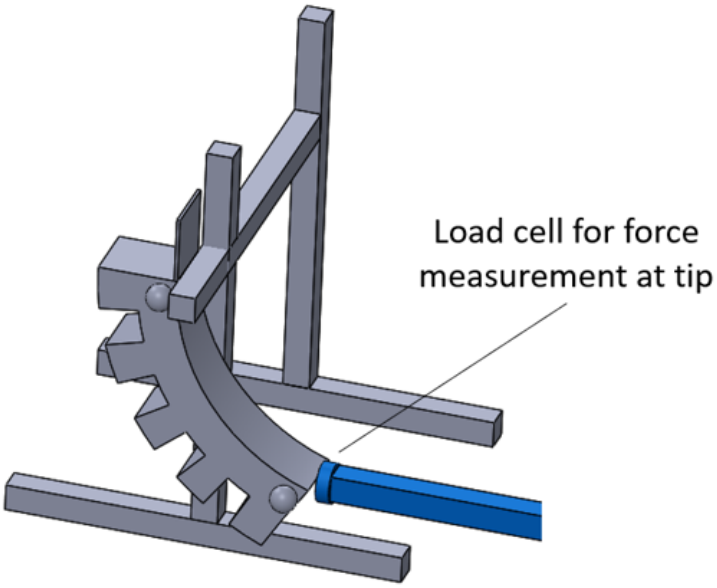


Figure 5.8: Diagram of how we obtain the force measurement at the tip of the actuator using a load cell.

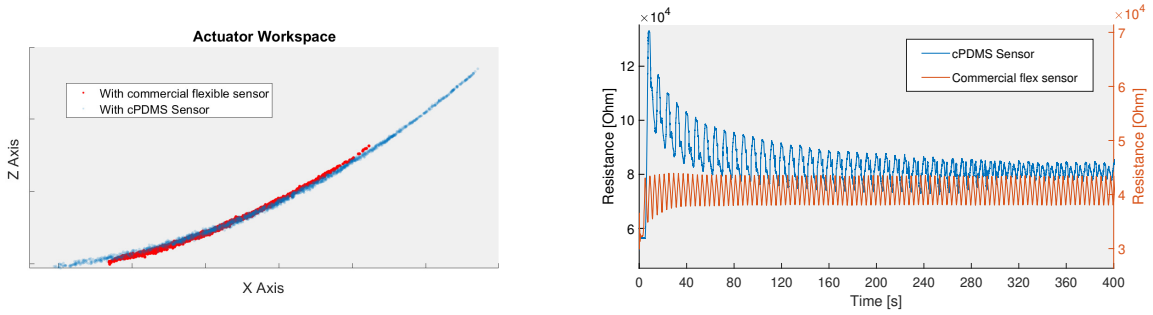
5.1.5 Long short-term memory for non-linear, time-varying material characteristics

Long short-term memory (LSTM) networks are a class of recurrent neural networks widely used for time series predictions [173]. We used the LSTM network provided by the MATLAB deep learning toolbox for creating our network. For all the trained networks, both for the cPDMS sensor and commercial flex sensor, we used the same network parameters. An LSTM layer size of 100 was taken with a dropout layer preceding the LSTM layer. The dropout rate was kept high at 0.5 for the graceful degradation test and at 0.1 for all the other tests. A fully connected layer which multiplied the output of the LSTM layer by a weight matrix and then added a bias vector provideds the final output from the network. L_2 regularization was also used to prevent over-fitting. The training data was normalized and split into two continuous blocks in the ratio 80:20 for training and testing. The network parameters were optimized using the *Adam* algorithm [174]. The mini batch size was 512.

5.2 Results

5.2.1 Kinematic modeling

To demonstrate the potential of the proposed methodology for full-body kinematic estimation, we performed a fundamental test from which scalability was evident. The test involved the finger following a random actuation pattern while being obstructed at unknown times by two fixed-point contacts. The height of the obstacles were fixed, but their placement along the X-axis varied. One contact was enforced at the tip of the finger and the other at an arbitrary location along the length of the finger. The same experiment was repeated with a finger where the soft cPDMS sensor was replaced by a commercial flex sensor. No adjustment to the learning approach was required in this case since it is agnostic to the type of sensors. In fact, kinematic estimation with the flex sensor was more accurate for the no-contact case due to the absence of any temporal nonlinearities (Figure 5.9b), but the high axial stiffness of the flex sensor reduced the effective compliance of the finger, thereby reducing the reachable workspace of the finger (Figure 5.9a).



(a) (b)

Figure 5.9: a) Difference in workspace, demonstrating how the sensor significantly affects the finger dynamics b) Drift effect prominent in the soft cPDMS sensor. The readings are shown for a cyclic activation of the actuator.

The training performance of the LSTM network is shown in Table 5.1 and the real-time test performance is shown in Figure 5.10. The number of samples required for the cPDMS sensor

Table 5.1: Training performance of the kinematic model.

Parameter	**cPDMS**	**Commercial flex sensor**
Samples	29000	10000
Training Error	$2.32 \pm 2.06mm$	$1.08 \pm 1.11mm$
Test Error	$3.58 \pm 2.83mm$	$1.69 \pm 1.51mm$

was higher than for the flex sensor. The reason higher samples are required for the cPDMS sensor is solely because drift is a slow dynamic process. As normalization of the data is performed using the sample data, it is necessary to make sure that the sensor reaches the 'boundaries' of working limit. Otherwise, during the testing phase the learned network would get saturated when the sensor readings go outside the sample ranges. The sampling rate was 10 Hz, so the whole sampling period for training lasted about 50 minutes. As expected, the prediction using the flex sensor was more accurate even during training and the real-time testing phase without contact. However, the prediction performance deteriorated upon contact. The soft sensors, on the other hand, performed consistently for all three cases. The trajectory of the finger tip and the predicted positions are shown in Figure 5.11b. A notable characteristic of the cPDMS sensor was the slight phase lag of the predictions. This could be due to the slower dynamics of the soft sensor [58] compared to the dynamics of the finger itself. Therefore kinematic information from body would become observable through the sensor only after a delay. This phase delay was not observed in the stiffer commercial flex sensor. The real-time test results were measured for a period of 20 seconds for each scenario. The error plots for both the test are shown in Figure 5.12. For scaling the current setup to accommodate more points of contact, we would need to embed more sensors and devise more training scenarios.

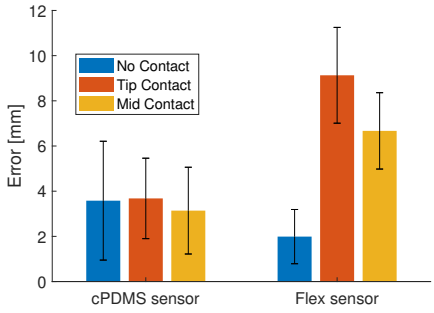


Figure 5.10: Real-time performance.

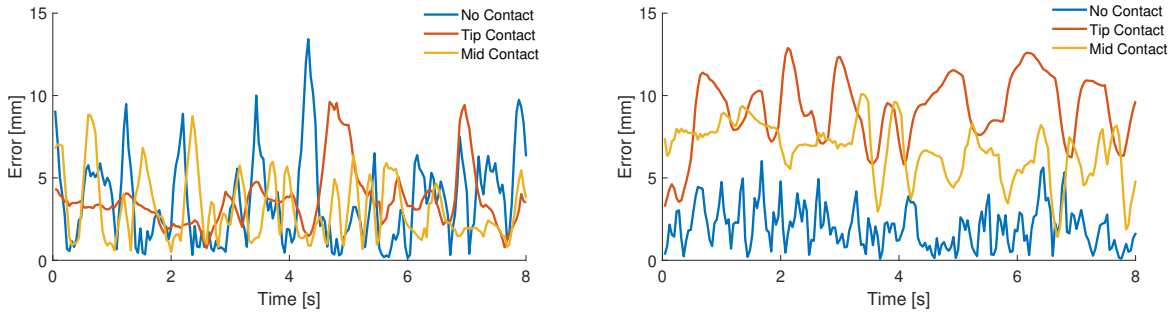
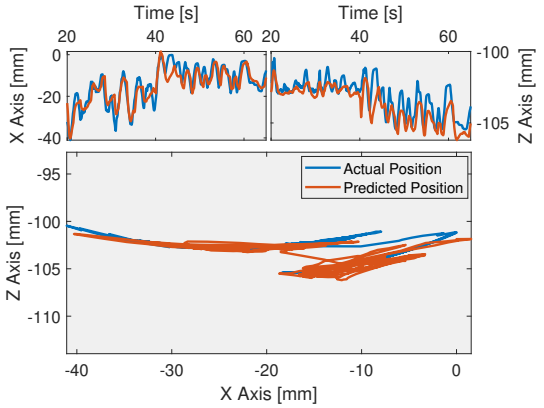
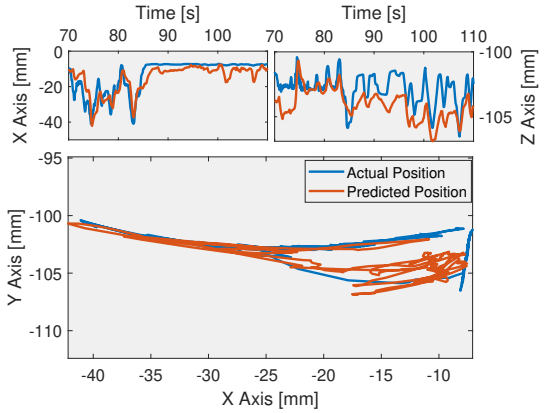


Figure 5.12: a) Error plot for tracking with the soft cPDMS sensor b) Error plot for tracking with the commercial flex sensor.

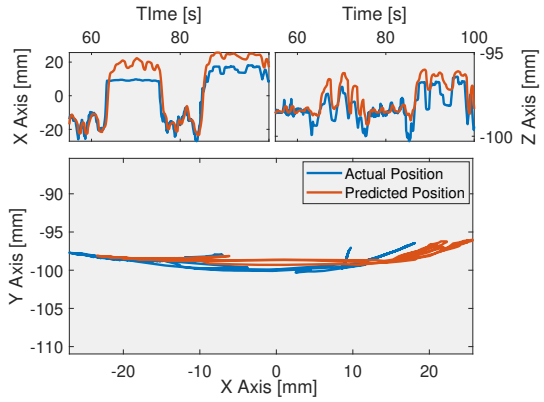
It is noteworthy that even after being constrained at the tip from one side, the soft cPDMS sensors still respond to actuation inputs, because of internal stress induced by the pneumatic pressure. This was not evident with the flex sensors because of the increased axial rigidity of the finger itself (Figure 5.13). Similarly, the independence of the three flex sensors was affected because of this unresponsiveness to contact (Figure 5.14). Thus the predictions with the flex sensor were more error prone to errors when in contact.



(a)

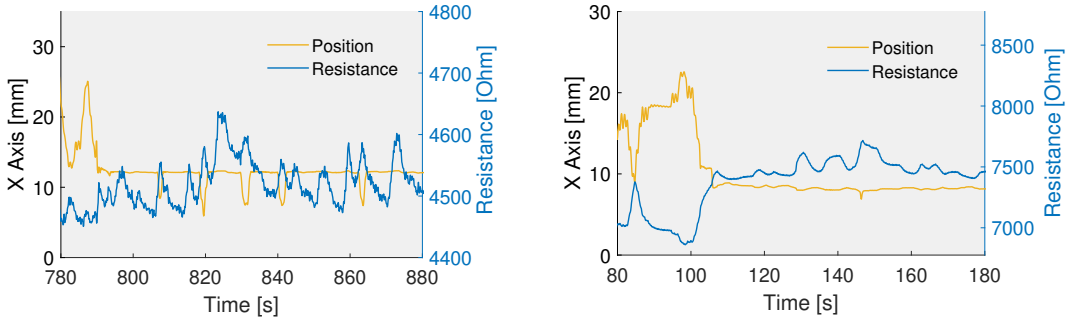


(b)



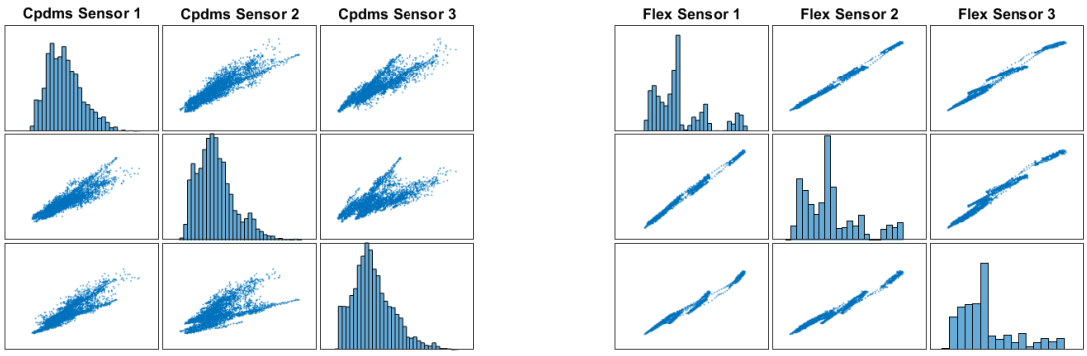
(c)

Figure 5.11: a) Predicted motion of the tip of the finger with the cPDMS sensors. The case of applying contact around the center of the finger is shown. The tip was still free to move after the constraint was applied but the kinematics changed. b) Predicted motion of the tip of the finger with the cPDMS sensors. The case of applying contact around at the tip of the finger is shown. c) Predicted motion of the tip of the finger with the flex sensor. Both cases of contact— one at the tip, and the other near the center of the finger— are shown. The first constraint was at the tip and the second constraint was near the center of the finger.



(a) (b)

Figure 5.13: a) Response of one among the three cPDMS sensor embedded in the soft finger to tip contact. The tip contact blocks the finger stopped it from moving in the positive X-axis direction b) Corresponding response of the flex sensor to tip contact



(a) (b)

Figure 5.14: a) Scatter plot matrix of the cPDMS sensor during a contact experiment with the diagonals showing histogram of resistance values and off-diagonals showing the scatter plots of two sensors for each discrete time period. Linearly uncorrelated information is observed from the three cPDMS sensors during the contact tasks. Note that if there are no contacts all the three sensors will be linearly correlated. b) Scatter plot matrix showing linearly correlated information from the three flex sensors during the contact tasks.

5.2.2 Force modeling

The force prediction model was learned using the same methodology, but we replaced the position signals with the forces applied by the tip of the finger. The tip forces were measured in the X-axis direction (i.e. parallel to the direction of travel of the tip of the finger in its resting

state) using a single axis load cell, and a total of 9500 samples were obtained for training. The inputs to the LSTM network remained the same as the kinematic model. The sampling rate was also kept the same at 10 Hz. The average force prediction error for the first 40 seconds of the real-time test was found to be 15.3% with respect to the total range. The prediction and error plot of the same test is shown in Figure 5.15. An additional uncalibrated test with a human hand was performed to ensure that the learning was not specific to the setup. The learned model performed with an average error of 0.05 ± 0.06 N in estimating the magnitude of error and to detect the onset of contact (implicitly), however, the system had exhibited a delay in detecting the cessation of contact. Similar phase lags observed in the kinematics estimator were also observed for this case.

The supplementary video, Movie S8, shows that the setup could theoretically be used for force prediction anywhere along the finger, but did not measure the exact magnitude of the applied force at every location with the current number of sensors. The actuator can respond to contact anywhere along the body because a single sensor runs along the body. This is one of the advantages of indirect force sensing. Direct force sensors, on the other hand, would not be responsive to contact in other locations. With more sensors, the methodology could be extended to estimate the exact magnitudes along the arm. Note that we do not need to explicitly mention the location of the contact for learning. Adding the fact that learning algorithms have very good generalization ability, we suspect that a few cases of contact would be sufficient to develop an approximate full body force estimate.

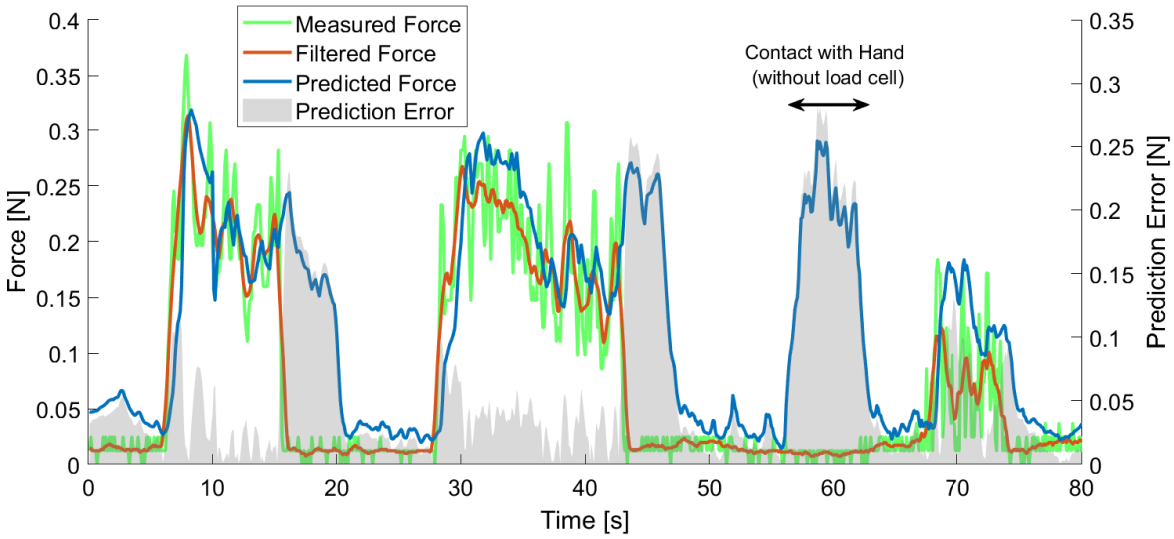


Figure 5.15: Force prediction at the finger tip. The raw load cell readings are filtered with a simple moving average filter with a one second window. External hand contact without the load cell is also shown.

5.2.3 Graceful degradation

Biological systems typically exhibit redundancies in their sensing modalities, which allow the organism to function despite damages to subcomponents of the system. This concept of graceful degradation suggests that we can use redundancy in the soft sensor network to maintain functional performance despite damage to the individual sensors. For the task of predicting the position of the tip of the finger without contact, our sensory architecture was redundant. Therefore, with appropriate training, the learned model could be made more robust to the loss of sensory information. We achieved this by increasing the dropout rate during training while using a small LSTM network. We expected, however, that this would reduce the accuracy of the model.

Here we show the results of fundamental tests to observe the predictive power of the pre-trained network in the face of abrupt loss of sensory information. All the results were obtained using the training data itself. For practical reasons, we were unable to physically remove sensors from the setup for real-time testing. To virtually simulate the removal of sensors, we set each row of our inputs to zero during the simulated test phase. The loss in accuracy in response to

sensor removal is show in figure 5.16. For both the cPDMS and flex sensor, a gradual decrease in accuracy can be observed upon virtual removal of each sensor and each combination of sensors. For the cPDMS sensors, each of the sensors appeared to contribute equally to the predictions. This can also be observed from the error distribution in the workspace (Figure 5.17a). Interestingly, the pressure information plays a significant role in prediction for the cPDMS sensors. This is because the pressure information plays a vital role in compensating for sensor drift. A model trained with a short training sample without pressure information shows significant drift in the test phase, whereas a model trained with the same data and pressure information is able to compensate for the sensor drift (Figure 5.18). Small variations in the performance of the model among sensors can be attributed to their signal to noise ratio and the variabilities in training. The same comparison for the contact scenario leads to drastic performance degradation (Table 5.16) and clear error distributions in the workspace indicating how each sensor contributes uniquely for different tasks (Figure 5.17b).

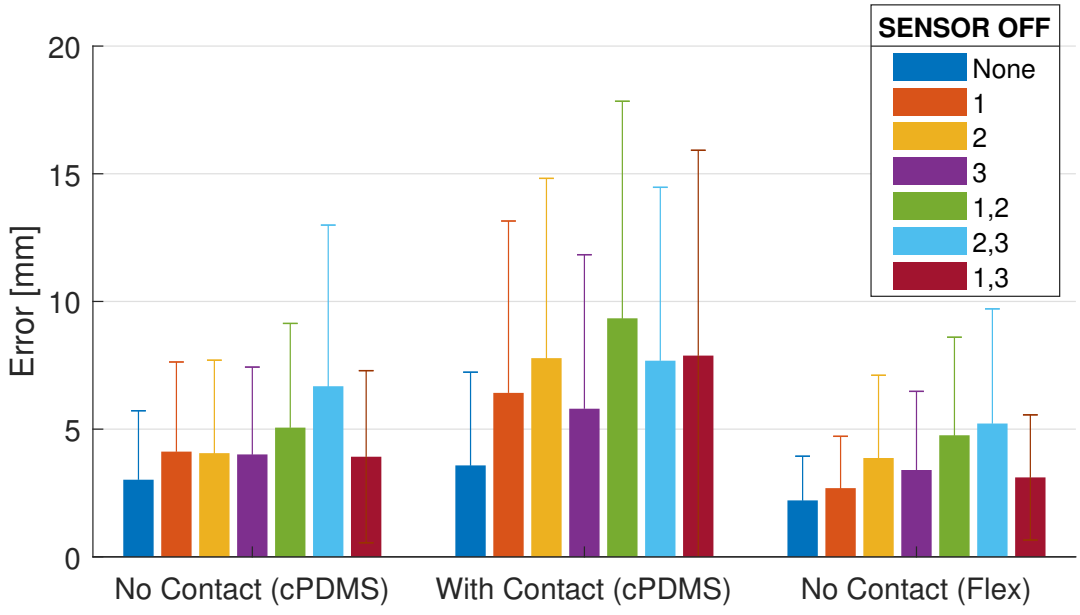


Figure 5.16: Test accuracy with virtual sensor removal. The performance is affected only a little when one of the sensor information is lost for the 'no contact' case. The accuracy is significantly affected even with one sensor removal for the 'with contact' case.

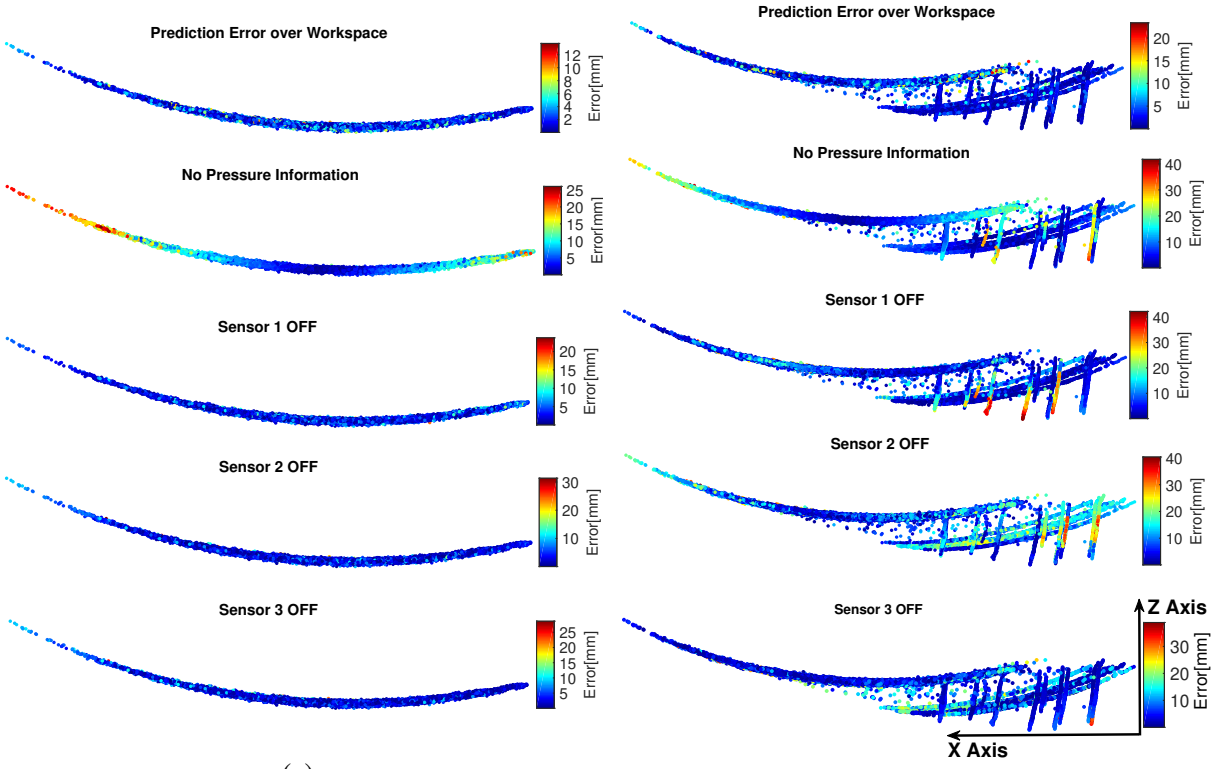
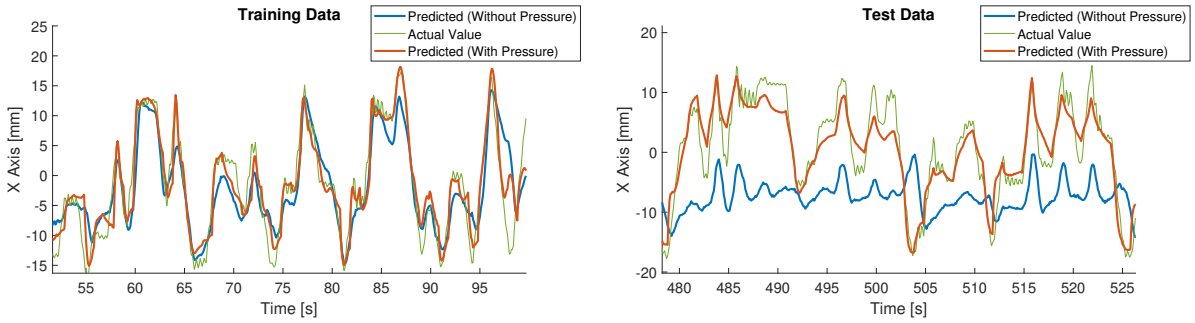


Figure 5.17: a) Division of labor among the sensors. For the case without contact, all the sensors have equal contribution to the underlying model. Hence, removing any one of them affects the prediction error slightly but equally in the workspace. For this case, removing the pressure information drastically reduces the accuracy, showing how motor action information is also important for accurate proprioception. b) Division of labor among the sensors once in contact. Here we can see clear division of labor among the sensors as there are no redundant sensors. Each sensor is 'specialized' to a particular kinematic case as can be seen from the error distribution in the workspace. Also, once in contact, the action inputs are not useful for proprioception.



(a) (b)

Figure 5.18: a) The performance of the learned model on the training data with and without pressure information b) The prediction errors on the test set deteriorate for the model without pressure information.

5.2.4 Multi-degree-of-freedom system

To validate the performance of the sensing methodology on a more complex system, we replicated the tests on two 2-DoF actuators. The 2-DoF-parallel actuator (Fig. 5.5a) is a non-planar 2-DoF actuator and the 2-DoF-serial actuator (Fig. 5.5b) is a planar 2-DoF actuator. The methodology remained the same, with identical actuator geometry for better comparison to the 1-DoF system. We demonstrated that this methodology worked for different sensor geometries by also testing variable sizes of sensors on the 2-DoF-parallel actuator. 10000 samples were obtained for each of the actuators for the kinematics estimation. The data is divided in the ratio 80:20 for training and testing and validation performances are measured on the test set. The non-planar actuator had a prediction accuracy of 2.43 ± 2.18 mm, while the planar 2-DoF actuator had a prediction accuracy of 2.17 ± 1.65 mm.

5.3 Conclusion and future work

This chapter presents a generalizable, model-less technique for real-time perception for a soft actuator using embedded soft sensors and recurrent neural networks. We followed a bio-inspired approach both for the hardware and software components. This allowed us to achieve

an accurate kinematic model of a soft finger even with highly nonlinear sensors. Although more accurate predictions were obtained with commercial flex sensors, their relative rigidity and in-extensibility made them undesirable for high dimensional deformations. With our proposed methodology, we demonstrated how full-body kinematic models could be learned. Additionally, following the same methodology, the system learned models of externally applied forces using the stress-strain relationship of the soft body. We validated the approach for a fundamental test, using a fabrication approach for which scaling to large numbers of sensors could be assured. We were able to accomplish this with irregularly shaped strain sensors. Due to the continuous distribution of the sensing module and the learning process, we can easily adjust the location of sensing. Due to our reliance on a pure learning-based model, it was possible to fuse the measured information from the sensors with the commanded information to the pressure regulators to achieve more accurate models. The role of action in perception is also a phenomenon observed in biological systems [162]. The methodology is highly generalizable with the ability to interchange sensors, mode of sensing and the system itself without any changes to the learning algorithm. Finally, we explored how sensor redundancy can make the system more robust to unexpected changes to the system.

Learning based approaches are very useful for modeling with minimal knowledge about the system, however, they also have inherent drawbacks. For example, these approaches do not afford the designer any physical intuition about the system. Thus, further analysis, for example to determine the optimal shape, placement and number of sensors, would be difficult, as would describing and correcting for sources of error. For this study, we used LSTM networks for training our time-dependent model. Although it is possible to train the same model with feedforward neural networks using appended input sequences, this makes the model memory inefficient [175]. Moreover, there is an additional step where the user has to hand-tune the fixed-input time-lags. Compared to other recurrent neural network architectures, LSTM was chosen mainly because of the ease in training LSTM networks for long time-lag tasks [173].

However, with the advancements in training recurrent neural networks, it would be meaningful to investigate other recurrent architectures.

The approach described here is demonstrated on a planar soft finger with only three embedded strain sensors. The main bottleneck for scaling to a larger number of sensors was the serial nature of the multiplexer circuit that we used to read the sensor signals from a single, high-precision inductance-capacitance-resistance (LCR) meter. This also led to signal mixing because of ghosting (or crosstalk) effects that became more prevalent at higher sampling frequency. Due to this, our sensing system had a maximum sampling rate of 10 Hz. Although 10 Hz was sufficient for this iteration of our experimental tasks, it will be insufficient for more dynamic tasks or actuators with additional degrees of freedom. This issue could be solved with improved data acquisition methods with multiple analog-to-digital channels.

A source of error for the cPDMS sensor was the lag of the predictions behind the actual values. The lag is not observed with the commercial flex sensor, which means it can be attributed to the slower dynamics of the soft, cPDMS sensor [58]. Nevertheless, this would affect the applicability of using embedded sensory feedback for highly dynamic tasks. Interestingly, devoid of the visual feedback system, the human proprioceptive system is also susceptible to erroneous drifts [176] and biases [177]. An important question to be investigated is whether the slow sensory response is intrinsic to all 'soft' sensors or whether it is due to the internal mechanics of our cPDMS sensor. A potential avenue towards improvement of the intrinsic errors in our cPDMS sensors could be to experiment with non-polymer-based materials, which may exhibit less significant time lag compared to cPDMS due to the molecular structure of the conductive material. However, the alternative sensor materials have their own challenges as discussed in the introduction.

Although our complete methodology closely resembles the human perceptive system, our reference feedback loops are well structured when compared to the biological counterparts. The tracking system and the load cell we use as ground truths provide physically meaningful

outputs that can be easily learned in supervisory manner using the LSTM network. However, in the human perceptive system, we map our sensor signals with multimodal raw signals coming from the ocular, vestibular, auditory, and muscular systems. For simplicity, we pre-process the raw images and force readings coming from the reference systems to obtain physically relevant variables. A faithful end-to-end replication of the human perceptive system, on the other hand, would require a direct mapping from the sensory space to the image space. This introduces additional complexities in the form of object recognition, calibration and coordinate referencing. The constant presence of the visual, inertial and auditory feedback is also important for adaptation in case of drastic system changes [162, 178]. Our methodology currently relies on independent external sensing technologies for reference feedback, which have to be removed for real world applications. However, if the entire system undergoes permanent physical changes like growth, stiffening, material deterioration, etc., the learned model would display biases. Hence, a potential future endeavor would be to integrate other sensing modalities like vision, inertial measurement units and force sensors directly into the soft system.

Chapter 5, in full, is a reprint of the material as it appears in T. G. Thuruthel*, **B. Shih***, C. Laschi, and M. T. Tolley, "Soft robot perception using embedded soft sensors and recurrent neural networks,", **Science Robotics**, 4:26, eaav1488, Jan 2019. The dissertation author was the co-primary investigator and author of this paper.

Chapter 6

Learning variabilities in materials and manufacturing for the control of soft robots 3D printed from TPU

Soft robots have great potential to solve a variety of challenges in many applications including manufacturing, healthcare, and environmental monitoring. 3D printing enables the rapid manufacture of soft robots customized for a specific task or user. However, variabilities in materials and manufacturing greatly limit our ability to design consistent controllers for soft robots. We propose to address this challenge by developing a learning method for the control of soft robots that takes into account experimentally determined material and manufacturing process variables, as well as knowledge gained in previous learning efforts for the same design. The result will be a general approach to learning controllers for soft robots that greatly expands the usability of these devices.

6.1 Customized soft robots enabled by 3D printing

3D printing technology has expanded substantially in recent years. Studies by Deloitte predict that enterprise 3D printers, materials, and services will surpass $3 billion in 2020 [179]. This method of rapid fabrication has improved our ability to design and fabricate functional devices and robots, at all levels of expertise and in various settings. In parallel with the growth of 3D printing, soft robotics has emerged as a promising application area for these rapid fabrication methods. Soft robots are systems that take advantage of material properties such as non-negligible compliance to simplify automation tasks or even automate tasks that were previously impossible [36]. These systems typically rely on pneumatic or hydraulic pressure for actuation, although smart material actuation is also possible. Promising areas of application include product handling [180, 181], medical devices [182], environmental monitoring [183, 184], and wearable devices for haptics [185] or rehabilitation [81]. Since complex and/or custom geometries are often required for soft robotics, the ability to 3D print soft robots is a key enabler [52, 105, 186].

However, material and manufacturing variability limit the reproducibility of soft robots. While 3D fabrication design files can be rapidly sent across the world, differences in manufacturing, such as environmental conditions that are challenging to control for including temperature, humidity, ambient pressure; and variability in material parameters quickly compound to affect the performance of soft robots. Since the performance of soft robots often depends directly on the intrinsic stiffness of their constituent materials and the effective stiffness of the manufactured designs (rather than just having a lower limit on stiffness, as in the case of rigid robots), they can be highly sensitive to these changes in materials and manufacturing.

Despite the additional variance compared to rigid systems, soft materials are growing increasingly popular in the robotic manipulation sector because there are several objects in settings such as industrial warehouses that may require a high degree of customization. Depending on the specific objects, these warehouses may want to design, fabricate, and control their own custom

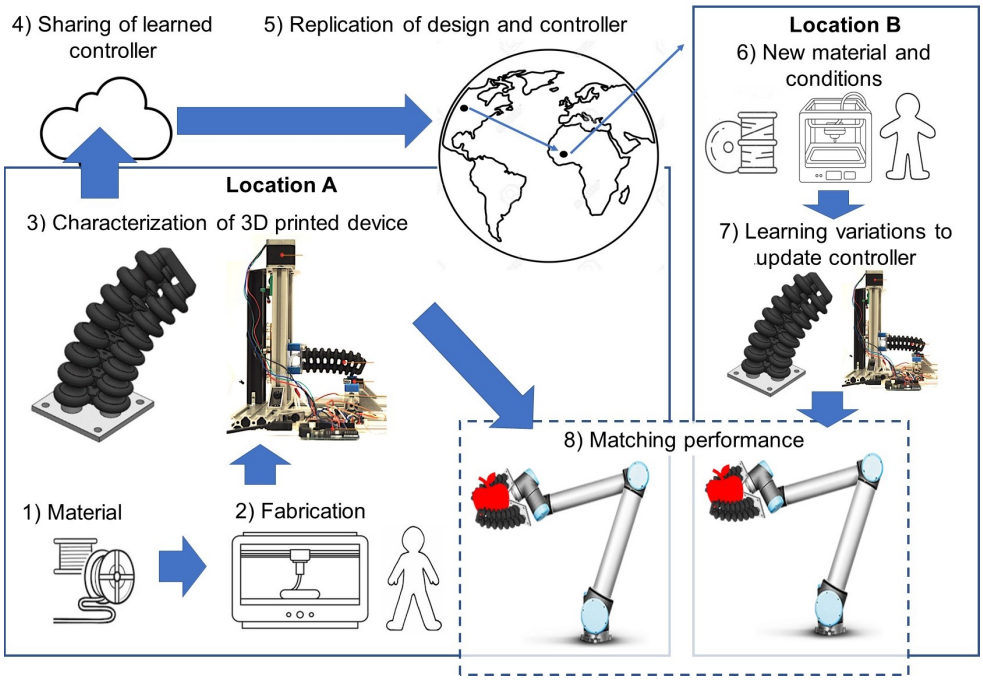


Figure 6.1: Envisioned behavior synchronization process for soft robotic actuators. 1,2) Initial user designs and manufactures a soft robotic actuator using her own materials and fabrication processes. 3) Initial user characterizes material properties and collects training data for her design. 4,5) The initial user uploads her material properties and trained model to a cloud network. 6,7) In other locations around the world, additional users receive identical digital copies of the initial user's design and fabricate their own copies. 8) The additional users download the material properties and trained model, which enables them to train their own model that remotely synchronizes the performance of their actuator to that of the initial user's. Subsequent data is fed back to the cloud for federated (collaborative) learning. 9) Users all around the world now have personalized controllers for performing identical tasks, despite variations in their individual materials, 3D printers, and manufacturing methods.

grippers that they make on site. In general, deformations resulting from physical contact are challenging to model analytically and computationally because of the numerous cases in which the contact can occur. Additionally, soft materials have the potential to reduce the computation complexity of interacting with delicate objects or humans due to their material compliance. In a previous study [11], we demonstrated that for soft materials, temporal-based machine learning techniques are capable of modeling arbitrary contacts. However, using this approach broadly would require re-training controllers for each device manufactured, which would be

computationally and experimentally expensive.

To address these challenges, we propose a method to compensate for varying inputs (materials and manufacturing conditions) to achieve identical outputs across multiple actuators and systems This method will enable any user to decouple the effects of variabilities in the performance of soft actuators introduced by manufacturing and materials and synchronize the performance of soft robotic actuators despite nuances in their performance and behavior. The goal is to improve the controllability of soft actuators by characterizing variabilities in both manufacturing and materials and incorporating this learned information into the control models.

Chapter 6, in part, is being prepared for submission for publication of the material. The dissertation author is the primary investigator and author of this paper.

Chapter 7

Classification of components of affective touch using rapidly manufacturable, soft, sensor skins

Affective touches play an important role in everyday communication because a significant amount of human interactions are through physical contacts. To facilitate robust, safe human-robot interactions (HRIs), we require robots with soft skins that can interpret affective touches. In this chapter, we describe the fabrication of rapidly manufacturable, soft sensor skins using liquid metal embedded silicone elastomer as a resistive element and trained a recurrent neural network (RNN) to distinguish between a variety of pokes and rubs from human users. On a 2×2 sensor array, we obtained an average classification accuracy of 97% for ten different types of pokes and rubs, demonstrating that the combination of a soft sensor and machine learning can classify the interactions. Our approach is a step towards intelligent soft robots that can understand social interactions through touches.

Recent work in soft robotics has spanned the design, control, and fabrication of robots using flexible and compliant materials [36, 187]. Many interesting mechanisms have emerged,

such as soft robots that can walk [188] and grasp [189], and the next generation has expanded to include ones that can swim [24], grow [23], and even play an instrument [190]. Within the field, soft sensing has become a desirable goal because of the need for feedback control [191]. Traditional tactile, strain, and pressure sensors often cannot conform to, adhere to, nor model the continuous motions that bioinspired soft robots exhibit, so researchers have built soft sensor skins to address these challenges [1–3, 15, 16, 52, 65]. In addition, machine learning is a useful tool for processing information as sensor arrays increase in density and interactions with the skins increase in complexity [8, 11, 35, 66, 69]. However, there currently still exists a gap between soft robot skins developed in the lab and robots with functional skins in practical applications [42, 191], particularly for processing information related to social interaction.

One area for which soft robots and skins may be especially useful is human-robot interaction (HRI). Collaborative robots that assist people with tasks have been improving in their capabilities and growing in popularity, but most are currently built with rigid materials. In contrast, soft materials provide morphological computation that reduces the burden of exact precision on the control system of a robot, making them safer for human interaction [192]. While physical safety is one element, HRI also includes interactions between robots and humans that may come in several forms including verbal, physical, visual, proximate, and remote [193].

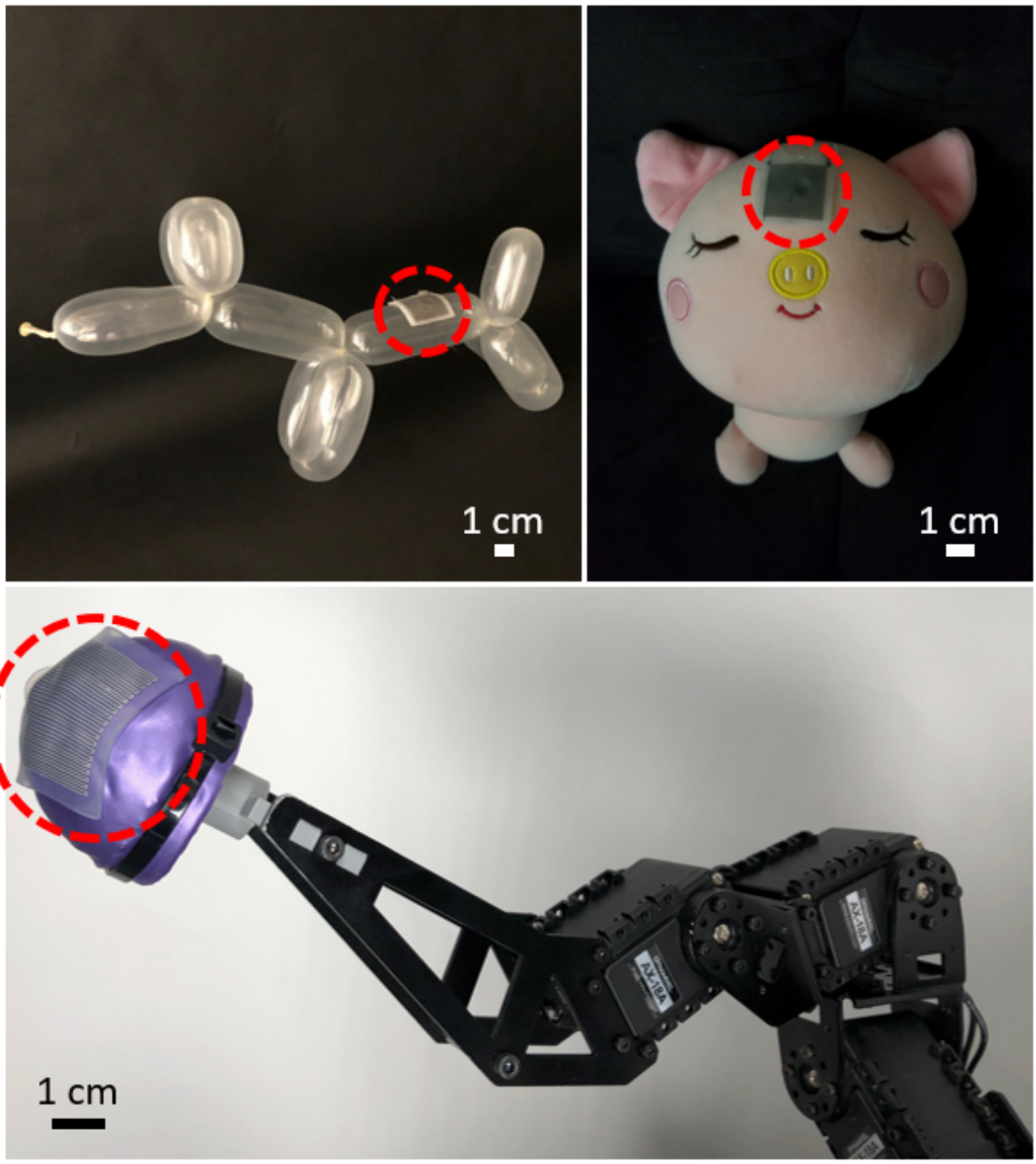


Figure 7.1: Concept figure for rapidly-manufacturable soft sensor skins that can detect and interpret physical contact for human-robot interaction. The soft sensors can classify various types of affective touches (e.g. pokes and rubs) on substrates with different stiffnesses including soft actuators, balloon animals, and stuffed animals. The sensors can provide collaborative, interactive robots and objects with a natural sense of touch and enable them to detect actions such as a pat on the back or head.

In particular, affective touch is social communication through physical interaction and it plays a significant role in our lives. It assists in the cognitive development of young children [194] and can help reduce social anxiety [195]. However, collaborative robots that are soft, safe, and interactive with people have not yet placed an emphasis on understanding and processing affective touch as they interact with humans. In this work, we studied how to use a rapidly manufacturable, soft, sensor array to interpret and classify basic forms of affective touch.

The main contributions of this chapter are:

- A method for classifying pokes and rubs at multiple locations on a rapidly-manufacturable soft sensor skin.
- An evaluation of how performance changes with respect to density of the sensor array.
- A comparison of classification accuracy when the soft skin is on a soft substrate as opposed to a rigid substrate.

Section 7.1 describes the rapid fabrication of soft sensor arrays. Section 7.2 discusses the machine learning tool that we used to classify affective touch. Section 7.3 details our abstraction of a wide variety of affective touches into simplified components for this chapter. Section 7.4 introduces our experiments. Section 7.5 presents our results and discussion. Lastly, Section 7.6 summarizes our findings and future work.

7.1 Design and fabrication of soft sensors

7.1.1 Design

We designed two soft sensors made of silicone elastomer with embedded liquid metal channels, which consist of arrays of various densities. Both the design and fabrication processes are based on previous work by Park et al. [2]. We designed the molds using computer modeling

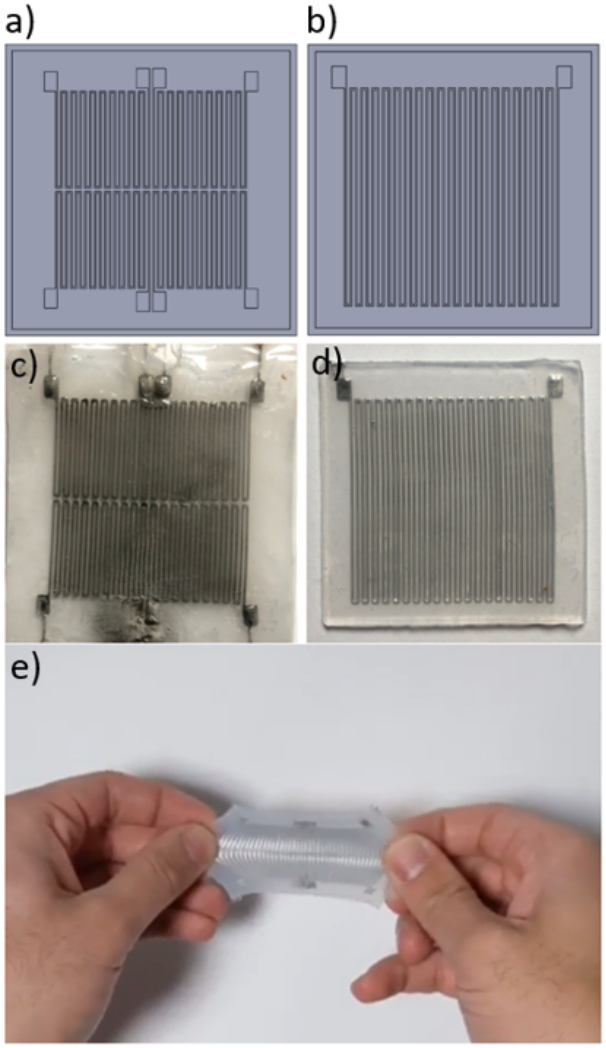


Figure 7.2: Designs of the various soft sensor arrays and the corresponding physical, soft sensors. a, b) Computer-aided design drawings for the 2x2 and 1x1 sensors. c, d) The sensors consist of microfluidic channels filled with liquid metal that are embedded within silicone rubber. e) Changes in the geometry of these sensors—which users can induce via contact, strain, or pressure—result in a change of the resistance. The changes in the resistance within a sensor array enable classification of different types of affective touch.

software (SolidWorks, Dassault) and 3D printed them (Connex3 Objet350, Stratasys). Each sensor has surface area of 30 x 30 mm (Fig. 7.2). The channel thickness of the traces was 0.25 mm and the spacing between the channels was 0.5 mm.

7.1.2 Fabrication

After the printer completed the molds, we heated them at 60C for a minimum of 3 hours to complete the curing of the surface finish. We then casted the bottom layer of the sensor using the 3D printed mold and spin-coated the top layer with a ramp up to 500 RPM over 5 seconds, hold for 30 seconds, and ramp down to 0 RPM over 5 seconds. Both layers were made of silicone (Ecoflex 00-30, Smooth-On). After the top and the bottom layers cured, we bonded the two layers by spin-coating a second layer of silicone on the top layer with a ramp up to 2000 RPM over 5 seconds, hold for 50 seconds, and ramp down to 0 RPM over 5 seconds. Before the second layer cured, we adhered the top and the bottom layers together to seal off the channels.

To fill the channels of the sensors with liquid metal, we covered the sensor on the top and the bottom with glass slides to ensure that the sensor remains level. Next, we inserted needles with beveled tips into the pads for the electrodes. We then filled the channels with Galinstan, an eutectic metal alloy of gallium, indium, and tin that flows in a liquid state at room temperature. Next, we soldered 0.1" spacing header pins to 44 American wire gauge (AWG) copper, enamel-coated wire. We inserted the stiffer, thicker, header pin side of the wire to each contact pad of the sensor electrodes. The electrode pads were then sealed with a silicone glue (Sil-Poxy, Smooth-On, Inc). Finally, we coated the surface of the sensor with talc powder (Clubman powder, Pinaud), which reduced the tackiness of the surface of the silicone.

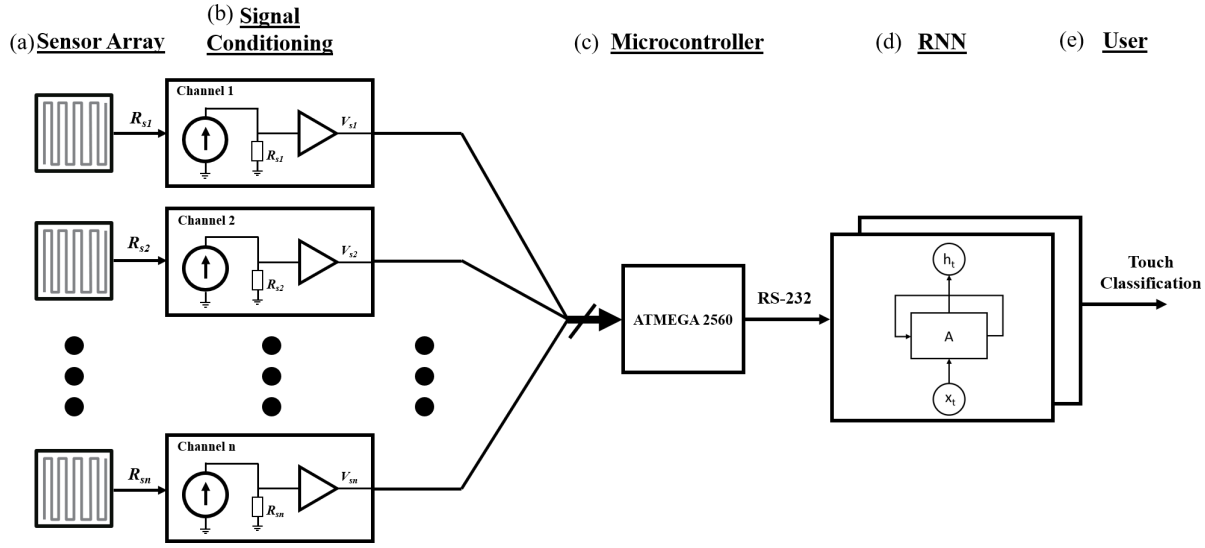


Figure 7.3: Information flow of the data acquisition circuit for a single sensor. a) Individual traces in the sensor array. b) Signal conditioning for the sensors, including a constant current source of 6 mA and amplifier with gain of 50 V/V. c) Data acquisition and serial communication. d) Machine learning for interpreting the signal measurements. e) User interaction and classification of affective touches.

7.1.3 Data acquisition

The data acquisition circuit consisted of a 6 mA constant current source to regulate the power flowing through the liquid metal sensor and a non-inverting amplifier to boost the strength of the signal (Fig. 7.3).

We then connected the sensor readings to the analog-to-digital conversion (ADC) ports of a microprocessor (Arduino Mega, Sparkfun) for data acquisition (Fig. 7.3). The micrprocessor aggregated data at a baud rate of 115,200 bps. We thresholded the data that the ADC collected based on a calibration phase upon startup and only sent data over serial communication when the sensor detected a contact. We then processed the information in software using an open-source machine learning library (Tensorflow in Python, Google).

7.2 Architecture of neural network

A recurrent neural network (RNN) is a type of neural network (NN) which is useful for modeling sequential phenomena. The key difference between RNNs and other types of NNs is a feedback loop that allows selected information to persist. Long Short-Term Memory networks (LSTM) are a type of RNN that can learn long-term dependencies in time series data [173]. The ability of the LSTM to retain information over multiple samples is what makes it conducive for time series data. This property makes them potentially very useful for distinguishing between different types of affective touches. LSTMs consist of a sequence of gates (called forget, input, and output) that control the information that the RNN stores in its cell state and the learning process updates the weights associated with each gate. Specifically, LSTMs differ from vanilla RNNs because of the cell state.

In previous work, we showed that LSTM is a suitable tool for modeling external deformations, forces, and contact in a soft actuator [11]. Other groups have also begun exploring the use of LSTMs for modeling, understanding, and interpreting the information that soft sensors produce [8, 66, 69]. In this work, we use LSTM to distinguish between various external deformations and forces that a user can apply to a soft sensor and interpret these actions in the context of affective touch.

7.3 Towards a framework for interpreting affective touch with soft sensors

Affective touch plays a significant role in human-human and human-robot interactions. In this chapter, we demonstrate how to use machine learning to enable the detection of various types of affective touches in HRI. Yohanan et al. presented a touch dictionary that lists human intent and expectations in touching a "haptic creature" [196] that describes types of actions that natural

organisms use to interact with each other. The dictionary presents several gestures, but in this work we simplify the list to poke and rub because we limit our inputs to a single finger.

We hypothesize that the parameters of contact duration, localization, frequency, and amplitude that represent an affective touch can capture the underlying properties of each type and was sufficient for distinguishing between various forms of contacts. For duration, we recorded the length that a sensor detected a contact. For localization, we obtained the information in the geometry and density of the sensor array. For frequency and amplitude, we captured the information in the time series of the sensor readings at each point in the array.

A prototypical poke resembles a short impulse with a large amplitude, whereas a prototypical rub appears with a longer duration but with a lower amplitude (Fig. 7.4). We anticipated slight variation in signals due to individual users (e.g. a long poke, short rub, gentle poke, hard rub depending on how an individual user interprets these actions) and inconsistencies (i.e. each time a user performs an affective touch, the force, duration, location, and frequency may not be exactly the same). Part of the challenges of developing a skin that can process and understand this information include accounting for these differences that users can introduce.

For this chapter, we abstracted the problem for simplification and selected pokes and rubs at various locations of the soft sensors to evaluate their classification accuracies (Fig. 7.5). Alonso et al. performed a similarly structured experiment on a rigid robot that detects contacts using vibrations that are detectable by acoustic sensors [197].

7.4 Experimental setup

7.4.1 Structure of our affective touch data

For our training set, we collected data on 10 classes of affective touch on the sensor array (Fig. 7.5). The classes consisted of: poke at bottom-left (Fig. 7.5.0); poke at bottom-right (Fig. 7.5.1); poke at top-left (Fig. 7.5.2); poke at top-right (Fig. 7.5.3); poke

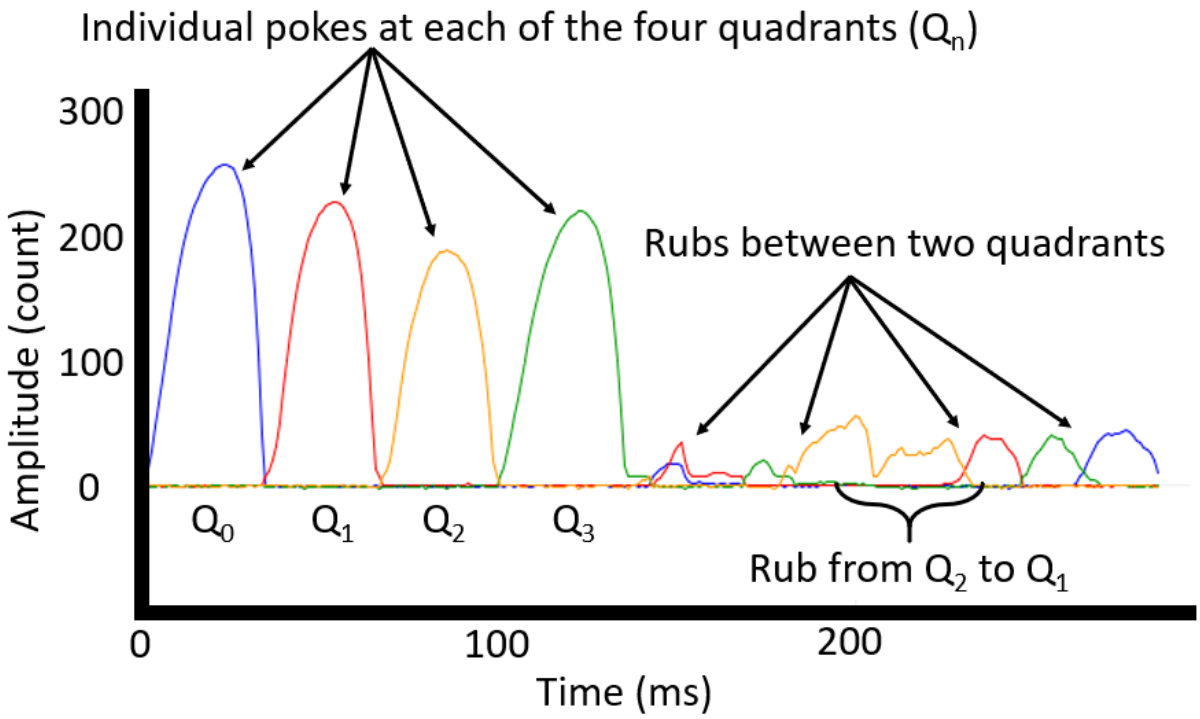


Figure 7.4: Heuristics for the sensor readings of pokes and rubs. Each of the Q_n represents touch at one of the four quadrants. These signals serve as general expectations for what defines a poke vs. a rub. Actual signals for individual users may differ, hence the use of LSTM to learn additional features in the time-series data.

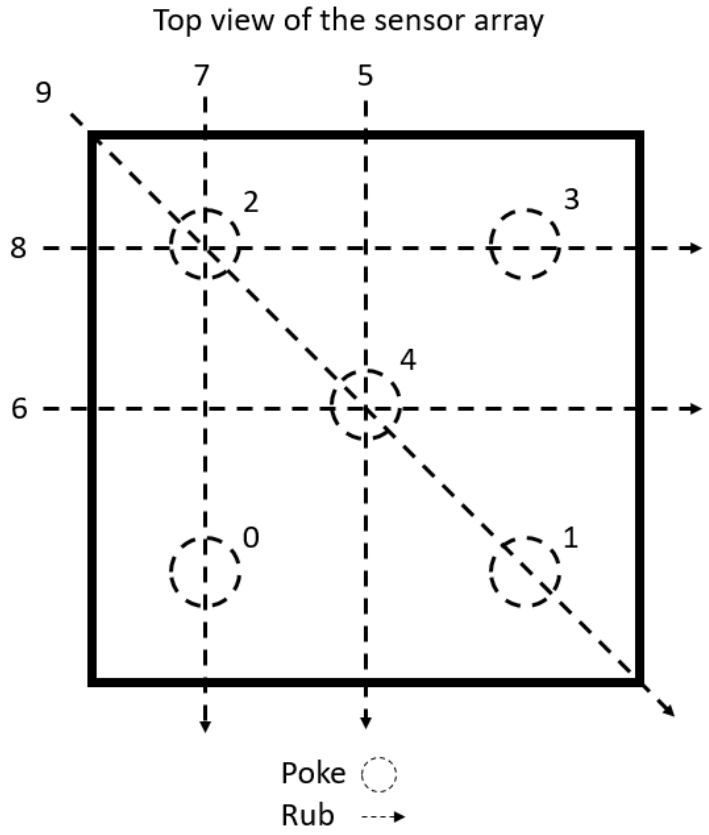


Figure 7.5: Visualization of the 10 types of touches that we classified. The circles correspond to pokes at the correpsonding location. The arrows represent the path and the direction of the rub.

at center (Fig. 7.5.4); rub from top-to-bottom along the middle (Fig. 7.5.5); rub from left-to-right along the middle (Fig. 7.5.6); rub from top-to-bottom along the left (Fig. 7.5.7); rub from left-to-right along the top (Fig. 7.5.8); and rub from top-left to bottom-right (Fig. 7.5.9). These 10 classes cover a comprehensive representation of the different types of pokes and rubs that a user might use to interact with the sensor. Our training data are available at: https://github.com/benshih/shih2020classificationgithub.com/benshih/shih2020classification.

7.4.2 Structure of LSTM

The input to our LSTM was the measurements from the sensor array (four inputs for the 2×2 array, one input for the 1x1 array), with ten output classes corresponding to the ten types of touch (Fig. 7.5). Because affective touch can vary in sample duration across different types of touches and consistency for individual users, we sampled a window of time around when the touch occurred, zero-padded the sensor readings, and fed that into the network. Our LSTM consisted of 85 nodes and 3 layers, each with dropout regularization of 0.2. We used softmax as the activation function for classification. The number of epochs was 50 and the batch size was 32. We saved the model parameters in the HDF5 format which enabled easy access during live deployment of the classification process.

The code for training the parameters for classification and for real-time deployment is available at: https://github.com/benshih/shih2020classificationgithub.com/benshih/shih2020classification.

7.4.3 Classification accuracy on the 2×2 sensor array

In the first experiment, we sought to assess how a rapidly manufacturable, 2×2, soft sensor array performs at classifying various types of affective touch. Based on the dictionary of touch, we selected ten classes that included various pokes and rubs (Fig. 7.5 and Section 7.4). Our hypothesis was that with this selection of affective touches, a 2×2 soft sensor array would be able to understand and distinguish between the various categories. Fig. 7.4 contains the heuristics for how the general shape of these forms of contacts appear as time series data.

We evaluated the classification accuracy by manually collecting training data from two users, building an LSTM model (Section 7.2) using an 80:20 ratio for training:testing data, and validating the learned model with five additional users. We chose to manually generate training data because a specific touch from one individual may differ from the same touch of another. In the experiments, our goal was to evaluate the performance of the learned models

despite variabilities between users. The training data consisted of 2400 samples and the test data consisted of 600 samples, which was an 80-20 random split for the training and testing data. Additionally, it consisted of samples from two individuals, to avoid overfitting to a specific individual. Finally, we evaluated the performance of the learned model by validating on five additional users.

7.4.4 Margin of return as related to scalability and density of sensor array

In the second experiment, our hypothesis was that a higher density of soft sensors in the array offers more information for distinguishing between classes of affective touch. With the appropriate data acquisition tools, we expected the 2×2 sensor to exhibit similar performances for all pokes regardless of location, while being able to distinguish between horizontal and vertical rubs because of the orientation characteristics of the serpentine pattern of the liquid metal sensors.

We evaluated the role that the density of the soft sensor array plays by comparing the performance of the 2×2 sensor to that of a 1x1 sensor. Instead of all ten classes like for the 2×2 sensor, we selected a subset of three classes: poke anywhere; rub from top-to-bottom along the middle (Fig. 7.5.5); and rub from left-to-right along the middle (Fig. 7.5.6). The structure of the LSTM for the 1×1 sensor was nearly identical to what was described in Section 7.4-B for the 2×2 sensor, except trained with 15 nodes instead of 85 because there were fewer classes to distinguish than for the 2×2 and less training data as a result. For the 1×1 sensor, we trained on 464 samples and validated on 116 samples.

7.4.5 Impact of soft vs. rigid substrate on soft sensor

In the third experiment, we hypothesized that while a rigid substrate provides higher signal amplitudes in terms of ground reaction forces during contact, the soft sensors would provide different but distinguishable amounts of information for classification when we performed the

same ten touches on a soft substrate (beneath the skin).

We evaluated the impact of a rigid vs. soft substrate by placing the 2×2 sensor array on a soft substrate (0.5" thick block of silicone (Ecoflex 00-50, Smooth-On)) while using the previously learned model from the rigid substrate (acrylic plate) to test the classification of the same ten types of affective touch (Fig. 7.5). We then validated on 139 samples. We retained the learned model that we trained on the rigid substrate to analyze how transferable the training data was on a different substrate and to quantify how much the performance changes compared to training on a rigid substrate.

7.4.6 Graceful degradation

In the fourth experiment, we hypothesized that despite damage to the sensor array, the predictions of the learned model would not fail catastrophically and instead provide reasonable, albeit diminished, results for classification [11].

We analyzed the ability of the 2×2 sensor to degrade gracefully by first removing and zeroing individual quadrants of the array. Then, we used the original learned model (with no sensors removed) to evaluate the classification accuracy of the data with individual sensors removed. For this experiment, we evaluated on 3000 samples as we removed individual sensors corresponding to each quadrant.

7.5 Results

7.5.1 Classification accuracy on the 2×2 sensor array

The average classification accuracy on the 2×2 sensor array was 97.1%, with a population standard deviation of 0.1% over five users. The value differed slightly for each instance of the training of the model because LSTMs are stochastic. We then validated the data on five users and

obtained accuracies of: 92%, 90%, 84%, 89%, and 81%.

Discussion The test data performed well on the training data. In the validation set, there was a larger decrease in performance for certain individuals compared to others, which we attribute to variance in force and duration due to each user's natural interpretation of what a poke and a rub feel like.

7.5.2 Margin of return as related to scalability and density of sensor array

The average classification accuracy of the 1x1 sensor array was 87.6%, with a population standard deviation of 0.5% over five users. We then validated the data using 100% of the training data and obtained an accuracy of 82%. However, the validation was inaccurate for other users not present in the training data: accuracy of 70% and 33% on a model trained from one user's touches.

Discussion We can attribute the lower accuracy of the 1×1 sensor array compared to that of the 2×2 sensor array to potential overfitting based on the large variability in model accuracy between individual users. Additionally, the lack of spatial resolution and reduced capability to interpret directionality may also contribute to the diminished performance and classification accuracy of the 1×1 sensor.

7.5.3 Impact of soft vs. rigid substrate on soft sensor

The average classification accuracy of the 2×2 sensor array that we intentionally trained using a rigid substrate but tested on a soft substrate was 69.5%, with a population standard deviation of 3.6% over four users.

Discussion This result shows that there is a decrease in performance of 19.5% when using the learned model (on a rigid substrate) for the 2×2 sensory array in conjunction with a soft substrate, which we can attribute to the soft substrate deforming along with the soft sensor, meaning that the elastomer channels do not experience as much deformation as on the rigid substrate and thus decreasing the amplitudes of the signal measurements from the sensor. It also suggests that a learned model specifically for the soft substrate may improve the performance compared to our current setup.

7.5.4 Graceful degradation

Removing the bottom-left sensor (Fig. 7.5.0) resulted in a classification accuracy of 71%, removing the bottom-right sensor (Fig. 7.5.1) resulted in a classification accuracy of 62%, removing the top-left sensor (Fig. 7.5.2) resulted in a classification accuracy of 61%, and removing the top-right sensor (Fig. 7.5.3) resulted in a classification accuracy of 72%. The average accuracy over five iterations of training the network was 97%, so the corresponding losses in accuracy for removal of the sensors was 26%, 35%, 36%, and 25%, respectively.

Discussion The sensor performance decreased, which was expected because of the overall loss of information compared to the full sensor array. However, it was promising to observe that the remaining sensors were able to partially compensate for the classification in spite of the loss of a quadrant (i.e. the array exhibited graceful degradation).

7.6 Conclusion and future work

Summary

Using LSTMs and liquid metal sensors, we enabled a sensor skin to distinguish between and classify a variety of pokes and rubs. We quantified the classification accuracy of a 2×2 sensor

array, compared the performance of the 2×2 sensor to a 1×1 sensor, evaluated the transferability of a learned model between substrates of different stiffness, and showed the graceful degradation of the 2×2 array when we disabled quadrants of the sensor. Our skin and learning approach are a step towards electronic skins for intelligent soft robots that can touch and feel with the sensitivity and perception of natural systems.

Future Work

Future work includes scaling up the size of the sensor array to increase the density and spatial resolution, to improve the electronics by using a higher sampling frequency than our current ADC to increase the temporal resolution, and to increase the sensitivity and range of amplitudes of the sensor measurements by modifying the geometry of the sensors. In addition, further exploration of techniques from transfer learning [198] will improve our understanding of how to contextualize and robustly interpret actions from multiple users despite individual variability. Finally, improving the robustness of the hardware system by securing the wires and deploying larger sensor skins in contextual, real-world examples would help demonstrate their practicality and usefulness for social interaction, e.g. for robots that can understand physical interactions such as a pat on the back.

One area of society that will benefit immediately from the implications of my research is socially assistive robots during infectious disease outbreaks. COVID-19 has demonstrated that robotics may help reduce the labor burden in many industries, particularly in healthcare. Soon, fully autonomous robots may collaborate with nurses and doctors or directly treat patients as caretakers. Additionally, with the pandemic transforming the landscape of physical interaction between people, haptics for soft robots could assist cognitive development of young children through educational robots that support or even substitute the daily physical interaction that students typically experience in the classroom.

Chapter 7, in full, is a reprint of the material as it appears in **B. Shih**, E. Lathrop, I. Adibnazari, R. Martin, Y.-L. Park, M. T. Tolley, "Classification of components of affective touch using rapidly manufacturable, soft, sensor skins", 2020 IEEE-RAS International Conference on Soft Robotics (**ROSO20**), pp. 182-187, Apr 2020. The dissertation author was the primary investigator and author of this paper.

Chapter 8

Electronic skins and machine learning for intelligent soft robots

Soft robots have garnered interest for real-world applications because of their intrinsic safety embedded at the material level. These robots use deformable materials capable of shape and behavioral changes and allow conformable physical contact for manipulation. Yet, with the introduction of soft and stretchable materials to robotic systems comes a myriad of challenges for sensor integration, including multimodal sensing capable of stretching, high-resolution but large-area sensor arrays, and sensor fusion with an increasing volume of data. This chapter explores the emerging confluence of e-skins and machine learning, with a focus on how roboticists can combine recent developments from the two fields to build autonomous, deployable soft robots, integrated with capabilities for informative touch and proprioception to stand up to the challenges of real-world environments.

8.1 Applications of e-skins

8.1.1 Shape sensing

Whereas environmental sensing helps a robot understand its surroundings, having a self-model of the robot's body is important for planning trajectories and actions within that environment. For robots primarily composed of rigid components, the geometry of each segment remains the same throughout the robot's lifetime, and relative rotations or translations of links provide enough additional information to fully specify the overall changes in shape. However, for soft robots, individual segments can continuously change their shapes, via both intentional and unintentional deformation modes, which complicates modeling and sensing schemes. Complementing recent work on soft sensing [42], the direct sensing of surface deformations would enhance the functionality of soft robots.

One approach to sensing the shape of soft robots involves pairing a model with a relatively low number of sensors, typically on the same order of magnitude as the number of controllable degrees of freedom in the system. A great deal of progress has been made in modeling manipulators that can be parameterized by a curve in 3D space [199]. These models have even been coupled with sensing mechanisms to enable closed-loop control of continuum manipulators [200]. Some approaches embedded sensors into other soft robotic components, such as bending actuators, to achieve closed-loop control in a low-dimensional task space [201].

The primary drawback of this type of approach is that when other unplanned deformation modes are introduced, such as buckling or a change of material properties through damage or natural material aging, the models accumulate error. In addition, it is unclear how to generalize these advances to reconfigurable soft robots [202] or robots that have more complex morphologies. For example, recent simulations suggest that there is a wide range of soft robot morphologies that could produce useful locomotion, including quadrupedal shapes and various oddly shaped exteriors [203]. All these classes of robots would benefit from sensing mechanisms with fewer

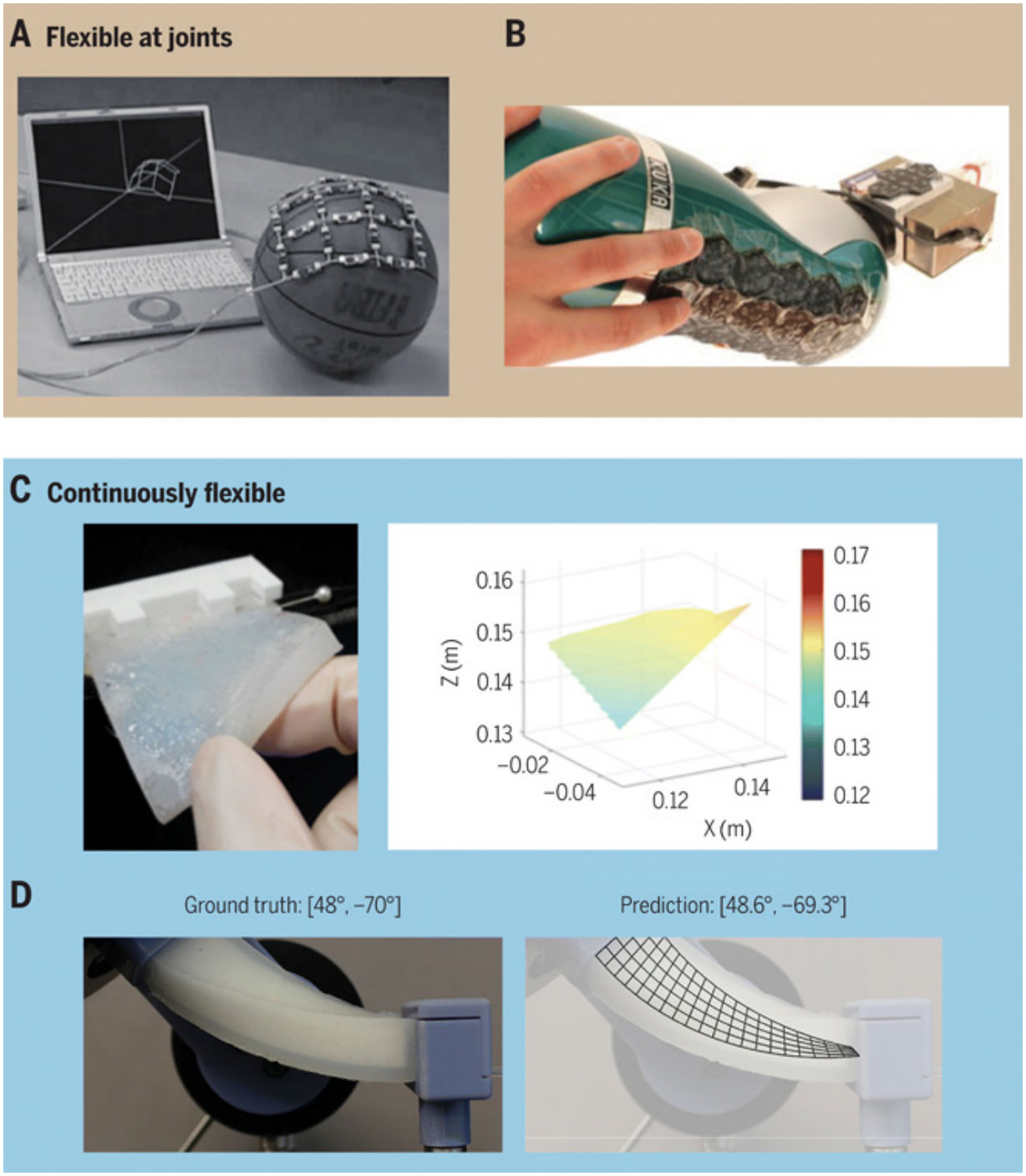


Figure 8.1: E-skins that can sense their shape in 3D. Recent advances in shape-sensing e-skins use several sensing modalities. (A and B) Accelerometers and/or magnetometers on rigid PCBs can rotate relative to each other and reconstruct their shape at discrete points. (A) "3D capture sheet" [32]. (B) Hexagonal PCBs with integrated accelerometers [33]. (C and D) Continuously flexible devices can sense deformation throughout their surface and estimate their resulting shape. Data-driven methods were then used in these examples to estimate the continuous shape of the e-skin. (C) Fiber Bragg gratings in silicone [34]. (D) Plastic optical fibers in silicone foam [35].

assumptions about the robot's mechanical properties.

The ideal shape-sensing system could stretch with the robot's surface without affecting its kinematics or dynamics, sense shape with- out external components, and be thin. E-skins designed for wearable applications should accommodate the strains of about 55 to 75% experienced by biological skin [53], and a similar range should be suitable for most soft robotic applications, although different robots experience different surface strains. Although a perfect solution for shape sensing of soft robots does not currently exist, recent advances in the field of flexible shape-sensing e-skins (Fig. 8.1) have the potential to greatly improve the capabilities of soft robots.

In contrast to that of soft skins, most work on shape-sensing e-skins treats the skin as an inextensible sheet of rigid elements joined by known axes of rotation (Fig. 8.1, A and B). The primary challenge is thus estimating the relative orientation between sections with known geometries to determine the spatial locations of discrete points within the sheet. In one early study, Hoshi and Shinoda arranged 24 printed circuit board (PCB) "nodes" into a mesh and estimated internode rotations using accelerometers and magnetometers [32] (Fig. 8.1A). Building upon this work, Mittendorfer and Cheng developed rigid sensorized hexagonal PCBs that could be integrated into semi-flexible sheets and wrapped around robots [56] (Fig. 8.1B). The nodes contained accelerometers similar to the work by Hoshi and Shinoda [32] and had similar assumptions (PCBs are free to rotate but cannot be stretched), but rotations between neighboring PCBs were calculated by obtaining at least two orientations of the skin-per-skin shape and solving a constrained Procrustes problem for aligning matrices of data points in real time. Hermanis et al. then used a grid-like arrangement of accelerometers and gravitometers on a flexible fabric sheet [33]. The sheets were demonstrated in a dynamic state estimation task where a user wore a shirt equipped with the shape- sensing sheets while bending and crouching.

In contrast to the discrete sampling methods mentioned above, other approaches leveraged techniques from machine learning and statistics to process various sensing signals and extract

a continuous estimate of the shape of the skins (Fig. 8.1, C and D). This kind of data-driven technique will be increasingly useful as the sensory spatial density increases, as discussed throughout this chapter. For instance, Rendl et al. used regularized least squares to process data from 16 piezoelectric bend sensors on a plastic sheet [polyethylene terephthalate (PET)] to approximate the shape of the sheet as a combination of several shape primitives [204]. This created a flexible system that could sense the bent state of the sheet with a roughly centimeter-level accuracy over an approximately A4-sized sheet. Another study used relatively inextensible optical fiber Bragg gratings arranged in a circle on the top and bottom of a silicone e-skin (Fig. 8.1C) [34]. The relation between the strains on the fiber and the shape of the sheet was extracted from training data using a feed-forward artificial neural network containing one hidden layer for computation between the input and output layers. In a similar spirit, an array of optical fibers were twisted through an elastomeric foam, and their outputs were sent to several machine learning algorithms (including kNN, SVM, neural networks, and decision trees) to predict the mode of deformation and angle of deformation of their structure (Fig. 8.1D) [35]. These approaches all dealt well with a limited set of deformations and, in principle, should work for a wider range of deformations when paired with a more expressive (deeper) network. However, none of these existing works can mechanically accommodate large in-plane strains, primarily because of the inextensibility of the optical fibers used.

8.1.2 Toward feedback control of soft robots

The intrinsic material compliance of soft robots can protect both the robot and the environment from damage when interacting with unstructured environments. This property makes soft robots appealing in contexts such as HRI and robotic manipulation, where safety around fragile objects can be important [45, 205]. E-skins have great potential to enable soft robots to interact intelligently with their environment.

In addition, tactile information obtained through skin is vital for a variety of general

robotic control tasks. The type of sensor modality to be used, the processing algorithm, and the response from the body all depend on the task at hand [206]. These tasks can be divided into three broad categories depending on the flow of information or energy and the primary system of concern (Fig. 8.2).

8.1.3 Manipulation

Robotic manipulation involves altering the state of an external object to a desired set point using internal actuators. The role of tactile sensors is mainly to obtain state information of the external object. As energy flows to the environment, stability of the object is of high concern. Grasp force optimization and stabilization is one of the most basic manipulation tasks involving tactile sensors [207]. Early works were built on the estimation of normal and tangential forces on the hand to detect slip and react accordingly [149]. Recent works used learning-based methods for slip onset prediction with adjustment and grasp failure detection with adjustment because of the ability of these methods to handle complex multimodal sensory information [208] and their generalizability [209].

Other manipulation studies used low-dimensional sensor space representations to improve performance in certain situations. Van Hoof et al. used autoencoders to generate a low-dimensional representation of their complex and continuous tactile data [210]. Control policies learned using this latent space representation required fewer rollouts and were more robust to noise. Another study was on calibration and self-modeling of a fully sensorized body for whole- body manipulation [211]. Recent work has shown that this process can be fully automated using control signal information and other sensor modalities, including inertial measurement units [212].

Perhaps the most complex manipulation task is in-hand manipulation, which imposes strict requirements on the body, brain, and sensors [213]. Current progress in in-hand manipulation using tactile sensors is primarily limited to rolling circular objects [30]. On the other hand, notable

developments toward in-hand manipulation have been achieved with external visual tracking systems [76]. However, control policies trained using vision alone are scene dependent and require large quantities of training data, motivating further research into using tactile sensing during in-hand manipulation.

8.1.4 Exploration

Tactile exploration is the process of voluntary motion of the body based on the somatosensory feedback for identifying environmental properties [214]. The environmental property of interest could be low-level features, such as surface texture [215, 216] or temperature [93], or mid-level tasks, such as object classification [82, 217]. However, to be fully autonomous, the higher-level process of selecting the best actions for obtaining better sensory information, also known as active exploration, must be considered. This is not trivial because the concept of an objective function and a reward function becomes difficult to define.

It is currently conjectured that human exploration is driven by a combination of extrinsic and intrinsic reward variables [218]. Extrinsic rewards are task specific, such as classification of objects, whereas intrinsic rewards are task independent and hence more general, such as curiosity-driven exploration. Experiments suggest that humans primarily use six types of exploratory movements when exploring objects to determine their properties [219]. Hence, there have been studies on acquiring these specialized closed-loop policies based on intrinsic rewards such as curiosity [220] or extrinsic rewards such as texture discrimination ability [221]. To achieve efficient exploration with soft robots, a combination of tactile and proprioceptive feedback will likely be useful for effectively implementing such reward functions.

A first step toward an autonomous tactile exploration control architecture, referred to as tactile servoing by the authors, was proposed by Li et al. [222]. By framing the control objective as the problem of following a trajectory in the sensor feature space, various autonomous sensory exploration strategies emerged. The emergent exploration strategies included maintaining contact

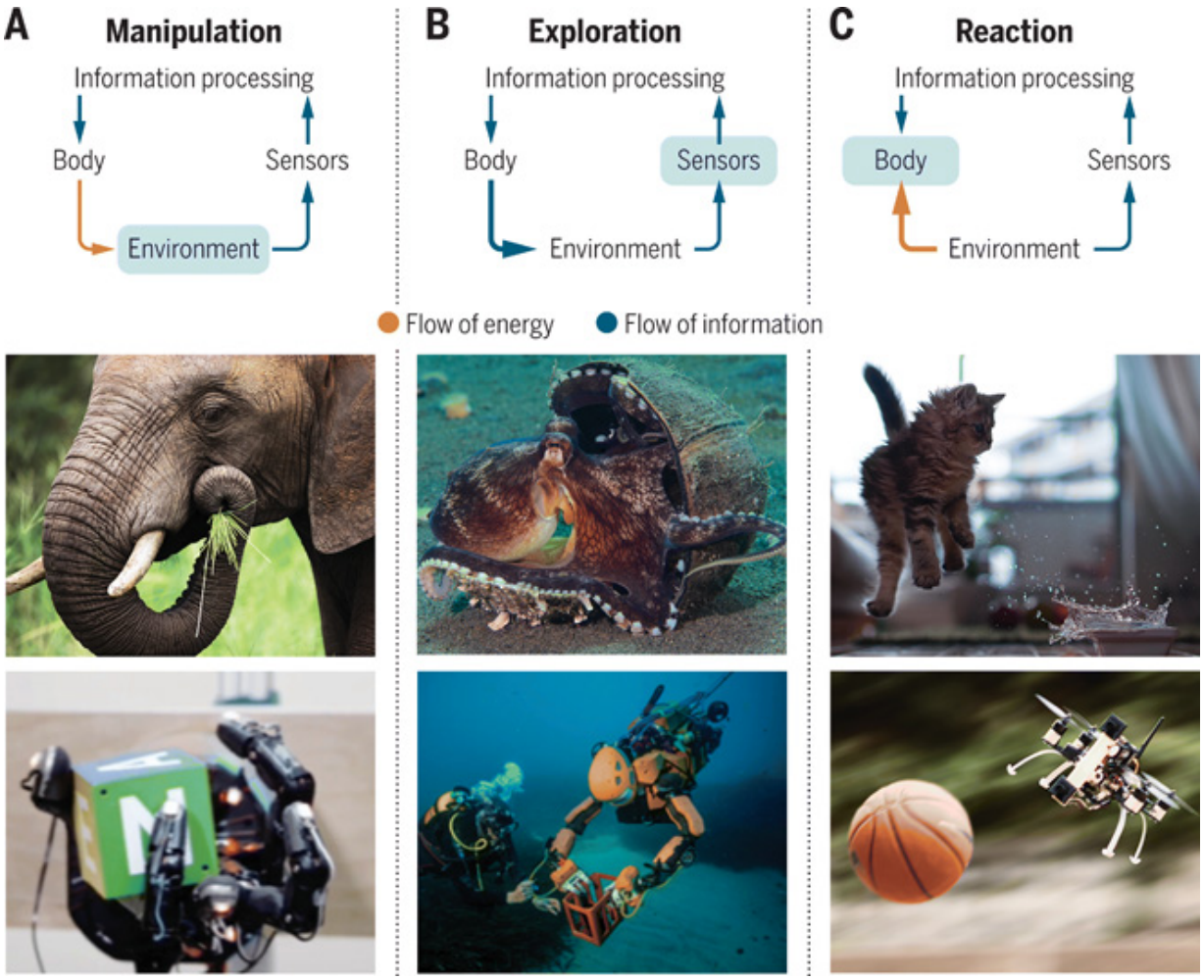


Figure 8.2: Closed-loop tasks where tactile sensing is essential. These tasks primarily differ depending on the system that determines the objective (denoted by the shaded boxes). The middle row consists of biological demonstrations of the tasks. The bottom row contains examples (69, 128, 129) of these capabilities in current rigid robots, which we expect to further improve in parallel with the integration of e-skins, soft robotics, and machine learning. Note that the presented division is not strict, and real-world tasks often involve a combination of all three elementary tasks. Yellow arrows indicate energy flow; blue arrows indicate information flow. (A) Manipulation involves altering the state of an external object to a desired set point using internal actuators. (B) Exploration involves motion of the body to account for uncertainties in the environment based on somatosensory feedback. (C) Reaction involves estimating and responding to environmental cues such that the body remains in a desired state.

with an object, edge tracking, and shape exploration of an unknown object. Exploration has also been framed as a force and pose control problem on an unknown object using tactile sensors for feedback [223]. Additional tactile information obtained during the process was then used to estimate the compliance of the object. Recent works integrated active exploration with object discrimination [224]. However, the mid-level processes were independent from the high-level exploration strategy, and the proposed algorithm was therefore relatively inefficient and slow. The next challenge in this area is to develop exploration strategies that run simultaneously and are regulated by the tactile feature extraction process. Such an algorithm would allow robots equipped with e-skins to efficiently process their sensory information to make informed decisions on how to move within the world to gather information and achieve at least locally optimal exploration strategies.

8.1.5 Reaction

Whole-body tactile skins are required for reacting to active environmental forces applied by external agents [225]. Here, the control objective is to estimate and react to external forces such that the body remains stable while executing a behavior. Often, the safety of the external agent, typically a human, becomes a higher priority than robot stability [226]. Because reaction typically involves HRI, additional challenges arise from safety, context prediction, and adaptation [130,227]. Otherwise, closed-loop reaction using tactile sensing is similar to the closed-loop manipulation problem and is often implemented in parallel with manipulation tasks as in the case of slip detection [228].

The main challenges in whole-body sensing are the organization and calibration of many spatially distributed multimodal tactile sensing elements [229]. Spatial calibration can be manually performed or automated using robot kinematics and action inference techniques [230]. Data-driven methods are also promising for end-to-end models without an explicit kinematic/dynamic calibration [231]. The most recent and comprehensive whole-body tactile sensing research was

able to self-organize and self-calibrate 1260 multimodal sensing units and implement a hierarchical task manager composed of the fusion of a balance controller, a self-collision avoidance system, and a skin compliance controller [232].

Chapter 8, in full, is a reprint of the material as it appears in **B. Shih**, D. S. Shah, J. Li, T. G. Thuruthel, Y.-L. Park, F. Iida, Z. Bao, R. Kramer-Bottiglio, M. T. Tolley, "Electronic skins and machine learning for intelligent soft robots", **Science Robotics**, 5:41, eaaz9239, April 2020. The dissertation author was the primary author of this paper.

Chapter 9

Conclusions

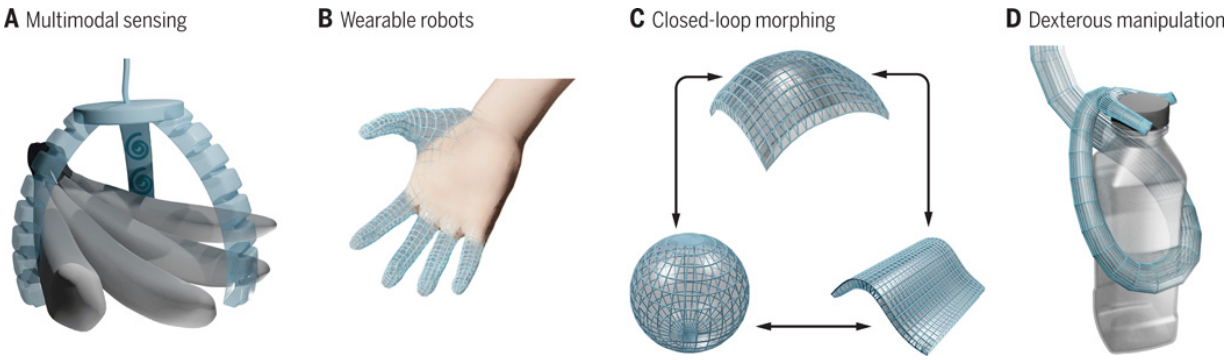


Figure 9.1: Tactile sensing and proprioception will enable soft robots to operate effectively in numerous challenging domains. **(A)** Multimodal sensing would be useful during manipulation, for detecting gripper states, object properties, and events such as contact and slip. **(B)** E-skins with an integrated human-robot interface could enable seamless assistive wearable robots and intuitive teleoperation of anthropomorphic robots. **(C)** When paired with the appropriate actuators, shape sensing would enable closed-loop changes of shape. **(D)** Closed-loop control algorithms would enable soft robots equipped with e-skins to succeed when performing complex tasks, including in-arm manipulation.

The fields of e-skins and soft robotics have both experienced rapid progress in recent years, demonstrating success in a wide range of domains. However, integrating advances from both fields to produce intelligent, autonomous soft robots is a challenging task which will require advances in several key areas (Fig. 9.1). Here, we outline major open questions in this area and identify areas of research which could provide solutions.

9.0.1 Open questions and future directions

Design and fabrication The primary future challenges of developing sensor arrays for soft robots will be to design stretchable sensory arrays with wide bandwidth and high dynamic range, resolution, and sensitivity. In addition, multimodal sensing would be useful for increasing robots' knowledge of their environment, leading to richer HRI (9.1A-B). Sensing of pressure, shear, vibration, and even detecting the presence of chemical and biological markers in the environment would be useful for a wide range of applications including manipulation, disaster response, and manufacturing. Recent efforts on integrating bacteria cells into soft robots have made it possible to directly detect and display chemical information on soft robots [17]. Another major design challenge is choosing how many sensors to integrate into a skin, and deciding how to place those intelligently. Resources are limited and require careful allocation. Where should sensors be placed along the skin's primary plane, and at what distance from the skin's surface? Are there "optimal" sensor distributions?

Machine learning and information processing Advancing the intelligence of soft robots will also require the community to develop computational models that can extract useful information from sensor arrays. However, the details of how to develop and implement such algorithms are unclear. What algorithms can most efficiently accomplish tasks in classification, regression, and fault detection? If neural networks are used, what architectures are easiest to train? Are there trade-offs between efficiency and reliability? Answering these questions will necessitate collaboration between computer and data scientists, materials engineers, and neuroscientists. The final result will be robots that are more aware of themselves, their environment, and their interactions with humans, yielding richer and more productive experiences for human end-users.

Affective touch is a crucial form of non-verbal communication that humans use daily, and is one application that would benefit from the combination of e-skins, soft robotics, and machine learning. In contrast, most robots currently are unable to understand gestures like a pat on the

back, because they either do not have the sensors necessary to measure the interaction or because they are not able to make sense of the affective contact.

Shape sensing Despite the recent progress in shape-sensing e-skins, it is unclear how to extend these advances to the wide range of soft robots presented in the literature. Soft robots experience large strains and complex deformations—how can stretchability be introduced into shape-sensing skins? How can resolution be increased to detect small local curvatures?

Once the field has reliable solutions for soft robot proprioception, it is conceivable that shape feedback would enable controlled shape-change in robots. Current soft robots do not have much ability to morph into specific configurations, yet even simple shape-change has led to innovative solutions for a wide range of tasks, such as obstacle avoidance [44], rolling locomotion [233], underwater locomotion [234] and camouflage [235]. Larger shape-change could result in robots which switch between morphologies and corresponding locomotion gaits on-demand (Fig. 9.1C).

Feedback control Using sensorized skins to close-the-loop has the potential to improve soft robots' ability to react to their environment, locomote, explore, and manipulate objects using their deformable bodies (Fig. 9.1D). The use of soft tactile sensors for closed-loop control is still in its nascency. The few relevant studies in this area use low-dimensional soft strain sensors for closed-loop kinematic or force control [201, 236, 237]. This is surprising given the wealth of literature on soft sensing technologies and considering the intended application of these sensors [42]. One reason for this discrepancy could be that soft sensors were originally developed for wearable devices and therefore used only for state estimation. Another reason could be the stiff performance expectations placed on soft sensors. Although it would be useful to develop drift-free, linear sensors with high gauge factors, biology suggests that workarounds are possible. For example, the human tactile sensing is hysteretic, nonlinear, time varying, and slow. Nature adapts to these drawbacks by developing hyper-redundant sensing networks and intelligent data

processing techniques [238].

Along the same lines, various sensor design strategies can be discovered by looking into nature. Tactile exploration likely requires the highest spatial resolution (around 2 mm), as evident from the dense mechanoreceptor distribution at the human fingertip [239, 240]. On the other end of the spectrum, tactile reaction likely requires the lowest spatial resolution, as suggested by the poor spatial resolution across other parts of the body. Tactile manipulation lies in between, with an expected spatial resolution of 5 mm [241].

The type and distribution of mechanoreceptors across the body also suggests the type of sensor technologies that would be useful for a particular task. It is clear that humans employ distinct sensors for static and dynamic cues. Low-bandwidth mechanoreceptors (10-50 Hz), can be found mainly in the fingertip, and would be essential for tactile exploration [242]. Higher bandwidth mechanoreceptors (50-400 Hz), that respond to the vibrations induced during object slippage, are distributed primarily at the palm of the hand [243]. The response and sensing area of the mechanoreceptors are strongly dependent on the skin morphology. Hence, it is vital to consider the design of the body and the motion capabilities for mimicking the dynamic receptors in our body.

Other insights can be gained by extending such an analysis to invertebrate biological organisms, such as octopuses. An octopus has a large number of receptors, primarily chemoreceptors, located on each sucker. Additionally, the octopus has strain receptors associated with its muscles and a relatively large brain for processing its receptor information. Despite these capabilities, it has a poor proprioceptive sense and cannot estimate the overall shape and location of external objects it is handling. There is local proprioceptive feedback in each arm for low-level control, but the only feedback to the central nervous system comes through vision [244]. Wells et al. conjectured that in flexible animals, motor control is hierarchical and proprioceptive information must be utilized locally [245]. Contrary to popular belief, the performance of the octopus in manipulation tasks is poor. Therefore, it might be necessary to incorporate rigid components in

fully-soft robots, if they are to be used for tactile-based closed-loop control tasks.

9.0.2 Outlook

This thesis focused on how the integration of soft sensor skins and machine learning enables soft robots to perceive physical interaction for complex haptic tasks. Part 1 on Soft Sensors (Chapters 2, 3, and 4) presented the design and fabrication of various types of soft strain sensors, using compliant materials such as silicones and polymers. Fabrication methods included soft lithography and 3D printing; performance of the sensors are characterized and modeled. Part 2 on Soft Robot Perception (Chapters 5 and 6) described how machine learning can be used to augment the performance of soft sensors and actuators. The method demonstrated how recurrent neural networks can be used for graceful degradation and learned perception of external contacts and forces despite not having a priori information about the individual sensors. Part 3 on Social Touch for Physical Human-Robot Interaction (Chapters 7 and 8) analyzed the use of the liquid metal sensors as robotic skins for the classification of affective (social) touch and builds towards the development of a framework for representing physical contact, for use at the human-robot interaction layer of abstraction.

In recent years, the concept of soft-bodied robots has rapidly grown in popularity. Researchers have developed many interesting forms of actuation that more closely mimic the functionality and capabilities found in nature. The next step for the field is to develop biologically-inspired tactile sensing for soft-bodied robots that can safely interact with—and explore—their environments. Current work concentrates on the design and fabrication of soft robots and sensors and explores how machine learning can enhance soft robot perception. In the short term, the field can focus on deployable, high-resolution sensor skins, algorithms for processing the dense sensor information, and reliable feedback control for soft robots. Building upon the fundamental work presented in this dissertation, the future consists of robots that can touch and feel with the sensitivity and perception of natural systems.

Bibliography

[1] H. A. Sonar, M. C. Yuen, R. Kramer-Bottiglio, and J. Paik, "An any-resolution pressure localization scheme using a soft capacitive sensor skin," in *2018 IEEE International Conference on Soft Robotics (RoboSoft)*, pp. 170–175, Apr. 2018.

[2] Y.-L. Park, B.-R. Chen, and R. J. Wood, "Design and fabrication of soft artificial skin using embedded microchannels and liquid conductors," *Sensors Journal, IEEE*, vol. 12, no. 8, pp. 2711–2718, 2012.

[3] T. Hellebrekers, O. Kroemer, and C. Majidi, "Soft magnetic skin for continuous deformation sensing," *Advanced Intelligent Systems*, vol. 1, no. 4, p. 1900025, 2019.

[4] B. C.-K. Tee, A. Chortos, A. Berndt, A. K. Nguyen, A. Tom, A. McGuire, Z. C. Lin, K. Tien, W.-G. Bae, H. Wang, P. Mei, H.-H. Chou, B. Cui, K. Deisseroth, T. N. Ng, and Z. Bao, "A skin-inspired organic digital mechanoreceptor," *Science*, vol. 350, pp. 313–316, Oct. 2015.

[5] D.-H. Kim, N. Lu, R. Ma, Y.-S. Kim, R.-H. Kim, S. Wang, J. Wu, S. M. Won, H. Tao, A. Islam, *et al.*, "Epidermal electronics," *Science*, vol. 333, no. 6044, pp. 838–843, 2011.

[6] M. Kaltenbrunner, T. Sekitani, J. Reeder, T. Yokota, K. Kuribara, T. Tokuhara, M. Drack, R. Schwödiauer, I. Graz, S. Bauer-Gogonea, *et al.*, "An ultra-lightweight design for imperceptible plastic electronics," *Nature*, vol. 499, no. 7459, p. 458, 2013.

[7] Z. Huang, Y. Hao, Y. Li, H. Hu, C. Wang, A. Nomoto, T. Pan, Y. Gu, Y. Chen, T. Zhang, *et al.*, "Three-dimensional integrated stretchable electronics," *Nature Electronics*, vol. 1, no. 8, p. 473, 2018.

[8] G. Soter, A. Conn, H. Hauser, and J. Rossiter, "Bodily aware soft robots: integration of proprioceptive and exteroceptive sensors," in *2018 IEEE international conference on robotics and automation (ICRA)*, pp. 2448–2453, IEEE, 2018.

[9] L. Chin, J. Lipton, M. C. Yuen, R. Kramer-Bottiglio, and D. Rus, "Automated recycling separation enabled by soft robotic material classification," in *2019 2nd IEEE International Conference on Soft Robotics (RoboSoft)*, pp. 102–107, IEEE, 2019.

[10] R. Deimel and O. Brock, "A novel type of compliant and underactuated robotic hand for dexterous grasping," *The International Journal of Robotics Research*, vol. 35, no. 1-3, pp. 161–185, 2016.

[11] T. G. Thuruthel, B. Shih, C. Laschi, and M. T. Tolley, "Soft robot perception using embedded soft sensors and recurrent neural networks," *Science Robotics*, vol. 4, no. 26, p. eaav1488, 2019.

[12] L. Scimeca, P. Maiolino, D. Cardin-Catalan, A. P. del Pobil, A. Morales, and F. Iida, "Non-destructive robotic assessment of mango ripeness via multi-point soft haptics," in *2019 International Conference on Robotics and Automation (ICRA)*, pp. 1821–1826, IEEE, 2019.

[13] R. A. Bilodeau, E. L. White, and R. K. Kramer, "Monolithic fabrication of sensors and actuators in a soft robotic gripper," in *Intelligent Robots and Systems (IROS), 2015 IEEE/RSJ International Conference on*, pp. 2324–2329, IEEE, 2015.

[14] N. Farrow and N. Correll, "A soft pneumatic actuator that can sense grasp and touch," in *Intelligent Robots and Systems (IROS), 2015 IEEE/RSJ International Conference on*, pp. 2317–2323, IEEE, 2015.

[15] B. Shih, D. Drotman, C. Christianson, Z. Huo, R. White, H. I. Christensen, and M. T. Tolley, "Custom soft robotic gripper sensor skins for haptic object visualization," in *Intelligent Robots and Systems (IROS), 2017 IEEE/RSJ International Conference on*, pp. 494–501, IEEE, 2017.

[16] H. Zhao, K. O'Brien, S. Li, and R. F. Shepherd, "Optoelectronically innervated soft prosthetic hand via stretchable optical waveguides," *Science Robotics*, vol. 1, no. 1, p. eaai7529, 2016.

[17] K. B. Justus, T. Helleb rekers, D. D. Lewis, A. Wood, C. Ingham, C. Majidi, P. R. LeDuc, and C. Tan, "A biosensing soft robot: Autonomous parsing of chemical signals through integrated organic and inorganic interfaces," *Science Robotics*, vol. 4, no. 31, p. eaax0765, 2019.

[18] A. Alspach, J. Kim, and K. Yamane, "Design of a soft upper body robot for physical human-robot interaction," in *2015 IEEE-RAS 15th International Conference on Humanoid Robots (Humanoids)*, pp. 290–296, IEEE, 2015.

[19] P. Mittendorfer, E. Dean, and G. Cheng, "3D spatial self-organization of a modular artificial skin," in *2014 IEEE/RSJ International Conference on Intelligent Robots and Systems*, pp. 3969–3974, Sept. 2014.

[20] J. W. Booth, D. Shah, J. C. Case, E. L. White, M. C. Yuen, O. Cyr-Choiniere, and R. Kramer-Bottiglio, "Omniskins: Robotic skins that turn inanimate objects into multifunctional robots," *Science Robotics*, vol. 3, no. 22, p. eaat1853, 2018.

[21] R. F. Shepherd, F. Ilievski, W. Choi, S. A. Morin, A. A. Stokes, A. D. Mazzeo, X. Chen, M. Wang, and G. M. Whitesides, "Multigait soft robot," *Proceedings of the national academy of sciences*, vol. 108, no. 51, pp. 20400–20403, 2011.

[22] D. Drotman, S. Jadhav, M. Karimi, M. T. Tolley, *et al.*, "3d printed soft actuators for a legged robot capable of navigating unstructured terrain," in *Robotics and Automation (ICRA), 2017 IEEE International Conference on*, pp. 5532–5538, IEEE, 2017.

[23] E. W. Hawkes, L. H. Blumenschein, J. D. Greer, and A. M. Okamura, "A soft robot that navigates its environment through growth," *Science Robotics*, vol. 2, no. 8, p. eaan3028, 2017.

[24] R. K. Katzschmann, J. DelPreto, R. MacCurdy, and D. Rus, "Exploration of underwater life with an acoustically controlled soft robotic fish," *Science Robotics*, vol. 3, no. 16, p. eaar3449, 2018.

[25] M. Wehner, R. L. Truby, D. J. Fitzgerald, B. Mosadegh, G. M. Whitesides, J. A. Lewis, and R. J. Wood, "An integrated design and fabrication strategy for entirely soft, autonomous robots," *Nature*, vol. 536, no. 7617, p. 451, 2016.

[26] S. Sundaram, P. Kellnhofer, Y. Li, J.-Y. Zhu, A. Torralba, and W. Matusik, "Learning the signatures of the human grasp using a scalable tactile glove," *Nature*, vol. 569, no. 7758, p. 698, 2019.

[27] K. Takei, T. Takahashi, J. C. Ho, H. Ko, A. G. Gillies, P. W. Leu, R. S. Fearing, and A. Javey, "Nanowire active-matrix circuitry for low-voltage macroscale artificial skin," *Nature materials*, vol. 9, no. 10, p. 821, 2010.

[28] W. Lee, Y. Liu, Y. Lee, B. K. Sharma, S. M. Shinde, S. D. Kim, K. Nan, Z. Yan, M. Han, Y. Huang, *et al.*, "Two-dimensional materials in functional three-dimensional architectures with applications in photodetection and imaging," *Nature communications*, vol. 9, no. 1, pp. 1–9, 2018.

[29] W. W. Lee, Y. J. Tan, H. Yao, S. Li, H. H. See, M. Hon, K. A. Ng, B. Xiong, J. S. Ho, and B. C. Tee, "A neuro-inspired artificial peripheral nervous system for scalable electronic skins," *Science Robotics*, vol. 4, no. 32, p. eaax2198, 2019.

[30] H. Van Hoof, T. Hermans, G. Neumann, and J. Peters, "Learning robot in-hand manipulation with tactile features," in *2015 IEEE-RAS 15th International Conference on Humanoid Robots (Humanoids)*, pp. 121–127, IEEE, 2015.

[31] A. D. Marchese, R. K. Katzschmann, and D. Rus, "A recipe for soft fluidic elastomer robots," *Soft Robotics*, vol. 2, no. 1, pp. 7–25, 2015.

[32] T. Hoshi and H. Shinoda, "3D shape measuring sheet utilizing gravitational and geomagnetic fields," in *2008 SICE Annual Conference*, pp. 915–920, Aug. 2008.

[33] A. Hermanis, R. Cacurs, and M. Greitans, "Acceleration and magnetic sensor network for shape sensing," *IEEE Sensors Journal*, vol. 16, pp. 1271–1280, Mar. 2016.

[34] T. L. T. Lun, K. Wang, J. D. L. Ho, K. Lee, K. Y. Sze, and K. Kwok, "Real-time surface shape sensing for soft and flexible structures using fiber Bragg gratings," *IEEE Robotics and Automation Letters*, vol. 4, pp. 1454–1461, Apr. 2019.

[35] I. Van Meerbeek, C. De Sa, and R. Shepherd, "Soft optoelectronic sensory foams with proprioception," *Science Robotics*, vol. 3, no. 24, p. eaau2489, 2018.

[36] D. Rus and M. T. Tolley, "Design, fabrication and control of soft robots," *Nature*, vol. 521, no. 7553, pp. 467–475, 2015.

[37] S. Wagner, S. P. Lacour, J. Jones, I. H. Pai-hui, J. C. Sturm, T. Li, and Z. Suo, "Electronic skin: architecture and components," *Physica E: Low-dimensional Systems and Nanostructures*, vol. 25, no. 2-3, pp. 326–334, 2004.

[38] J. Case, M. Yuen, M. Mohammed, and R. Kramer, "Sensor skins: An overview," in *Stretchable Bioelectronics for Medical Devices and Systems*, pp. 173–191, Springer, 2016.

[39] M. Amjadi, K.-U. Kyung, I. Park, and M. Sitti, "Stretchable, skin-mountable, and wearable strain sensors and their potential applications: a review," *Advanced Functional Materials*, vol. 26, no. 11, pp. 1678–1698, 2016.

[40] N. Yogeswaran, W. Dang, W. T. Navaraj, D. Shakthivel, S. Khan, E. O. Polat, S. Gupta, H. Heidari, M. Kaboli, L. Lorenzelli, *et al.*, "New materials and advances in making electronic skin for interactive robots," *Advanced Robotics*, vol. 29, no. 21, pp. 1359–1373, 2015.

[41] R. Dahiya, N. Yogeswaran, F. Liu, L. Manjakkal, E. Burdet, V. Hayward, and H. Jörntell, "Large-area soft e-skin: The challenges beyond sensor designs," *Proceedings of the IEEE*, vol. 107, no. 10, pp. 2016–2033, 2019.

[42] H. Wang, M. Totaro, and L. Beccai, "Toward perceptive soft robots: Progress and challenges," *Advanced Science*, p. 1800541, 2018.

[43] K. Chin, T. Hellebrekers, and C. Majidi, "Machine learning for soft robotic sensing and control," *Advanced Intelligent Systems*, 2020.

[44] D. S. Shah, M. C. Yuen, L. G. Tilton, E. J. Yang, and R. Kramer-Bottiglio, "Morphing robots using robotic skins that sculpt clay," *IEEE Robotics and Automation Letters*, vol. 4, pp. 2204–2211, Apr. 2019.

[45] T. Arnold and M. Scheutz, "The tactile ethics of soft robotics: designing wisely for human–robot interaction," *Soft robotics*, vol. 4, no. 2, pp. 81–87, 2017.

[46] J. Viventi, D.-H. Kim, L. Vigeland, E. S. Frechette, J. A. Blanco, Y.-S. Kim, A. E. Avrin, V. R. Tiruvadi, S.-W. Hwang, A. C. Vanleer, *et al.*, "Flexible, foldable, actively multiplexed, high-density electrode array for mapping brain activity in vivo," *Nature neuroscience*, vol. 14, no. 12, p. 1599, 2011.

[47] D.-H. Kim, J.-H. Ahn, W. M. Choi, H.-S. Kim, T.-H. Kim, J. Song, Y. Y. Huang, Z. Liu, C. Lu, and J. A. Rogers, "Stretchable and foldable silicon integrated circuits," *Science*, vol. 320, no. 5875, pp. 507–511, 2008.

[48] T. Someya, Y. Kato, T. Sekitani, S. Iba, Y. Noguchi, Y. Murase, H. Kawaguchi, and T. Sakurai, "Conformable, flexible, large-area networks of pressure and thermal sensors with organic transistor active matrixes," *Proceedings of the National Academy of Sciences*, vol. 102, no. 35, pp. 12321–12325, 2005.

[49] T. Sekitani, Y. Noguchi, K. Hata, T. Fukushima, T. Aida, and T. Someya, "A rubberlike stretchable active matrix using elastic conductors," *Science*, vol. 321, no. 5895, pp. 1468–1472, 2008.

[50] X. Ren, K. Pei, B. Peng, Z. Zhang, Z. Wang, X. Wang, and P. K. Chan, "A low-operating-power and flexible active-matrix organic-transistor temperature-sensor array," *Advanced Materials*, vol. 28, no. 24, pp. 4832–4838, 2016.

[51] S. Wang, J. Xu, W. Wang, G.-J. N. Wang, R. Rastak, F. Molina-Lopez, J. W. Chung, S. Niu, V. R. Feig, J. Lopez, *et al.*, "Skin electronics from scalable fabrication of an intrinsically stretchable transistor array," *Nature*, vol. 555, no. 7694, p. 83, 2018.

[52] B. Shih, C. Christianson, K. Gillespie, S. Lee, J. Mayeda, Z. Huo, and M. T. Tolley, "Design considerations for 3D printed, soft, multimaterial resistive sensors for soft robotics," *Frontiers in Robotics and AI*, vol. 6, p. 30, 2019.

[53] A. Chortos, J. Liu, and Z. Bao, "Pursuing prosthetic electronic skin," *Nature materials*, vol. 15, no. 9, p. 937, 2016.

[54] Y. Kim, A. Chortos, W. Xu, Y. Liu, J. Y. Oh, D. Son, J. Kang, A. M. Foudeh, C. Zhu, Y. Lee, *et al.*, "A bioinspired flexible organic artificial afferent nerve," *Science*, vol. 360, no. 6392, pp. 998–1003, 2018.

[55] P. A. Xu, A. Mishra, H. Bai, C. Aubin, L. Zullo, and R. Shepherd, "Optical lace for synthetic afferent neural networks," *Science Robotics*, vol. 4, no. 34, p. eaaw6304, 2019.

[56] P. Mittendorfer and G. Cheng, "3D surface reconstruction for robotic body parts with artificial skins," in *2012 IEEE/RSJ International Conference on Intelligent Robots and Systems*, pp. 4505–4510, Oct. 2012.

[57] R. K. Kramer, C. Majidi, R. Sahai, and R. J. Wood, "Soft curvature sensors for joint angle proprioception," in *Intelligent Robots and Systems (IROS), 2011 IEEE/RSJ International Conference on*, pp. 1919–1926, IEEE, 2011.

[58] J. T. Muth, D. M. Vogt, R. L. Truby, Y. Mengüç, D. B. Kolesky, R. J. Wood, and J. A. Lewis, "Embedded 3d printing of strain sensors within highly stretchable elastomers," *Advanced Materials*, vol. 26, no. 36, pp. 6307–6312, 2014.

[59] A. Alspach, J. Kim, and K. Yamane, "Design and fabrication of a soft robotic hand and arm system," in *2018 IEEE International Conference on Soft Robotics (RoboSoft)*, pp. 369–375, Apr. 2018.

[60] J. Jung, M. Park, D. W. Kim, and Y.-L. Park, "Optically sensorized elastomer air chamber for proprioceptive sensing of soft pneumatic actuators," *IEEE Robotics and Automation Letters*, 2020.

[61] G. Schwartz, B. C.-K. Tee, J. Mei, A. L. Appleton, D. H. Kim, H. Wang, and Z. Bao, "Flexible polymer transistors with high pressure sensitivity for application in electronic skin and health monitoring," *Nature communications*, vol. 4, p. 1859, 2013.

[62] J. Byun, Y. Lee, J. Yoon, B. Lee, E. Oh, S. Chung, T. Lee, K.-J. Cho, J. Kim, and Y. Hong, "Electronic skins for soft, compact, reversible assembly of wirelessly activated fully soft robots," *Science Robotics*, vol. 3, no. 18, p. eaas9020, 2018.

[63] H. Jeong, L. Wang, T. Ha, R. Mitbander, X. Yang, Z. Dai, S. Qiao, L. Shen, N. Sun, and N. Lu, "Modular and reconfigurable wireless e-tattoos for personalized sensing," *Advanced Materials Technologies*, p. 1900117, 2019.

[64] Y. Mengüç, Y.-L. Park, H. Pei, D. Vogt, P. M. Aubin, E. Winchell, L. Fluke, L. Stirling, R. J. Wood, and C. J. Walsh, "Wearable soft sensing suit for human gait measurement," *The International Journal of Robotics Research*, vol. 33, no. 14, pp. 1748–1764, 2014.

[65] C. M. Boutry, M. Negre, M. Jorda, O. Vardoulis, A. Chortos, O. Khatib, and Z. Bao, "A hierarchically patterned, bioinspired e-skin able to detect the direction of applied pressure for robotics," *Science Robotics*, vol. 3, no. 24, p. eaau6914, 2018.

[66] P. Piacenza, S. Sherman, and M. Ciocarlie, "Data-driven super-resolution on a tactile dome," *IEEE Robotics and Automation Letters*, vol. 3, no. 3, pp. 1434–1441, 2018.

[67] C. Larson, J. Spjut, R. Knepper, and R. Shepherd, "A deformable interface for human touch recognition using stretchable carbon nanotube dielectric elastomer sensors and deep neural networks," *Soft robotics*, vol. 6, no. 5, pp. 611–620, 2019.

[68] D. Kim, J. Kwon, B. J. Jeon, and Y.-L. Park, "Adaptive calibration of soft sensors using optimal transportation transfer learning for mass production and long-term usage," *Advanced Intelligent Systems*, 2020.

[69] D. Kim, J. Kwon, S. Han, Y.-L. Park, and S. Jo, "Deep full-body motion network (dfm-net) for a soft wearable motion sensing suit," *IEEE/ASME Transactions on Mechatronics*, 2018.

[70] M. Riesenhuber and T. Poggio, "Hierarchical models of object recognition in cortex," *Nature neuroscience*, vol. 2, no. 11, p. 1019, 1999.

[71] Y. Bengio, A. Courville, and P. Vincent, "Representation learning: A review and new perspectives," *IEEE transactions on pattern analysis and machine intelligence*, vol. 35, no. 8, pp. 1798–1828, 2013.

[72] P. Mirowski, R. Pascanu, F. Viola, H. Soyer, A. J. Ballard, A. Banino, M. Denil, R. Goroshin, L. Sifre, K. Kavukcuoglu, *et al.*, "Learning to navigate in complex environments," *arXiv preprint arXiv:1611.03673*, 2016.

[73] T. Chen, S. Gupta, and A. Gupta, "Learning exploration policies for navigation," *arXiv preprint arXiv:1903.01959*, 2019.

[74] J. Fu, S. Levine, and P. Abbeel, "One-shot learning of manipulation skills with online dynamics adaptation and neural network priors," in *2016 IEEE/RSJ International Conference on Intelligent Robots and Systems (IROS)*, pp. 4019–4026, IEEE, 2016.

[75] A. Rajeswaran, V. Kumar, A. Gupta, G. Vezzani, J. Schulman, E. Todorov, and S. Levine, "Learning complex dexterous manipulation with deep reinforcement learning and demonstrations," *arXiv preprint arXiv:1709.10087*, 2017.

[76] M. Andrychowicz, B. Baker, M. Chociej, R. Jozefowicz, B. McGrew, J. Pachocki, A. Petron, M. Plappert, G. Powell, A. Ray, *et al.*, "Learning dexterous in-hand manipulation," *arXiv:1808.00177*, 2018.

[77] D. P. Bertsekas, *Dynamic programming and optimal control*, vol. 1. Athena scientific, 1995.

[78] C. Laschi, B. Mazzolai, and M. Cianchetti, "Soft robotics: Technologies and systems pushing the boundaries of robot abilities," *Science Robotics*, vol. 1, no. 1, p. eaah3690, 2016.

[79] S. Kim, C. Laschi, and B. Trimmer, "Soft robotics: a bioinspired evolution in robotics," *Trends in biotechnology*, vol. 31, no. 5, pp. 287–294, 2013.

[80] R. Pfeifer, M. Lungarella, and F. Iida, "The challenges ahead for bio-inspired 'soft' robotics," *Communications of the ACM*, vol. 55, no. 11, pp. 76–87, 2012.

[81] P. Polygerinos, Z. Wang, K. C. Galloway, R. J. Wood, and C. J. Walsh, "Soft robotic glove for combined assistance and at-home rehabilitation," *Robotics and Autonomous Systems*, vol. 73, pp. 135–143, 2015.

[82] B. S. Homberg, R. K. Katzschmann, M. R. Dogar, and D. Rus, "Haptic identification of objects using a modular soft robotic gripper," in *Intelligent Robots and Systems (IROS), 2015 IEEE/RSJ International Conference on*, pp. 1698–1705, IEEE, 2015.

[83] R. Deimel and O. Brock, "A novel type of compliant and underactuated robotic hand for dexterous grasping," *The International Journal of Robotics Research*, p. 0278364915592961, 2015.

[84] K. Suzumori, S. Iikura, and H. Tanaka, "Applying a flexible microactuator to robotic mechanisms," *Control Systems, IEEE*, vol. 12, no. 1, pp. 21–27, 1992.

[85] H. Ritter and R. Haschke, "Hands, dexterity, and the brain," in *Humanoid Robotics and Neuroscience: Science, Engineering and Society*, pp. 49–77, CRC Press, 2014.

[86] S. Li, H. Zhao, and R. F. Shepherd, "Flexible and stretchable sensors for fluidic elastomer actuated soft robots," *MRS Bulletin*, vol. 42, no. 2, pp. 138–142, 2017.

[87] J. Kim, A. Alspach, and K. Yamane, "3d printed soft skin for safe human-robot interaction," in *Intelligent Robots and Systems (IROS), 2015 IEEE/RSJ International Conference on*, pp. 2419–2425, IEEE, 2015.

[88] A. M. Okamura, M. L. Turner, and M. R. Cutkosky, "Haptic exploration of objects with rolling and sliding," in *Robotics and Automation, 1997. Proceedings., 1997 IEEE International Conference on*, vol. 3, pp. 2485–2490, IEEE, 1997.

[89] H. A. Sonar and J. Paik, "Soft pneumatic actuator skin with piezoelectric sensors for vibrotactile feedback," *Frontiers in Robotics and AI*, vol. 2, p. 38, 2015.

[90] N. Gorges, S. E. Navarro, D. Göger, and H. Wörn, "Haptic object recognition using passive joints and haptic key features," in *Robotics and Automation (ICRA), 2010 IEEE International Conference on*, pp. 2349–2355, IEEE, 2010.

[91] R. D. P. Wong, R. B. Hellman, and V. J. Santos, "Haptic exploration of fingertip-sized geometric features using a multimodal tactile sensor," in *SPIE Sensing Technology+ Applications*, pp. 911605–911605, International Society for Optics and Photonics, 2014.

[92] A. J. Spiers, M. V. Liarokapis, B. Calli, and A. M. Dollar, "Single-grasp object classification and feature extraction with simple robot hands and tactile sensors," *IEEE transactions on haptics*, vol. 9, no. 2, pp. 207–220, 2016.

[93] H. Yousef, M. Boukallel, and K. Althoefer, "Tactile sensing for dexterous in-hand manipulation in robotics – a review," *Sensors and Actuators A: physical*, vol. 167, no. 2, pp. 171–187, 2011.

[94] R. R. Ma and A. M. Dollar, "On dexterity and dexterous manipulation," in *Advanced Robotics (ICAR), 2011 15th International Conference on*, pp. 1–7, IEEE, 2011.

[95] J. Fraś, J. Czarnowski, M. Maciaś, J. Główka, M. Cianchetti, and A. Menciassi, "New stiff-flop module construction idea for improved actuation and sensing," in *Robotics and Automation (ICRA), 2015 IEEE International Conference on*, pp. 2901–2906, IEEE, 2015.

[96] S. Sareh, A. Jiang, A. Faragasso, Y. Noh, T. Nanayakkara, P. Dasgupta, L. D. Seneviratne, H. A. Wurdemann, and K. Althoefer, "Bio-inspired tactile sensor sleeve for surgical soft manipulators," in *Robotics and Automation (ICRA), 2014 IEEE International Conference on*, pp. 1454–1459, IEEE, 2014.

[97] B. C. Mac Murray, X. An, S. S. Robinson, I. M. van Meerbeek, K. W. O'Brien, H. Zhao, and R. F. Shepherd, "Poroelastic foams for simple fabrication of complex soft robots," *Advanced Materials*, vol. 27, no. 41, pp. 6334–6340, 2015.

[98] C.-X. Liu and J.-W. Choi, "Patterning conductive pdms nanocomposite in an elastomer using microcontact printing," *Journal of Micromechanics and Microengineering*, vol. 19, no. 8, p. 085019, 2009.

[99] D. P. Holland, E. J. Park, P. Polygerinos, G. J. Bennett, and C. J. Walsh, "The soft robotics toolkit: Shared resources for research and design," *Soft Robotics*, vol. 1, no. 3, pp. 224–230, 2014.

[100] L. d. F. D. Costa and R. M. Cesar Jr, *Shape analysis and classification: theory and practice*. CRC Press, Inc., 2000.

[101] H. Lipson and M. Kurman, *Fabricated: The new world of 3D printing*. John Wiley & Sons, 2013.

[102] Y. Wang, X. Yang, Y. Chen, D. K. Wainwright, C. P. Kenaley, Z. Gong, Z. Liu, H. Liu, J. Guan, T. Wang, *et al.*, "A biorobotic adhesive disc for underwater hitchhiking inspired by the remora suckerfish," *Science Robotics*, vol. 2, no. 10, p. eaan8072, 2017.

[103] K. Kumar, J. Liu, C. Christianson, M. Ali, M. T. Tolley, J. Aizenberg, D. E. Ingber, J. C. Weaver, and K. Bertoldi, "A biologically inspired, functionally graded end effector for soft robotics applications," *Soft robotics*, vol. 4, no. 4, pp. 317–323, 2017.

[104] M. J. Pearson, B. Mitchinson, J. C. Sullivan, A. G. Pipe, and T. J. Prescott, "Biomimetic vibrissal sensing for robots," *Philosophical Transactions of the Royal Society B: Biological Sciences*, vol. 366, no. 1581, pp. 3085–3096, 2011.

[105] N. W. Bartlett, M. T. Tolley, J. T. Overvelde, J. C. Weaver, B. Mosadegh, K. Bertoldi, G. M. Whitesides, and R. J. Wood, "A 3d-printed, functionally graded soft robot powered by combustion," *Science*, vol. 349, no. 6244, pp. 161–165, 2015.

[106] H. Lipson, "A grand challenge for additive manufacturing: Can we print a robot that will walk out of the printer?," *3D Printing and Additive Manufacturing*, vol. 2, no. 2, pp. 41–41, 2015.

[107] S. Felton, M. Tolley, E. Demaine, D. Rus, and R. Wood, "A method for building self-folding machines," *Science*, vol. 345, no. 6197, pp. 644–646, 2014.

[108] R. MacCurdy, R. Katzschmann, Y. Kim, and D. Rus, "Printable hydraulics: a method for fabricating robots by 3d co-printing solids and liquids," in *Robotics and Automation (ICRA), 2016 IEEE International Conference on*, pp. 3878–3885, IEEE, 2016.

[109] I. Ieropoulos, J. Greenman, C. Melhuish, I. Horsfield, *et al.*, "Ecobot-iii-a robot with guts.," in *ALIFE*, vol. 733, p. e40, 2010.

[110] J. M. Florez, B. Shih, Y. Bai, and J. Paik, "Soft pneumatic actuators for legged locomotion," in *IEEE International Conference on Robotics and Biomimetics*, no. EPFL-CONF-205047, 2014.

[111] N. Kellaris, V. G. Venkata, G. M. Smith, S. K. Mitchell, and C. Keplinger, "Peano-hasel actuators: Muscle-mimetic, electrohydraulic transducers that linearly contract on activation," *Science Robotics*, vol. 3, no. 14, p. eaar3276, 2018.

[112] F. Connolly, C. J. Walsh, and K. Bertoldi, "Automatic design of fiber-reinforced soft actuators for trajectory matching," *Proceedings of the National Academy of Sciences*, vol. 114, no. 1, pp. 51–56, 2017.

[113] A. Miriyev, K. Stack, and H. Lipson, "Soft material for soft actuators," *Nature communications*, vol. 8, no. 1, p. 596, 2017.

[114] A. T. Conn, M. J. Pearson, A. G. Pipe, J. Welsby, and J. Rossiter, "Dielectric elastomer vibrissal system for active tactile sensing," in *Electroactive Polymer Actuators and Devices (EAPAD) 2012*, vol. 8340, p. 83400F, International Society for Optics and Photonics, 2012.

[115] L. Scimeca, P. Maiolino, and F. Iida, "Soft morphological processing of tactile stimuli for autonomous category formation," in *2018 IEEE International Conference on Soft Robotics (RoboSoft)*, pp. 356–361, IEEE, 2018.

[116] B. S. Homberg, R. K. Katzschmann, M. R. Dogar, and D. Rus, "Robust proprioceptive grasping with a soft robot hand," *Autonomous Robots*, pp. 1–16, 2018.

[117] T. Kalisky, Y. Wang, B. Shih, D. Drotman, S. Jadhav, E. Aronoff-Spencer, and M. T. Tolley, "Differential pressure control of 3d printed soft fluidic actuators," in *Intelligent Robots and Systems (IROS), 2017 IEEE/RSJ International Conference on*, pp. 6207–6213, IEEE, 2017.

[118] T. Umedachi, V. Vikas, and B. A. Trimmer, "Highly deformable 3-d printed soft robot generating inching and crawling locomotions with variable friction legs," in *Intelligent Robots and Systems (IROS), 2013 IEEE/RSJ International Conference on*, pp. 4590–4595, IEEE, 2013.

[119] W. Felt, M. J. Telleria, T. F. Allen, G. Hein, J. B. Pompa, K. Albert, and C. D. Remy, "An inductance-based sensing system for bellows-driven continuum joints in soft robots," in *Robotics: Science and Systems*, 2017.

[120] M. J. Pearson, B. Mitchinson, J. Welsby, T. Pipe, and T. J. Prescott, "Scratchbot: Active tactile sensing in a whiskered mobile robot," in *International Conference on Simulation of Adaptive Behavior*, pp. 93–103, Springer, 2010.

[121] S. Bauer, S. Bauer-Gogonea, I. Graz, M. Kaltenbrunner, C. Keplinger, and R. Schwödiauer, "25th anniversary article: a soft future: from robots and sensor skin to energy harvesters," *Advanced Materials*, vol. 26, no. 1, pp. 149–162, 2014.

[122] H. A. Sonar and J. Paik, "Soft pneumatic actuator skin with piezoelectric sensors for vibrotactile feedback," *Frontiers in Robotics and AI*, vol. 2, p. 38, 2016.

[123] H. Devaraj, T. Giffney, A. Petit, M. Assadian, and K. Aw, "The development of highly flexible stretch sensors for a robotic hand," *Robotics*, vol. 7, no. 3, p. 54, 2018.

[124] M.-Y. Cheng, C.-L. Lin, Y.-T. Lai, and Y.-J. Yang, "A polymer-based capacitive sensing array for normal and shear force measurement," *Sensors*, vol. 10, no. 11, pp. 10211–10225, 2010.

[125] A. Frutiger, J. T. Muth, D. M. Vogt, Y. Mengüç, A. Campo, A. D. Valentine, C. J. Walsh, and J. A. Lewis, "Capacitive soft strain sensors via multicore–shell fiber printing," *Advanced Materials*, vol. 27, no. 15, pp. 2440–2446, 2015.

[126] E. L. White, M. C. Yuen, J. C. Case, and R. K. Kramer, "Low-cost, facile, and scalable manufacturing of capacitive sensors for soft systems," *Advanced Materials Technologies*, vol. 2, no. 9, p. 1700072, 2017.

[127] D. J. Lipomi, M. Vosgueritchian, B. C. Tee, S. L. Hellstrom, J. A. Lee, C. H. Fox, and Z. Bao, "Skin-like pressure and strain sensors based on transparent elastic films of carbon nanotubes," *Nature nanotechnology*, vol. 6, no. 12, pp. 788–792, 2011.

[128] J. Yin, V. J. Santos, and J. D. Posner, "Bioinspired flexible microfluidic shear force sensor skin," *Sensors and Actuators A: Physical*, vol. 264, pp. 289–297, 2017.

[129] S. Han, T. Kim, D. Kim, Y.-L. Park, and S. Jo, "Use of deep learning for characterization of microfluidic soft sensors," *IEEE Robotics and Automation Letters*, vol. 3, no. 2, pp. 873–880, 2018.

[130] D. Silvera-Tawil, D. Rye, and M. Velonaki, "Artificial skin and tactile sensing for socially interactive robots: A review," *Robotics and Autonomous Systems*, vol. 63, pp. 230–243, 2015.

[131] C. Majidi, "Soft robotics: a perspective—current trends and prospects for the future," *Soft Robotics*, vol. 1, no. 1, pp. 5–11, 2014.

[132] B. Shih, J. Mayeda, Z. Huo, C. Christianson, and M. T. Tolley, "3d printed resistive soft sensors," in *2018 IEEE International Conference on Soft Robotics (RoboSoft)*, IEEE, 2018.

[133] Stratasys, "Objet tangoblackplus flx980 data sheet." http://usglobalimages.stratasys.com/Main/Secure/MSDS/Rubber-like\%20Materials/DOC-06133-Objet-TangoBlackPlus-FLX980-US.pdf, 2014.

[134] Stratasys, "Polyjet materials data sheet." usglobalimages.stratasys.com/Main/Files/Material_Spec_Sheets/MSS_PJ_PJMaterialsDataSheet.pdf, 2016.

[135] Y.-S. Kim, J. Lu, B. Shih, A. Gharibans, Z. Zou, K. Matsuno, R. Aguilera, Y. Han, A. Meek, J. Xiao, M. T. Tolley, and T. P. Coleman, "Scalable manufacturing of solderable and stretchable physiologic sensing systems," *Advanced Materials*, vol. 29, no. 39, 2017.

[136] A. M. Wessendorf and D. J. Newman, "Dynamic understanding of human-skin movement and strain-field analysis," *IEEE Transactions on Biomedical Engineering*, vol. 59, no. 12, pp. 3432–3438, 2012.

[137] C. Creton and M. Ciccotti, "Fracture and adhesion of soft materials: a review," *Reports on Progress in Physics*, vol. 79, no. 4, p. 046601, 2016.

[138] V. Slesarenko and S. Rudykh, "Towards mechanical characterization of soft digital materials for multimaterial 3d-printing," *arXiv preprint arXiv:1710.05187*, 2017.

[139] Y.-L. Park, C. Majidi, R. Kramer, P. Bérard, and R. J. Wood, "Hyperelastic pressure sensing with a liquid-embedded elastomer," *Journal of Micromechanics and Microengineering*, vol. 20, no. 12, p. 125029, 2010.

[140] X. Wang, M. Jiang, Z. Zhou, J. Gou, and D. Hui, "3d printing of polymer matrix composites: A review and prospective," *Composites Part B: Engineering*, vol. 110, pp. 442–458, 2017.

[141] Stratasys, "Objet tangoplus flx980 data sheet." http://usglobalimages.stratasys.com/Main/Secure/MSDS/Rubber-like\%20Materials/DOC-06128-Objet-TangoPlus-FLX930-US.pdf, 2014.

[142] Stratasys, "Objet veroclear rgd810 data sheet." http://usglobalimages.stratasys.com/Main/Secure/MSDS/Transparent\%20Materials/DOC-06119-Objet-VeroClear-RGD810-EU.pdf, 2014.

[143] Stratasys, "Objet support705 sup705 data sheet." https://www.stratasys.com/\~/media/Main/Files/SDS/Support-Materials/SDS_Objet-Support-SUP705-US.pdf, 2014.

[144] W. Zhang, A. A. Dehghani-Sanij, and R. S. Blackburn, "Carbon based conductive polymer composites," *Journal of materials science*, vol. 42, no. 10, pp. 3408–3418, 2007.

[145] B. Calli, A. Singh, J. Bruce, A. Walsman, K. Konolige, S. Srinivasa, P. Abbeel, and A. M. Dollar, "Yale-cmu-berkeley dataset for robotic manipulation research," *The International Journal of Robotics Research*, vol. 36, no. 3, pp. 261–268, 2017.

[146] B. Mosadegh, P. Polygerinos, C. Keplinger, S. Wennstedt, R. F. Shepherd, U. Gupta, J. Shim, K. Bertoldi, C. J. Walsh, and G. M. Whitesides, "Pneumatic networks for soft robotics that actuate rapidly," *Advanced functional materials*, vol. 24, no. 15, pp. 2163–2170, 2014.

[147] A. W. Mahoney, T. L. Bruns, P. J. Swaney, and R. J. Webster, "On the inseparable nature of sensor selection, sensor placement, and state estimation for continuum robots or "where to put your sensors and how to use them"," in *Robotics and Automation (ICRA), 2016 IEEE International Conference on*, pp. 4472–4478, IEEE, 2016.

[148] P. Polygerinos, N. Correll, S. A. Morin, B. Mosadegh, C. D. Onal, K. Petersen, M. Cianchetti, M. T. Tolley, and R. F. Shepherd, "Soft robotics: Review of fluid-driven intrinsically soft devices; manufacturing, sensing, control, and applications in human-robot interaction," *Advanced Engineering Materials*, vol. 19, no. 12, p. 1700016, 2017.

[149] N. Wettels, V. J. Santos, R. S. Johansson, and G. E. Loeb, "Biomimetic tactile sensor array," *Advanced Robotics*, vol. 22, no. 8, pp. 829–849, 2008.

[150] R. Patel, R. Cox, and N. Correll, "Integrated proximity, contact and force sensing using elastomer-embedded commodity proximity sensors," *Autonomous Robots*, pp. 1–16, 2018.

[151] T. Yamada, Y. Hayamizu, Y. Yamamoto, Y. Yomogida, A. Izadi-Najafabadi, D. N. Futaba, and K. Hata, "A stretchable carbon nanotube strain sensor for human-motion detection," *Nature nanotechnology*, vol. 6, no. 5, p. 296, 2011.

[152] C. Mattmann, F. Clemens, and G. Tröster, "Sensor for measuring strain in textile," *Sensors*, vol. 8, no. 6, pp. 3719–3732, 2008.

[153] L. Wang, F. Ma, Q. Shi, H. Liu, and X. Wang, "Study on compressive resistance creep and recovery of flexible pressure sensitive material based on carbon black filled silicone rubber composite," *Sensors and Actuators A: Physical*, vol. 165, no. 2, pp. 207–215, 2011.

[154] Q. Zheng, J. Zhou, and Y. Song, "Time-dependent uniaxial piezoresistive behavior of high-density polyethylene/short carbon fiber conductive composites," *Journal of materials research*, vol. 19, no. 9, pp. 2625–2634, 2004.

[155] D. M. Vogt, Y.-L. Park, and R. J. Wood, "Design and characterization of a soft multi-axis force sensor using embedded microfluidic channels," *IEEE Sensors Journal*, vol. 13, no. 10, pp. 4056–4064, 2013.

[156] B. Gwandu, X. Shu, Y. Liu, W. Zhang, L. Zhang, and I. Bennion, "Simultaneous measurement of strain and curvature using superstructure fibre bragg gratings," *Sensors and Actuators A: Physical*, vol. 96, no. 2-3, pp. 133–139, 2002.

[157] S. Ozel, N. A. Keskin, D. Khea, and C. D. Onal, "A precise embedded curvature sensor module for soft-bodied robots," *Sensors and Actuators A: Physical*, vol. 236, pp. 349–356, 2015.

[158] V. Wall, G. Zöller, and O. Brock, "A method for sensorizing soft actuators and its application to the rbo hand 2," in *Robotics and Automation (ICRA), 2017 IEEE International Conference on*, pp. 4965–4970, IEEE, 2017.

[159] R. L. Truby, M. Wehner, A. K. Grosskopf, D. M. Vogt, S. G. Uzel, R. J. Wood, and J. A. Lewis, "Soft somatosensitive actuators via embedded 3d printing," *Advanced Materials*, vol. 30, no. 15, p. 1706383, 2018.

[160] J. Morrow, H.-S. Shin, C. Phillips-Grafflin, S.-H. Jang, J. Torrey, R. Larkins, S. Dang, Y.-L. Park, and D. Berenson, "Improving soft pneumatic actuator fingers through integration of soft sensors, position and force control, and rigid fingernails," *2016 IEEE International Conference on Robotics and Automation (ICRA)*, pp. 5024–5031, 2016.

[161] N. Sornkarn and T. Nanayakkara, "Can a soft robotic probe use stiffness control like a human finger to improve efficacy of haptic perception?," *IEEE transactions on haptics*, vol. 10, no. 2, pp. 183–195, 2017.

[162] U. Proske and S. C. Gandevia, "The proprioceptive senses: their roles in signaling body shape, body position and movement, and muscle force," *Physiological reviews*, vol. 92, no. 4, pp. 1651–1697, 2012.

[163] K. Fiehler and F. Rösler, "Plasticity of multisensory dorsal stream functions: evidence from congenitally blind and sighted adults," *Restorative neurology and neuroscience*, vol. 28, no. 2, pp. 193–205, 2010.

[164] G. Cappagli, E. Cocchi, and M. Gori, "Auditory and proprioceptive spatial impairments in blind children and adults," *Developmental science*, vol. 20, no. 3, p. e12374, 2017.

[165] R. J. van Beers, A. C. Sittig, and J. J. van der Gon Denier, "How humans combine simultaneous proprioceptive and visual position information," *Experimental Brain Research*, vol. 111, no. 2, pp. 253–261, 1996.

[166] K. Elgeneidy, N. Lohse, and M. Jackson, "Bending angle prediction and control of soft pneumatic actuators with embedded flex sensors–a data-driven approach," *Mechatronics*, vol. 50, pp. 234–247, 2018.

[167] C. Larson, J. Spjut, R. Knepper, and R. Shepherd, "Orbtouch: Recognizing human touch in deformable interfaces with deep neural networks," *Preprint at http://https://arxiv.org/abs/1706.02542*, 2017.

[168] T. George Thuruthel, Y. Ansari, E. Falotico, and C. Laschi, "Control strategies for soft robotic manipulators: A survey," *Soft robotics*, vol. 5, no. 2, pp. 149–163, 2018.

[169] K. Xu and N. Simaan, "An investigation of the intrinsic force sensing capabilities of continuum robots," *IEEE Transactions on Robotics (TRO)*, vol. 23, no. 3, pp. 576–587.

[170] A. Bajo and N. Simaan, "Finding lost wrenches: Using continuum robots for contact detection and estimation of contact location," in *Robotics and Automation (ICRA), 2010 IEEE International Conference on*, pp. 3666–3673, IEEE, 2010.

[171] R. E. Goldman, A. Bajo, and N. Simaan, "Compliant motion control for continuum robots with intrinsic actuation sensing," in *Robotics and Automation (ICRA), 2011 IEEE International Conference on*, pp. 1126–1132, IEEE, 2011.

[172] F. Khan, R. J. Roesthuis, and S. Misra, "Force sensing in continuum manipulators using fiber bragg grating sensors," in *Proc. IEEE/RSJ Int. Conf. Intelligent Robots and Systems (IROS)*, pp. 2531–2536, 2017.

[173] S. Hochreiter and J. Schmidhuber, "Long short-term memory," *Neural computation*, vol. 9, no. 8, pp. 1735–1780, 1997.

[174] D. P. Kingma and J. Ba, "Adam: A method for stochastic optimization," *arXiv preprint arXiv:1412.6980*, 2014.

[175] R. J. Williams and D. Zipser, "A learning algorithm for continually running fully recurrent neural networks," *Neural computation*, vol. 1, no. 2, pp. 270–280, 1989.

[176] A. Tsay, G. Savage, T. Allen, and U. Proske, "Limb position sense, proprioceptive drift and muscle thixotropy at the human elbow joint," *The Journal of physiology*, vol. 592, no. 12, pp. 2679–2694, 2014.

[177] R. J. van Beers, A. C. Sittig, and J. J. D. van der Gon, "The precision of proprioceptive position sense," *Experimental Brain Research*, vol. 122, no. 4, pp. 367–377, 1998.

[178] P. B. Matthews, "Mammalian muscle receptors and their central actions," *American Journal of Physical Medicine & Rehabilitation*, vol. 53, no. 3, pp. 143–144, 1974.

[179] Deloitte, "3d printing growth accelerates again," 2018.

[180] J. Amend, N. Cheng, S. Fakhouri, and B. Culley, "Soft robotics commercialization: Jamming grippers from research to product," *Soft robotics*, vol. 3, no. 4, pp. 213–222, 2016.

[181] J. A. Sandoval, S. Jadhav, H. Quan, D. D. Deheyn, and M. T. Tolley, "Reversible adhesion to rough surfaces both in and out of water, inspired by the clingfish suction disc," *Bioinspiration & biomimetics*, vol. 14, no. 6, p. 066016, 2019.

[182] S. Liu, M. Majit, S. Horgan, T. M. T., W. Weston-Dawkes, and E. Ochoa, "Programmable stiffness tissue displacement device," filed 2017. U.S. Patent App. No. 62/524034.

[183] C. Christianson, N. N. Goldberg, D. D. Deheyn, S. Cai, and M. T. Tolley, "Translucent soft robots driven by frameless fluid electrode dielectric elastomer actuators," *Science Robotics*, vol. 3, no. 17, p. eaat1893, 2018.

[184] J. Luong, P. Glick, A. Ong, M. S. deVries, S. Sandin, E. W. Hawkes, and M. T. Tolley, "Eversion and retraction of a soft robot towards the exploration of coral reefs," in *2019 2nd IEEE International Conference on Soft Robotics (RoboSoft)*, pp. 801–807, IEEE, 2019.

[185] S. Jadhav, V. Kannanda, B. Kang, M. T. Tolley, and J. P. Schulze, "Soft robotic glove for kinesthetic haptic feedback in virtual reality environments," *Electronic Imaging*, vol. 2017, no. 3, pp. 19–24, 2017.

[186] D. Drotman, M. Ishida, S. Jadhav, and M. T. Tolley, "Application-driven design of soft, 3-d printed, pneumatic actuators with bellows," *IEEE/ASME Transactions on Mechatronics*, vol. 24, no. 1, pp. 78–87, 2018.

[187] G. M. Whitesides, "Soft robotics," *Angewandte Chemie International Edition*, vol. 57, no. 16, pp. 4258–4273, 2018.

[188] M. T. Tolley, R. F. Shepherd, B. Mosadegh, K. C. Galloway, M. Wehner, M. Karpelson, R. J. Wood, and G. M. Whitesides, "A resilient, untethered soft robot," *Soft robotics*, vol. 1, no. 3, pp. 213–223, 2014.

[189] R. Deimel and O. Brock, "Soft hands for reliable grasping strategies," in *Soft Robotics*, pp. 211–221, Springer, 2015.

[190] J. Hughes, P. Maiolino, and F. Iida, "An anthropomorphic soft skeleton hand exploiting conditional models for piano playing," *Science Robotics*, vol. 3, no. 25, p. eaau3098, 2018.

[191] B. Shih, D. S. Shah, J. Li, T. G. Thuruthel, Y.-L. Park, F. Iida, Z. Bao, R. Kramer-Bottiglio, and M. T. Tolley, "Electronic skins and machine learning for intelligent soft robots," *Science Robotics*.

[192] R. Pfeifer and J. Bongard, *How the body shapes the way we think: a new view of intelligence*. 2006.

[193] M. A. Goodrich, A. C. Schultz, *et al.*, "Human–robot interaction: a survey," *Foundations and Trends in Human–Computer Interaction*, vol. 1, no. 3, pp. 203–275, 2008.

[194] T. Field, "Touch for socioemotional and physical well-being: A review," *Developmental review*, vol. 30, no. 4, pp. 367–383, 2010.

[195] M. von Mohr, L. P. Kirsch, and A. Fotopoulou, "The soothing function of touch: affective touch reduces feelings of social exclusion," *Scientific reports*, vol. 7, no. 1, p. 13516, 2017.

[196] S. Yohanan and K. E. MacLean, "The role of affective touch in human-robot interaction: Human intent and expectations in touching the haptic creature," *International Journal of Social Robotics*, vol. 4, no. 2, pp. 163–180, 2012.

[197] F. Alonso-Martín, J. Gamboa-Montero, J. Castillo, Á. Castro-González, and M. Salichs, "Detecting and classifying human touches in a social robot through acoustic sensing and machine learning," *Sensors*, vol. 17, no. 5, p. 1138, 2017.

[198] S. J. Pan and Q. Yang, "A survey on transfer learning," *IEEE Transactions on knowledge and data engineering*, vol. 22, no. 10, pp. 1345–1359, 2009.

[199] J. Burgner-Kahrs, D. C. Rucker, and H. Choset, "Continuum robots for medical applications: A survey," *IEEE Transactions on Robotics*, vol. 31, pp. 1261–1280, Dec. 2015.

[200] T. George Thuruthel, Y. Ansari, E. Falotico, and C. Laschi, "Control strategies for soft robotic manipulators: A survey," *Soft Robotics*, Jan. 2018.

[201] J. Morrow, H. Shin, C. Phillips-Grafflin, S. Jang, J. Torrey, R. Larkins, S. Dang, Y.-L. Park, and D. Berenson, "Improving soft pneumatic actuator fingers through integration of soft sensors, position and force control, and rigid fingernails," in *2016 IEEE International Conference on Robotics and Automation (ICRA)*, pp. 5024–5031, May 2016.

[202] S. Y. Kim, R. Baines, J. Booth, N. Vasios, K. Bertoldi, and R. Kramer-Bottiglio, "Reconfigurable soft body trajectories using unidirectionally stretchable composite laminae," *Nature Communications*, vol. 10, p. 3464, Aug. 2019.

[203] N. Cheney, R. MacCurdy, J. Clune, and H. Lipson, "Unshackling evolution: evolving soft robots with multiple materials and a powerful generative encoding," in *Proceedings of the 15th annual conference on Genetic and evolutionary computation*, pp. 167–174, ACM, 2013.

[204] C. Rendl, D. Kim, S. Fanello, P. Parzer, C. Rhemann, J. Taylor, M. Zirkl, G. Scheipl, T. Rothländer, M. Haller, and S. Izadi, "Flexsense: A transparent self-sensing deformable surface," in *Proceedings of the 27th Annual ACM Symposium on User Interface Software and Technology*, UIST '14, (New York, NY, USA), pp. 129–138, ACM, 2014. event-place: Honolulu, Hawaii, USA.

[205] L. Pinto, D. Gandhi, Y. Han, Y.-L. Park, and A. Gupta, "The curious robot: Learning visual representations via physical interactions," in *European Conference on Computer Vision*, pp. 3–18, Springer, 2016.

[206] M. R. Cutkosky, R. D. Howe, and W. R. Provancher, "Force and tactile sensors," *Springer Handbook of Robotics*, pp. 455–476, 2008.

[207] M. Li, Y. Bekiroglu, D. Kragic, and A. Billard, "Learning of grasp adaptation through experience and tactile sensing," in *2014 IEEE/RSJ International Conference on Intelligent Robots and Systems*, pp. 3339–3346, Ieee, 2014.

[208] F. Veiga, J. Peters, and T. Hermans, "Grip stabilization of novel objects using slip prediction," *IEEE transactions on haptics*, vol. 11, no. 4, pp. 531–542, 2018.

[209] Y. Chebotar, M. Kalakrishnan, A. Yahya, A. Li, S. Schaal, and S. Levine, "Path integral guided policy search," in *2017 IEEE international conference on robotics and automation (ICRA)*, pp. 3381–3388, IEEE, 2017.

[210] H. Van Hoof, N. Chen, M. Karl, P. van der Smagt, and J. Peters, "Stable reinforcement learning with autoencoders for tactile and visual data," in *2016 IEEE/RSJ International Conference on Intelligent Robots and Systems (IROS)*, pp. 3928–3934, IEEE, 2016.

[211] Y. Ohmura and Y. Kuniyoshi, "Humanoid robot which can lift a 30kg box by whole body contact and tactile feedback," in *2007 IEEE/RSJ International Conference on Intelligent Robots and Systems*, pp. 1136–1141, IEEE, 2007.

[212] P. Mittendorfer, E. Yoshida, and G. Cheng, "Realizing whole-body tactile interactions with a self-organizing, multi-modal artificial skin on a humanoid robot," *Advanced Robotics*, vol. 29, no. 1, pp. 51–67, 2015.

[213] K. Hertkorn, M. A. Roa, and C. Borst, "Planning in-hand object manipulation with multifingered hands considering task constraints," in *2013 IEEE International Conference on Robotics and Automation*, pp. 617–624, IEEE, 2013.

[214] G. E. Loeb, G. A. Tsianos, J. A. Fishel, N. Wettels, and S. Schaal, "Understanding haptics by evolving mechatronic systems," in *Progress in brain research*, vol. 192, pp. 129–144, Elsevier, 2011.

[215] N. Jamali and C. Sammut, "Majority voting: Material classification by tactile sensing using surface texture," *IEEE Transactions on Robotics*, vol. 27, no. 3, pp. 508–521, 2011.

[216] J. Sinapov, V. Sukhoy, R. Sahai, and A. Stoytchev, "Vibrotactile recognition and categorization of surfaces by a humanoid robot," *IEEE Transactions on Robotics*, vol. 27, no. 3, pp. 488–497, 2011.

[217] N. Jamali and C. Sammut, "Material classification by tactile sensing using surface textures," in *2010 IEEE International Conference on Robotics and Automation*, pp. 2336–2341, IEEE, 2010.

[218] J. Gottlieb, P.-Y. Oudeyer, M. Lopes, and A. Baranes, "Information-seeking, curiosity, and attention: computational and neural mechanisms," *Trends in cognitive sciences*, vol. 17, no. 11, pp. 585–593, 2013.

[219] S. J. Lederman and R. L. Klatzky, "Hand movements: A window into haptic object recognition," *Cognitive psychology*, vol. 19, no. 3, pp. 342–368, 1987.

[220] L. Pape, C. M. Oddo, M. Controzzi, C. Cipriani, A. Förster, M. C. Carrozza, and J. Schmidhuber, "Learning tactile skills through curious exploration," *Frontiers in neurorobotics*, vol. 6, p. 6, 2012.

[221] J. A. Fishel and G. E. Loeb, "Bayesian exploration for intelligent identification of textures," *Frontiers in neurorobotics*, vol. 6, p. 4, 2012.

[222] Q. Li, C. Schürmann, R. Haschke, and H. Ritter, "A control framework for tactile servoing," 2013.

[223] Z. Su, J. A. Fishel, T. Yamamoto, and G. E. Loeb, "Use of tactile feedback to control exploratory movements to characterize object compliance," *Frontiers in neurorobotics*, vol. 6, p. 7, 2012.

[224] M. Kaboli, K. Yao, D. Feng, and G. Cheng, "Tactile-based active object discrimination and target object search in an unknown workspace," *Autonomous Robots*, vol. 43, no. 1, pp. 123–152, 2019.

[225] H. Iwata and S. Sugano, "Whole-body covering tactile interface for human robot coordination," in *Proceedings 2002 IEEE International Conference on Robotics and Automation (Cat. No. 02CH37292)*, vol. 4, pp. 3818–3824, IEEE, 2002.

[226] M. Frigola, A. Casals, and J. Amat, "Human-robot interaction based on a sensitive bumper skin," in *2006 IEEE/RSJ International Conference on Intelligent Robots and Systems*, pp. 283–287, IEEE, 2006.

[227] S. Haddadin and E. Croft, "Physical human–robot interaction," in *Springer handbook of robotics*, pp. 1835–1874, Springer, 2016.

[228] G. Canepa, R. Petrigliano, M. Campanella, and D. De Rossi, "Detection of incipient object slippage by skin-like sensing and neural network processing," *IEEE Transactions on Systems, Man, and Cybernetics, Part B (Cybernetics)*, vol. 28, no. 3, pp. 348–356, 1998.

[229] G. Cheng, E. Dean-Leon, F. Bergner, J. R. G. Olvera, Q. Leboutet, and P. Mittendorfer, "A comprehensive realization of robot skin: Sensors, sensing, control, and applications," *Proceedings of the IEEE*, vol. 107, no. 10, pp. 2034–2051, 2019.

[230] A. Del Prete, S. Denei, L. Natale, F. Mastrogiovanni, F. Nori, G. Cannata, and G. Metta, "Skin spatial calibration using force/torque measurements," in *2011 IEEE/RSJ International Conference on Intelligent Robots and Systems*, pp. 3694–3700, IEEE, 2011.

[231] R. Calandra, S. Ivaldi, M. P. Deisenroth, E. Rueckert, and J. Peters, "Learning inverse dynamics models with contacts," in *2015 IEEE International Conference on Robotics and Automation (ICRA)*, pp. 3186–3191, IEEE, 2015.

[232] E. Dean-Leon, J. R. Guadarrama-Olvera, F. Bergner, and G. Cheng, "Whole-body active compliance control for humanoid robots with robot skin," in *2019 International Conference on Robotics and Automation (ICRA)*, pp. 5404–5410, IEEE, 2019.

[233] E. Steltz, A. Mozeika, N. Rodenberg, E. Brown, and H. M. Jaeger, "JSEL: Jamming skin enabled locomotion," in *2009 IEEE/RSJ International Conference on Intelligent Robots and Systems*, pp. 5672–5677, Oct. 2009.

[234] M. Ishida, D. Drotman, B. Shih, M. Hermes, M. Luhar, and M. T. Tolley, "Morphing structure for changing hydrodynamic characteristics of a soft underwater walking robot," *IEEE Robotics and Automation Letters*, vol. 4, no. 4, pp. 4163–4169, 2019.

[235] J. H. Pikul, S. Li, H. Bai, R. T. Hanlon, I. Cohen, and R. F. Shepherd, "Stretchable surfaces with programmable 3D texture morphing for synthetic camouflaging skins," *Science*, vol. 358, pp. 210–214, Oct. 2017.

[236] H. A. Sonar, A. P. Gerratt, S. P. Lacour, and J. Paik, "Closed-loop haptic feedback control using a self-sensing soft pneumatic actuator skin," *Soft robotics*, 2019.

[237] J. Wirekoh, L. Valle, N. Pol, and Y.-L. Park, "Sensorized, flat, pneumatic artificial muscle embedded with biomimetic microfluidic sensors for proprioceptive feedback," *Soft robotics*, vol. 6, no. 6, pp. 768–777, 2019.

[238] R. S. Dahiya, G. Metta, M. Valle, and G. Sandini, "Tactile sensing - from humans to humanoids," *IEEE transactions on robotics*, vol. 26, no. 1, pp. 1–20, 2009.

[239] J. C. Stevens, "Aging and spatial acuity of touch," *Journal of gerontology*, vol. 47, no. 1, pp. P35–P40, 1992.

[240] R. S. Johansson and A. Vallbo, "Tactile sensibility in the human hand: relative and absolute densities of four types of mechanoreceptive units in glabrous skin," *The Journal of physiology*, vol. 286, no. 1, pp. 283–300, 1979.

[241] F. Mancini, A. Bauleo, J. Cole, F. Lui, C. A. Porro, P. Haggard, and G. D. Iannetti, "Whole-body mapping of spatial acuity for pain and touch," *Annals of neurology*, vol. 75, no. 6, pp. 917–924, 2014.

[242] Å. Vallbo and R. Johansson, "Properties of cutaneous mechanoreceptors in the human hand related to touch sensation," *Human neurobiology*, vol. 3, no. 1, pp. 3–14, 1984.

[243] R. S. Johansson and J. R. Flanagan, "Coding and use of tactile signals from the fingertips in object manipulation tasks," *Nature Reviews Neuroscience*, vol. 10, no. 5, p. 345, 2009.

[244] M. J. Wells, *Octopus: physiology and behaviour of an advanced invertebrate*. Springer Science & Business Media, 2013.

[245] M. Wells, "Tactile discrimination of surface curvature and shape by the octopus," *Journal of Experimental Biology*, vol. 41, no. 2, pp. 433–445, 1964.